iScience

CellPress
OPEN ACCESS

Review

# A review of organ-on-chip fabrication methods: From early developments to overcoming inert barriers

Claudia Olaizola-Rodrigo,[1,2,*] Clara Bayona,[1,3] Sara Oliván,[1,3,*] and Rosa Monge[2,*]
[1]Tissue Microenvironment (TME) Lab, Aragón Institute of Engineering Research (I3A), University of Zaragoza, 50018 Zaragoza, Spain
[2]Beonchip S.L., 50018 Zaragoza, Spain
[3]Institute for Health Research Aragón (IIS Aragón), 50009 Zaragoza, Spain
*Correspondence: colaizola@unizar.es (C.O.-R.), soligar@unizar.es (S.O.), rmonge@beonchip.com (R.M.)
https://doi.org/10.1016/j.isci.2025.113992

## SUMMARY

Organ-on-chip (OOC) systems represent a significant advance in the effort to replicate human physiology *in vitro*, providing versatile models that extend beyond the limitations of static culture and animal experimentation. The fabrication methods and materials underlying these platforms play a decisive role in determining their structural accuracy, biological relevance, and potential for large-scale adoption. This review surveys the historical progression of OOC manufacturing, beginning with established microfabrication techniques such as photolithography, soft lithography, hot embossing, microinjection molding, and xurography and extending to recent innovations in additive manufacturing. Particular attention is given to emerging barrier-free strategies, including laminar flow patterning, hydrogel photopatterning, phaseguide design, and surface treatment patterning that permit direct tissue-tissue communication. These methods aim to enhance biomimicry by reducing artificial interfaces, thereby improving the simulation of intercellular gradients, multicellular crosstalk, and pathophysiological dynamics. Alongside their benefits, the review discusses the practical challenges these approaches introduce in terms of reproducibility, throughput, and scalability. By integrating advances in materials science, fabrication techniques, and microphysiological design, this review highlights the potential of next-generation OOC devices to provide predictive, translationally relevant platforms that narrow the divide between preclinical experimentation and clinical application.

## INTRODUCTION

In the field of microtechnologies designed to replicate controlled biological environments, OOC devices represent a significant advancement. These systems incorporate miniature engineered or natural tissues cultivated within microfluidic platforms, created using advanced microchip fabrication techniques. OOC systems typically contain chambers seeded with living cells, where biological fluids are steadily perfused, closely simulating the physiological conditions of organs and tissues, offering a valuable tool for studying biological processes.[1,2] By replicating dynamic microenvironments, precise tissue interfaces, and vascular perfusion, OOCs achieve levels of functionality that far surpass those of conventional 2D or static 3D culture systems.[3,4] Furthermore, they enable high-resolution real-time imaging and *in vitro* analysis of biochemical, genetic, and metabolic activities of living cells in a functional organ-like context. This technology has significant potential to facilitate advancements in the study of tissue development, organ physiology, and disease mechanisms. These systems represent a critical step toward reducing dependence on animal models and enabling personalized medicine.[5,6] Building upon the success of single-organ models, multi-organ-on-chip systems have been developed to capture systemic processes such as drug absorption, metabolism, and inter-organ communication, further broadening the applications of the technology.[2,7–9]

While these biological applications are transformative, the evolution and impact of OOC technology are inseparable from fabrication. Microfabrication techniques and material selection dictate nearly every aspect of device performance, including channel geometry, fluidic control, cellular microenvironment, optical accessibility, and compatibility with biochemical assays. The fabrication process not only defines the structural fidelity of the device but also influences its scalability, reproducibility, and regulatory acceptance, all of which are essential for translational impact. Early OOC platforms were predominantly fabricated via soft lithography in polydimethylsiloxane (PDMS), a material prized for prototyping but limited by small-molecule absorption and its gas permeability that can be either advantageous or restrictive depending on the application.[10,11] These drawbacks encouraged a shift toward thermoplastics and hybrid substrates. More recently, barrier-free fabrication strategies—eliminating inert membranes or other artificial interfaces—have emerged to improve physiological relevance, though they still represent a combination of traditional fabrication methods and innovative advances developed throughout the history of OOCs.

These technical developments now intersect with significant regulatory and economic shifts. In April 2025, the US Food and Drug Administration (FDA) announced plans to phase out mandatory animal testing requirements for certain drug classes in favor of New Approach Methodologies (NAMs), including OOC systems and advanced computational models.[12] The agency aims to make animal studies the exception rather than the norm within the next 5 years, signaling a major transition in preclinical evaluation. This regulatory momentum is mirrored by market expansion: the global OOC market, valued at approximately USD 157 million in 2024, is projected to reach nearly USD 950 million by 2030, corresponding to a compound annual growth rate of 35.11%.[13] Such growth reflects not only scientific innovation but also the increasing alignment of industrial strategies and regulatory frameworks with human-relevant testing platforms. Together, these shifts are accelerating the translation of OOC devices from academic prototypes into scalable, regulatory-accepted tools for biomedical research and drug development.

The present review provides a structured overview of the manufacturing strategies that have enabled OOC development, from traditional microfabrication methods, including photolithography, replication (soft lithography, hot embossing, injection molding), xurography, and 3D printing, to recent barrier-free innovations. Beyond describing each technique, we critically examine their advantages and limitations in relation to OOC performance and translational potential. Particular attention is given to emerging strategies designed to eliminate inert interfaces, a pivotal step toward creating platforms that more faithfully replicate human physiology. Taken together, these advances illustrate both the progress achieved and the challenges that remain, underscoring the potential of OOC technologies to reshape experimental biology and foster new avenues in translational research.

## FROM THE ORIGINS OF MICROFLUIDICS TO ORGAN-ON-CHIP

The advent of microfluidics in the final decades of the 20th century has profoundly impacted our understanding of biomedical sciences, with their diverse applications spanning a multitude of fields. These include optics, semiconductors, microelectronics, drug discovery, point-of-care clinical diagnostics, and bioanalytical systems.[14–17] It is therefore evident that microfluidics plays a significant role in this technological revolution.

Microfluidics focuses on the controlled manipulation of fluids within microscale environments, typically involving volumes in the microliter to picoliter range. These systems rely on microchannels or microcapillaries to direct fluid flow with exceptional precision.[18,19]

The origins of this technology can be traced back to the 1960s, with the advent of micro-electromechanical systems (MEMS) marking a significant development. These advancements, in turn, emerged from a series of prior innovations in semiconductor manufacturing and micromachining technology. MEMS represented a pioneering integration of mechanical and electrical components at the micro-scale. A significant landmark was achieved in 1965 with the development of the first silicon resonator by Nathanson, which integrated a vibrating mechanical structure with a field-effect transistor on the same chip.[20,21] This innovation enabled mechanical motion to modulate electronic signals, laying the foundation for future MEMS technologies. Subsequent decades witnessed a rapid advancement in MEMS technologies, with their applications expanding to automotive systems, medical devices, and consumer electronics. The 1980s witnessed the emergence of Biomedical MEMS (BioMEMS), a specialized extension of MEMS with a focus on applications in healthcare and biology, such as implantable sensors and microfluidic devices for biological analysis.[22] These advances subsequently catalyzed the development of micro-total analysis systems (micro-TAS) with the development of the first miniature gas chromatograph with a thermal conductivity detector on a silicon wafer at Stanford University.[23] Pioneered by researchers such as Andreas Manz, micro-TAS relied heavily on microfabrication and microfluidics, directly inheriting methods from MEMS to enable automated chemical and biological analyses with unprecedented efficiency and scale (Figure 1).[29,30] The first microfluidic devices were silicon-based, largely due to the early reliance on integrated circuit (IC) manufacturing techniques and materials.[31,32]

In the early 1990s, the utilization of microfabricated analysis systems for electrophoresis-based separations was first proposed.[33,34] Subsequently, microfabrication utilizing photolithography and etching techniques (Figure 1; early 1990s) was employed to pattern microchannels on silicon and glass substrates, mirroring processes used in integrated circuit fabrication.[35] In 1998, the introduction of the silicone-based elastomer PDMS in microsystems fabrication marked the start of soft lithography and subsequently promoted the widespread adoption of microfluidics beyond engineering laboratories (Figure 1).[25,36] PDMS transformed microfluidic device fabrication by offering unprecedented flexibility, ease of use, and reduced production cost. In the following years, alternative materials such as plastics, low-temperature ceramics, and different polymers were employed. More recently, polymers in particular have further diversified material options, especially in biomedical applications, due to their scalability, simplicity, and flexibility.[3,37]

Microfluidic systems facilitate high-throughput experimentation with minimal reagent volumes, while automating complex processes at reduced cost.[38,39] The aforementioned advantages render microfluidic technology particularly well suited to cellular research, given its micrometric dimensions, which are comparable to those of cells. Therefore, in the mid-2000s, cell culture in microfluidic devices was initiated using both silicon substrates and PDMS chips. Silicone-based systems enabled interaction between lung and liver cells,[26] while PDMS platforms were primarily used to study liver tissue.[40] By the end of the decade, PDMS was the material of choice for most microdevices used to study cell culture and simulate biological environments, enabling the study of organs such as the lung (Figure 1; 2007)[28] or the intestine.[41]

The integration of porous membranes into microfluidic devices further enhanced their ability to reproduce biomimetic environments by facilitating compartmentalized co-cultures and selective molecular transport. However, the dynamic simulation of physiological conditions arises primarily from microfluidic

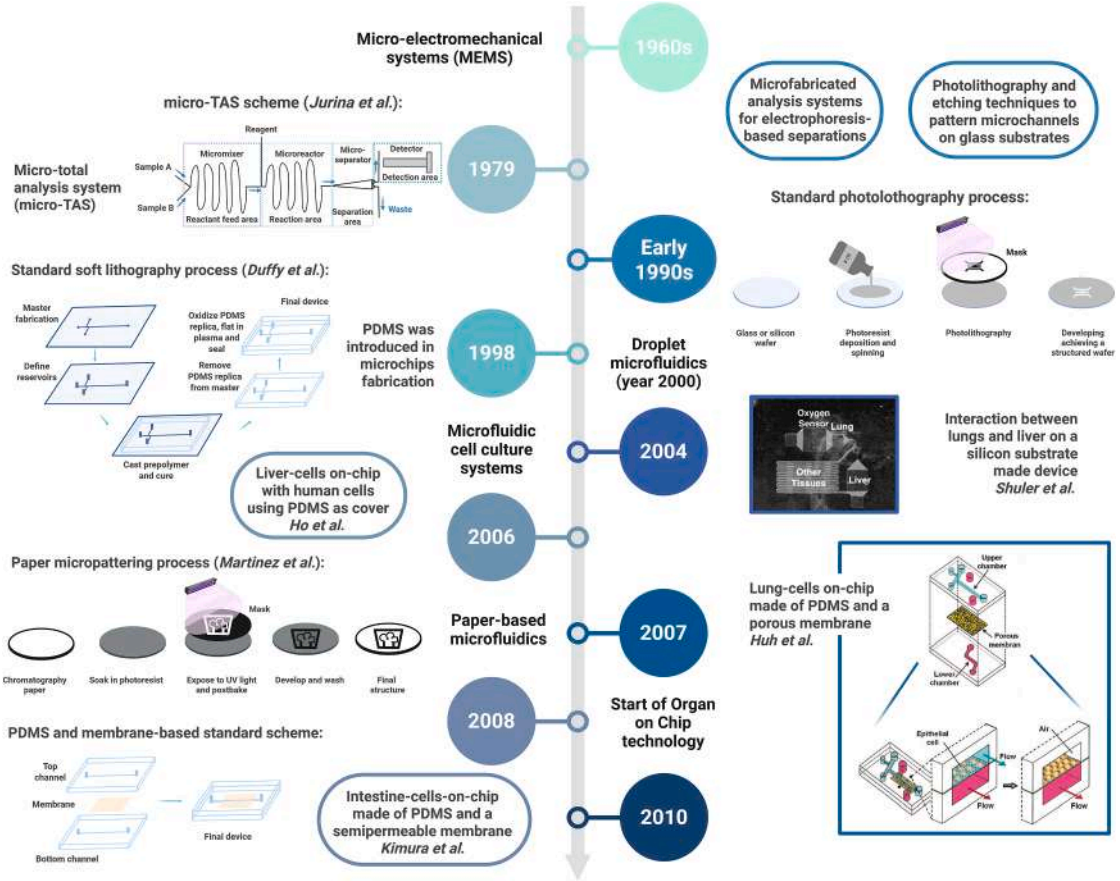


**Figure 1. Historical development of fabrication techniques, new devices, and materials**

The micro-TAS development in 1979, scheme adapted from Jurina et al.[24] under the terms and conditions of the CC BY 4.0 license (https://creativecommons.org/licenses/by/4.0/). PDMS introduction in 1998; soft lithography process adapted with permission from Duffy et al.,[25] copyright 1998 American Chemical Society. Interaction between lungs and liver on a silicon substrate reprinted with permission from Sin et al.,[26] Wiley. Paper-based microfluidics in 2007, paper micropatterning process in Whitesides' laboratory adapted with permission from Martinez et al.,[27] Wiley. Same year, a lung-cells on-chip of PDMS and porous membrane creation, image reprinted from Huh et al.,[28] copyright (2007) National Academy of Sciences.

perfusion, which enables controlled flow and nutrient exchange. This conceptual origin of membrane-based culture systems dates back to the1960s with the introduction of the Transwell, which consists of a porous membrane insert or filter that separates the culture dish into two media-filled compartments.[42] These conventional platforms, however, provide a static environment with limited physiological relevance. The subsequent incorporation of membranes into microfluidic architectures allowed the establishment of continuous perfusion systems that more closely mimic *in vivo* conditions for cell culture. At this juncture, Whitesides introduced paper as a material for constructing microfluidic devices (Figure 1; 2007),[27,43,44] thus inaugurating the field of point-of-care (POC) diagnostics.[45–48] POC devices, typically compact and easy to use, allow healthcare providers, and even patients, to perform diagnostic tests and obtain rapid results directly at the site of care, without relying on centralized laboratories.

Following these initial steps, OOC technology truly began to be developed around 2010. By definition, an organ-on-chip is a microfluidic device that integrates 3D cell cultures to replicate specific physiological functions of an organ or tissue, providing a more accurate model for studying biological processes and disease mechanisms.[2,49] The future goal is to create integrated body-on-chip systems that can simulate multi-organ interactions, potentially reducing the need for animal testing in specific research areas.

In 2010, Huh et al.[10] developed a lung-on-chip that reconstructed the critical functional alveolar-capillary interface of human lungs (Figure 2, 2010). In the same year, Domansky et al.[57] developed a multiwell-dish-based platform, which could also be called liver-on-chip, in which tissue units were perfused with cell culture medium circulating in the dish by means of integrated pneumatic membrane micropumps.

The following year, when the Defense Advanced Research Projects Agency (DARPA) provided funding for OOC research, Nakao et al.[50] developed a liver-on-chip and Jang et al.[58] a kidney-on-chip, both using photolithography and soft lithography techniques. In 2012, vessels-on-chip were achieved creating a microstructured silicone stamp as a master on which collagen with cells were injected creating the *in vitro* vessels.[59,60] At the

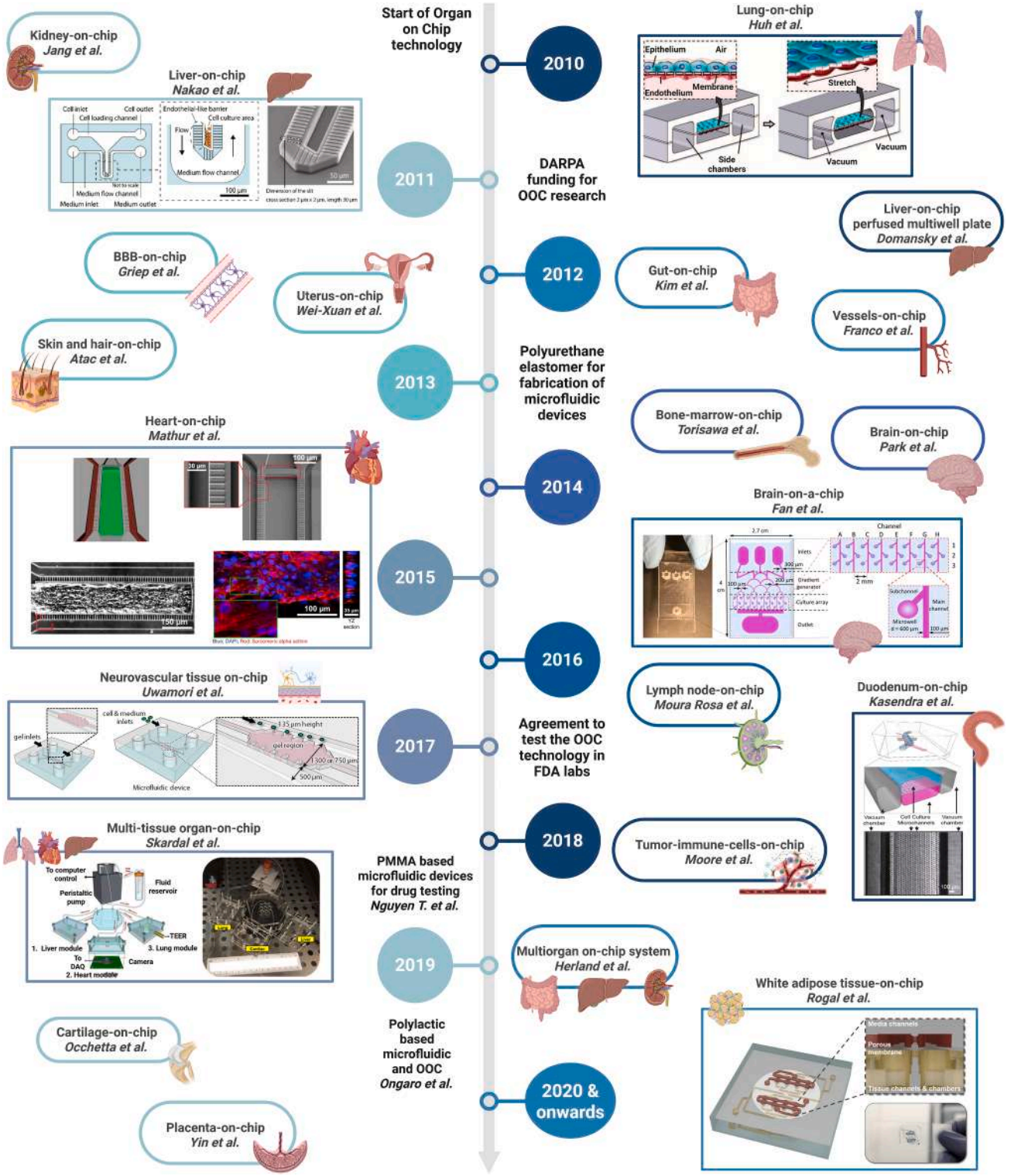


**Figure 2. Evolution of OOC technology**

Temporal line indicates various organs developed within microfluidic devices, thereby demonstrating the evolution of OOCs over the past two decades. From top to bottom part, list of adapted figures: lung-on-chip reproduced with permission from Huh et al.,[10] AAAS. Liver-on-chip reproduced with permission from

*(legend continued on next page)*

same time, a gut-on-chip model was developed[61] adapting a soft lithography technique that was used to create the lung-on-chip device by the same authors.[10] A uterus-on-chip was created by using PDMS top (zigzag-shaped channel) and bottom (four parallel rectangular channels) compartments separated by a polycarbonate (PC) porous membrane.[62] In 2013, a blood-brain-barrier-on-chip was performed following the same structure: two PDMS layers with specific designs and a PC porous membrane separating compartments.[63] Concurrently, the initial multi-organ-on-chip model for skin and hair culture was engineered, employing a PDMS-based platform integrated with a micropump.[64] A bone-marrow-on-chip was developed in 2014, emerging from a PDMS structure that incorporated a central cylindrical cavity. This cavity was designed to house bone-inducing materials for future bone formation.[65]

Through soft lithography, a brain-on-chip was fabricated in 2015, consisting of a PDMS-based device with cellulose membrane windows enabling an osmotic micropump.[66] The same year, a new heart-on-chip was developed[51]—knowing that in 2013[67] a heart system was made initiating this area of study—made of PDMS containing a central chamber where cells were seeded and two lateral channels for nutrients (Figure 2, 2015). Next year was marked by the development of a one-step UV lithography-based technique using a photo-polymerizable polyethylene glycol diacrylate (PEGDA) hydrogel, creating a brain-on-chip (Figure 2; 2016),[52] as well as a lymph-node-on-chip[68] based on soft lithography.

In 2017, the FDA initiated its first collaborative agreement to evaluate OOC technology, illustrating its early commitment to advancing and validating these human-relevant testing platforms.[69] That same year, Skardal et al.[54] developed a multi-organ-on-chip consisting of three platforms connected by a fourth one, which was also linked to a peristaltic pump (Figure 2, 2017). In parallel, a neurovascular-tissue-on-chip was developed the same year, a PDMS platform where neurogenesis and angiogenesis models were combined.[53]

Fabricated from cyclic olefin copolymer (COC), a transparent thermoplastic characterized by its low permeability, a tumor immune-on-chip comprising 12 parallel channels was introduced in 2018.[70] In the same year, a duodenum-on-chip[55] was also developed (Figure 2; 2018), which had the same structure as the lung-on-chip and the gut-on-chip of previous years.[10,61] It comprised a PDMS device consisting of an upper and lower channel separated by a porous membrane and two lateral vacuum chambers.

In 2019, a device based on polymethyl methacrylate (PMMA) was developed for drug testing purposes.[71] It consisted of a transparent, biocompatible, and rigid material that could be modified by laser cutting, and its parts may be unified by chemical bonding. That year, a cartilage-on-chip was developed.[72] This device consisted of a PDMS structure with two chambers, separated by a PDMS membrane. Additionally, a PDMS placenta-on-chip was developed to investigate nanoparticle exposure at the placental barrier.[73] In 2020, a white adipose-tissue-on-chip was developed to maintain, monitor, and manipulate human adipocytes.[56] This was a PDMS-based device (Figure 2; 2020 and onwards). Same year, the multiorgan-on-chip developed by Herland et al.[74] had the channels vascularized, thus demonstrating a continued evolution in similarity to the *in vivo* system. In this instance, gut-on-chip, liver-on-chip, and kidney-on-chip were attached, with all three components connected to a reservoir of fresh blood substitute medium. In 2021, a mucus-on-chip was developed using soft lithography. It facilitated the transportation of nanoparticles through mucus.[75] Over the past few years, significant improvements have been made in the manufacturing and materials used in OOC, as will be discussed in the next sections.

## FABRICATION TECHNIQUES FOR ORGAN-ON-CHIP DEVICES

As OOC technology evolves, the fabrication techniques for such devices also go forward, as might be expected. This section analyses traditional OOC manufacturing techniques and their variants.

Fabrication techniques can be divided into four main categories, each offering different advantages depending on the application's specific requirements. Such techniques include photolithography-based methods for high-precision patterning and creating master molds, as well as replication techniques like soft lithography, hot embossing, and microinjection molding, which rely on molds to reproduce patterns. In addition, xurography offers a simple and cost-effective approach for cutting and shaping materials, while 3D printing enables the fabrication of complex and customizable microfluidic devices (Table 1).

### Photolithography

Photolithography, which uses UV radiation in the wavelength range of 360–410 nm, is the most widely used form of lithography. The use of this technique to produce DNA arrays was one of the first examples to attract widespread attention.[106–109] Photolithography-based techniques are characterized by the use of light to define the desired pattern on a photosensitive material, which can be used either as a structural material or to transfer the pattern to another structural material. The photolithographic process used to obtain microfluidic devices is based on the deposition of the resin onto a wafer using a spin-coating process to obtain a succession of very thin layers of controlled thickness (Figure 3A). In a subsequent step, the wafers are exposed to UV light with the mask containing the desired pattern interposed between light source and substrate. Lastly, resin developer is used to eliminate the residual resin, thus obtaining the devices to be used as masters for soft lithography.[110] The most commonly used material is SU-8, a negative photoresist that allows devices to be fabricated on substrates such as glass or silicon, or to be fabricated entirely in SU-8.[111] This photoresist

**Table 1. Comparative analysis of traditional microfabrication methods for OOC devices**

| Method | Feature size (resolution) | Scalability/ Commercial readiness | Material compatibility | Strengths | Limitations | Relevance for OOC |
|---|---|---|---|---|---|---|
| Photolithography | ~1–5 μm | low/mainly academic, prototype mold fabrication | silicon, glass, SU-8 photoresist, PDMS replicas | high precision, sub-micron accuracy, established protocols | expensive, requires cleanroom, limited scalability | prototype molds, academic devices[76,77] |
| Replication—soft lithography | ~10 μm | low/widely used in research, limited industrial scalability | PDMS | rapid prototyping, optical transparency | small-molecule absorption, poor scalability | widely used for OOCs[78–84] |
| Replication—hot embossing | ~1–100 μm (depending on mold) | medium/suitable for pilot production and thermoplastic OOCs | thermoplastics | high-fidelity replication, reproducibility | long cycle times, thermal stresses, limited for multilayer | suitable for thermoplastic OOCs[85,86] |
| Replication—microinjection molding | ~1 μm | high (industrial)/ dominant for commercial disposable chips | thermoplastics | mass production, reproducibility, scalable manufacturing, cost-efficient at scale | high tooling cost, material restrictions | disposable or high-throughput OOCs[87–91] |
| Xurography | ~100–300 μm | low-medium/ inexpensive, mostly academic prototyping | adhesive tapes, thin polymer sheets | inexpensive, equipment-light | low resolution, poor reproducibility, limited durability | quick prototyping, used for OOCs[92–94] |
| 3D printing—Light-polymerized | ~10–50 μm (depending on printer) | low/research-level use | photopolymers, resins | complex 3D geometries, no molds needed | surface roughness, cytotoxic resins, optical limitations | exploratory OOCs[95–99] |
| 3D printing—Inkjet | ~20–50 μm droplets | low/research-level use | photopolymers, hydrogels, bioinks | multi-material deposition, patterned biomolecules | limited resolution, nozzle clogging | droplet generation, 3D culture OOC platforms[100,101] |
| 3D printing—microextrusion | ~50–200 μm filaments | low-medium/ expanding for tissue bioprinting, not yet industrial | hydrogels, thermoplastics, bioinks | bioprinting of cell-laden hydrogels | low resolution, shear stress on cells | rigid and flexible OOCs[102–105] |

exhibits stable mechanical, thermal, and chemical properties, can be coated to thicknesses greater than 1 mm, and can be patterned to produce high aspect ratio microstructures, unparalleled in conventional photoresists.[112,113]

Concerning the manufacturing techniques employed throughout the development of OOC chip technology, photolithography is the most widely utilized. In fact, most of the devices presented in the previously outlined timeline follow this fabrication approach, often in combination with soft lithography,[10,50,53,55,58] the latter being a replication-based method that will be discussed in the following section. In recent years, OOC devices have been fabricated solely using photolithography to replicate biological processes such as neural necrosis and glioblastoma multiforme pseudopalisading.[76,77] Both devices originate from the fabrication technique developed by Blanco et al., which is based on photopatterning thick SU-8 layers on substrates followed by low-temperature adhesive bonding of two fully crosslinked SU-8 structures.[114] In the first case, Figure 3B, the fabrication process consists of spin-coating and photopatterning a single SU-8 layer directly onto a glass substrate to define the microstructures, including channels and micropillar arrays. The device is enclosed using a mechanical clamping system or a coverslip, without any bonding between SU-8 layers (Figure 3Bi). By contrast, Ayuso et al. follow the full multilayer bonding protocol described by Blanco et al., including photopatterning SU-8 layers on separate substrates and performing low-temperature bonding under pressure to form sealed microchannels that are showed in Figure 3Ci. Therefore, although both methods derive from the same core principles of SU-8-based photolithography, they diverge in complexity and execution, with Ayuso et al. adopting the full bonding strategy introduced by Blanco et al. and Esteve et al. employing a monolithic, single-layer approach.

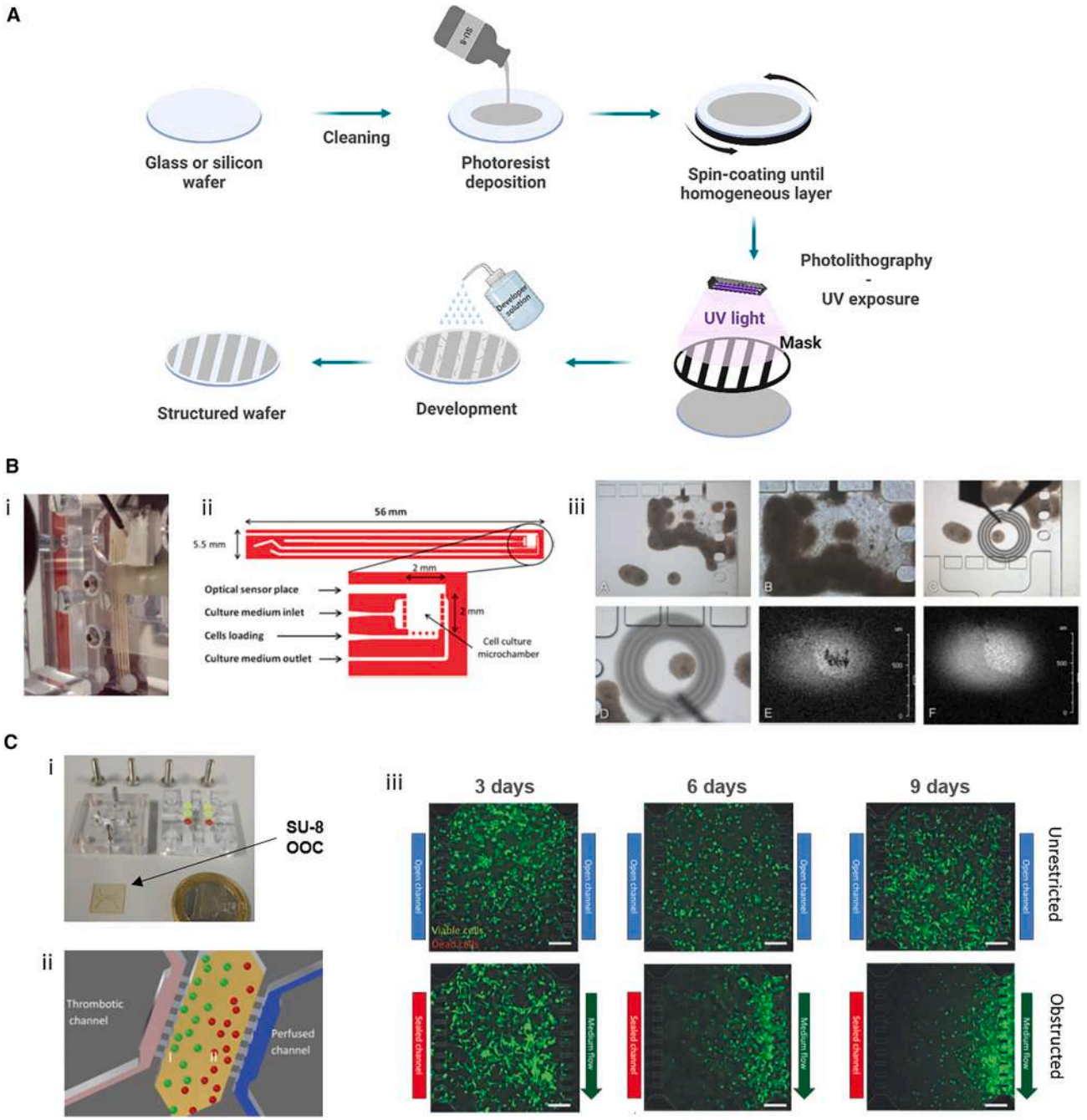


**Figure 3. Photolithography microfabrication technique and OOC models recreated in photolithography-based devices**

(A) Photolithography process.

(B) Neural necrosis OOC. (Bi) Device placed on the monitoring base. (Bii) Top-down view of the microfluidic chip layout highlighting the main structural features and dimensions. (Biii) Representative images of neurospheres cultured within the device. (A) Several neurospheres merged and expanded near the corner at the entrance of the cell-guidance channel. (B) Differentiated cells extend outward from the aggregated mass, forming a three-dimensional outgrowth.

(C and D) Optical micrographs of a neurosphere positioned in the microchamber with the microcoil superimposed; image (D) corresponds to an inverted orientation of (C) to facilitate comparison with subsequent data.

(E and F) NMR microimages obtained at two cross-sections separated by 180 μm; only the region encompassed by the microcoil is visualized. In (E), a central area consistent with necrosis is apparent, whereas it is absent in the more superficial slice in (F). The in-plane resolution is 8 × 8 μm with a slice thickness of 50 μm. Reprinted from Esteve et al.,[76] with the permission of AIP Publishing. (C) Glioblastoma-on-chip model. (Ci) Fabricated microdevice and packaging tool. (Cii) Diagram of the microdevice showing obstructed conditions with nutrient-poor (I) and nutrient-rich (II) regions. (Ciii) Pseudopalisade formation under free and obstructed flow. U-251 cells ($4\times10^6$ mL$^{-1}$) in collagen hydrogel (1.5 mg mL$^{-1}$) were cultured in the device. Viability over time was assessed with calcein (green) and propidium iodide (red). Device posts (50 × 100 μm) are marked with white dashed lines. Reproduced with permission from Ayuso et al.[77] Neuro-Oncology, 2017.

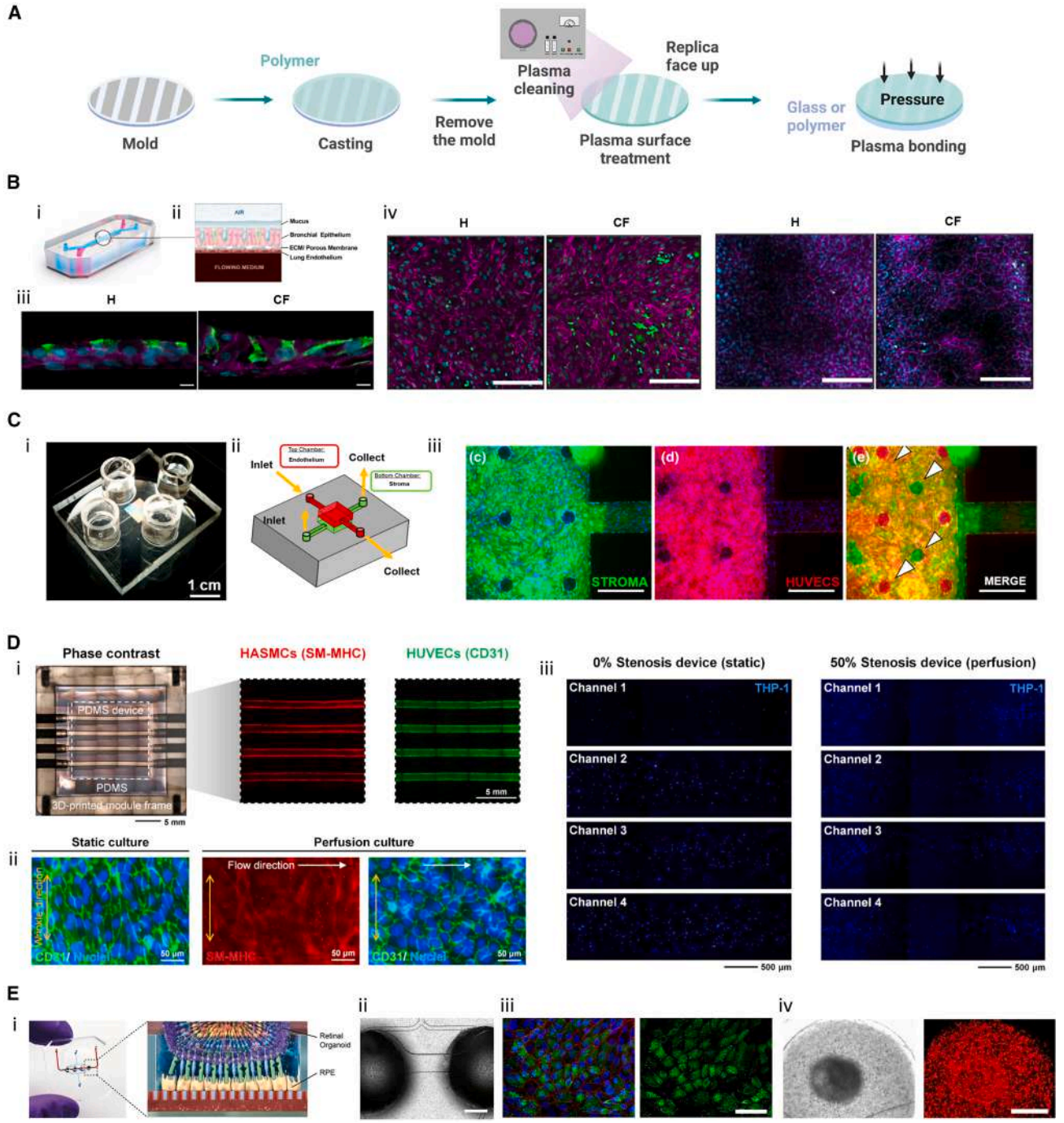


**Figure 4. Soft lithography technique and examples of its application to obtain OOC models**

(A) Soft lithography technique step by step.

(B) Lung-on-chip model. (Bi) Chip-S1 stretchable chip from emulate.[121] (Bii) Schematic of the airway chip with bronchial epithelium cultured at an air-liquid interface above a porous membrane and human lung endothelial cells below under fluid flow. (Biii) Confocal sections of healthy (H) and cystic fibrosis (CF) chips showing ciliated (β-tubulin IV, green), basal (CK5, magenta), goblet (MUC5AC, green), and club cells (CC-10, green). Scale bars, 10 μm. (Biv) Baseline inflammatory phenotype, with PMNs (green) adhering to CD31$^+$ endothelium (magenta). Reprinted from Plebani et al.,[78] Journal of Cystic Fibrosis, 2022.

(C) Endometrium-on-chip. (Ci) Photograph of the assembled PDMS device with four inlet/outlet reservoirs; the porous membrane appears translucent. (Cii) Schematic of the perivascular stroma model. (Ciii) Stroma compartment showing a confluent cell layer (c) and endothelial compartment with CD31$^+$ HUVECs (d). (e) Merged channels (DAPI, FITC, and CY5) reveal the identity of each cell layer within the compartments. Circular pillars (arrows) allow visualization of individual cell types (DAPI nuclei, blue). Scale bars, 400 μm.

*(legend continued on next page)*

While this technique represents a significant advancement in micro- and nano-scale systems, it has inherent limitations when applied to biological and biotechnological systems. Such limitations include restricted control over surface properties, high cost of substrates (mainly silicon and glass) and cleanrooms, limited accessibility to some biological researchers, and the lengthy and costly process from initial conception to final production. Moreover, examples such as the neurosphere culture chip by Esteve et al. highlight specific constraints of some photolithography-based platforms: the use of rigid, inert microstructures like micropillars, as shown in Figures 3Bii and 3Biii, hinders the dynamic interaction between compartments. This prevents the spatial organization of multiple cell types or physiological gradients, reducing the model's relevance for complex organotypic scenarios. Similarly, the glioblastoma-on-chip model developed by Ayuso et al., which successfully recreates pseudopalisade formation under hypoxic conditions, is limited by its pillar-based architecture (Figures 3Cii and 3Ciii). This restricts cells from behaving as they naturally would, since inert barriers separate tissues.

In light of these examples, it is evident that while photolithography enabled the first generation of OOC devices, its present use has shifted considerably. Rather than serving as the primary method for fabricating complete microfluidic platforms, photolithography today is employed predominantly for the production of SU-8 replica molds (as mentioned in the section before and will be explained in next section) and for the microfabrication of ultrathin membranes or integrated components that are subsequently incorporated into hybrid devices.[115–117] This evolution reflects both the strengths of the technique—precision, reproducibility, and compatibility with semiconductor processes—and its limitations in terms of cost, accessibility, and the rigidity of silicon and glass substrates. As a result, photolithography now occupies a complementary role, supplying high-fidelity features that support soft-lithography or thermoplastic-based platforms, rather than defining the entire chip architecture.

## Replication

Replication-based techniques rely on the use of a mold, which is employed to transfer the desired pattern onto a softer material through direct physical contact. These approaches can be further classified into three main categories: soft lithography, hot embossing, and injection molding.

### *Soft lithography*

Soft lithography provides tools for micro-patterning that complement and extend conventional fabrication methods.[36] Two of the key features of soft lithography are the use of elastomeric materials to produce pattern transfer elements through molding and the development of techniques to create complex biochemical patterns.[118–120]

The fabrication process begins with the preparation of a mixture comprising a base elastomer and a curing agent. This mixture is poured into a mold that defines the desired microfluidic circuit. Once the material solidifies, it forms a polymer that can be sealed by bonding to a substrate, such as glass or another polymer film (Figure 4A). Typically, such devices are made of PDMS, a silicone-based polymer widely employed in microfluidic fabrication due to its versatility and compatibility with soft lithography. Its isotropic and homogeneous properties, lower cost compared to silicon, and ability to replicate submicron features for microstructure development further enhance its appeal.[11,122]

As previously mentioned, soft lithography using PDMS was the foundational technique that enabled the development of OOC systems. This approach was pioneered by Ingber and colleagues at the Wyss Institute. They developed a series of organ models built upon a standardized PDMS-based platform (presented in the timeline of Figure 2), consisting of two parallel microchannels vertically stacked separated by a porous, flexible membrane (Figure 4Bi). Several OOC devices have been derived from this design. One of the most extensively studied is the lung-on-chip. In the model described by Plebani et al.,[78] the microfluidic device recreates a human airway by culturing a pseudostratified bronchial epithelium under air-liquid interface (ALI) conditions on the upper surface of the porous membrane, while the lower vascular channel is lined with human lung microvascular endothelial cells (PMVECs) exposed to dynamic fluid flow (Figure 4Bii). This configuration allows for the recreation of key features of airway physiology and pathology. The authors engineered both healthy and cystic fibrosis (CF) airway models and analyzed their structural and functional characteristics. Confocal immunofluorescence imaging revealed distinct cellular compositions, including ciliated, goblet, basal, and club cells, with disease-specific alterations in the CF model (Figure 4Biii). Furthermore, differences in inflammatory phenotypes were observed at baseline, with increased neutrophil adhesion to the endothelium in the CF model compared to the healthy counterpart (Figure 4Biv). This airway chip platform has also been employed in other studies to investigate pulmonary edema,[10] asthma-like inflammation,[123] and viral infections such as influenza and SARS-CoV-2,[124] among others, highlighting its versatility in modeling human respiratory pathophysiology.

This widely used OOC platform has been extended to models of other human organs. The duodenum intestine-on-chip system, incorporating cyclic strain and fluid flow, promotes villus-like architecture, enables co-culture with commensal microbiota, and preserves epithelial barrier function, offering key

Adapted from Gnecco et al.,[79] under CC BY 4.0 license (https://creativecommons.org/licenses/by/4.0/).

(D) Vessel-on-chip model. (Di) Phase-contrast and immunofluorescence images of HASMCs and the HUVEC layer in a perfused multichannel coculture module. (Dii) Expression of smooth muscle myosin heavy chain (SM-MHC) and CD31 under static and perfusion conditions. (Diii) Adhesion of THP-1 monocytic cells in the inflammation model: left, recruitment in a nonstenotic device under static culture; right, recruitment in a 50% stenosed device under perfusion. Adapted from Cho and Park,[80] under CC BY 4.0 license.

(E) Retina-on-chip (ROC) model. (Ei) Photograph of the ROC (left) and schematic of photoreceptor-RPE interactions (right). (Eii) RPE cells seeded within the device. Scale bars, 500 μm. (Eiii) Marker expression and polarization of RPE cells: gp100 (green) and ZO-1 (red). (Eiv) ROC as a pharmacological testing platform, showing brightfield and fluorescence images after 6-day treatment with 0.5 mg/mL gentamicin. Adapted from Achberger et al.,[81] under CC BY 4.0 license.

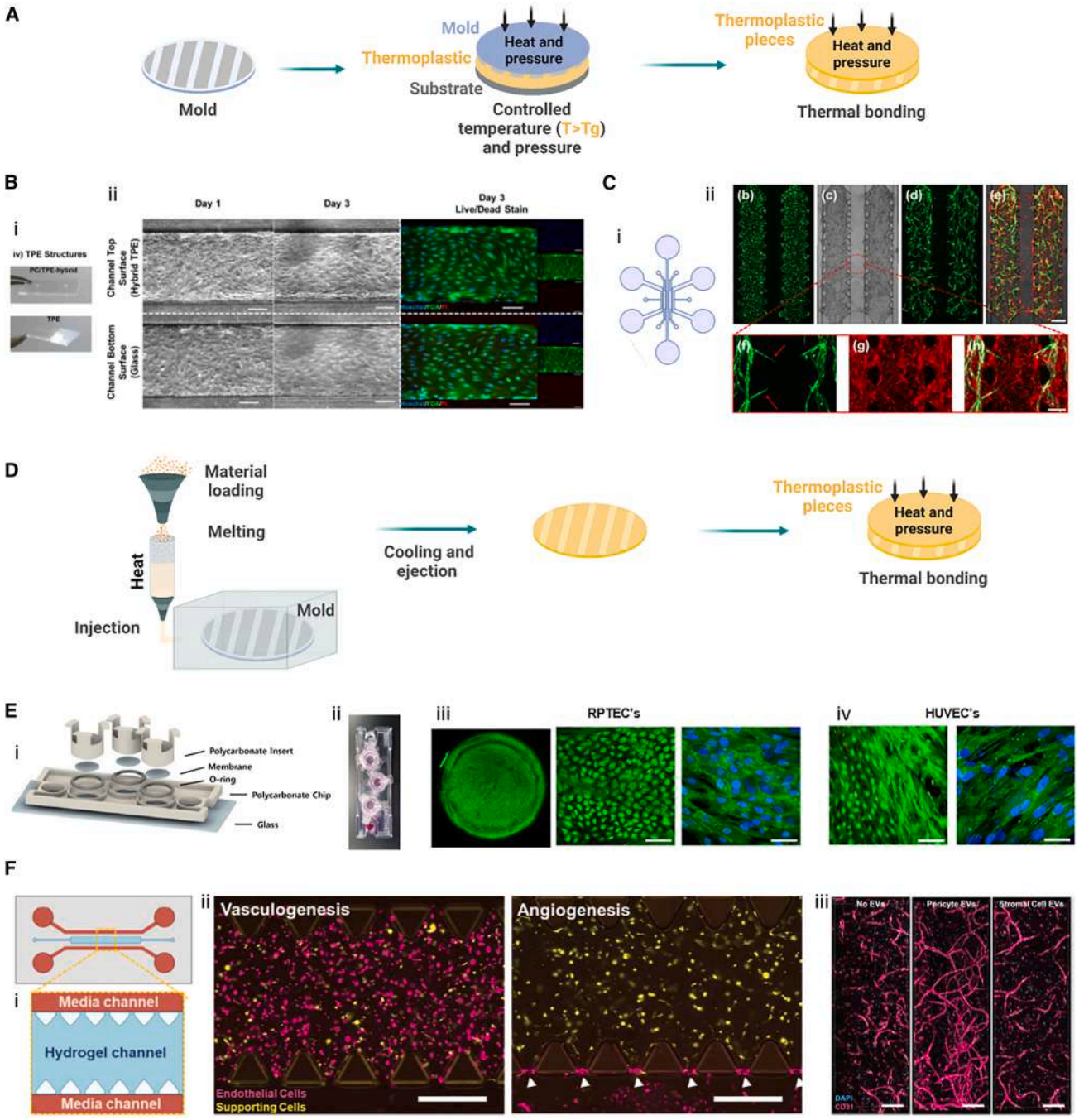


**Figure 5. Hot embossing and microinjection molding techniques and examples of OOCs made by these methods**

(A) Hot embossing basic steps.

(B) Hot embossed device for OOC applications. (Bi) TPE and PC/TPE-hybrid microfluidic platforms. (Bii) Phase-contrast micrographs showing cell adhesion and growth from day 1 to day 3 on both substrates (left) and live/dead staining by fluorescence microscopy on day 3 (composite image left; individual color channels right). Scale bars, 100 μm. $n = 3$. Adapted from Schneider et al.,[85] under CC BY 4.0 license (https://creativecommons.org/licenses/by/4.0/).

(C) Microvessels-on-chip. (Ci) Design of the multi-vessel loading chamber. (Cii) Visualization of GFP-HUVECs after seeding. (C–E) Bright-field (C), GFP fluorescence (D), and merged bright-field/GFP/RFP channels (E) on day 8. (F–H) Individual GFP (F), RFP (G), and merged (H) images showing angiogenic sprouting from pre-existing vessels, indicated by red arrows in (F). Cells were cultured an additional 4 days under hydrostatic flow induced by rocker motion every 10 min. Scale bars, 500 μm (E), 200 μm (H). Adapted from Moon et al.,[86] RSC, under CC BY 3.0 (https://creativecommons.org/licenses/by/3.0/).

(D) Microinjection molding fabrication method step by step.

(E) Tubule-on-chip. (Ei) Injection-molded chip with insert module installed. (Eii) Actual photograph of injection-molded chip and insert. (Eiii) RPTEC's L&D images (4× and 20×) and immunofluorescence images (40×) were observed in I-M Chip with 3 μm pore size using a confocal microscope, live-dead cell image

*(legend continued on next page)*

advantages over static cultures and organoids.[55] Colon-on-chip models have applied similar principles to investigate disease-specific mechanisms such as barrier dysfunction and cytokine responses in inflammatory bowel disease.[82] The liver-on-chip supports drug metabolism and hepatotoxicity studies and has shown high sensitivity and specificity in detecting compounds associated with drug-induced liver injury.[83] Brain-on-chip systems incorporating neurovascular units under dynamic flow have been used to study blood-brain barrier integrity and neuroinflammation,[84] and more models were reproduced in this device. These organ-specific PDMS-based platforms implement physiological mechanical cues—such as cyclic strain in intestinal models and shear flow in hepatic, renal, vascular, and lymphoid systems—demonstrating the adaptability, mechanobiological fidelity, and translational relevance of the emulate system architecture.

Other models with distinct microfluidic designs have also been developed to address specific organ functions. For example, Gnecco et al. designed a uterus-on-chip platform that recapitulates key features of the female reproductive tract by mimicking hormonal cycling and endometrial remodeling *in vitro* (Figure 4Ci).[79] This device integrates endometrial epithelial and stromal cells within a microfluidic chamber and applies sequential hormone perfusion to simulate the estrous cycle (Figure 4Cii). The system successfully reproduced physiological responses such as decidualization and cyclic gene expression patterns, offering a dynamic and controllable alternative to static 2D cultures or explants (Figure 4Ciii). Importantly, this model provides a valuable platform for investigating hormone-regulated processes, implantation mechanisms, and female reproductive disorders under near-physiological conditions.

In a different approach, Cho and Park developed a vessel-on-chip designed to replicate key aspects of human vascular physiology and pathology (Figure 4Di).[80] The device consists of a modular, multichannel 3D platform featuring circular microchannels lined with human endothelial and smooth muscle cells, enabling coculture under physiologically relevant conditions (Figure 4Dii). Through tunable geometries and flow conditions, the system can reproduce vascular stenosis and inflammation, including shear stress-induced endothelial responses and tumor necrosis factor alpha (TNF-α)-mediated immune cell recruitment (Figure 4Diii). This platform not only allows for high-throughput studies across multiple conditions but also offers a valuable tool for investigating early events in vascular disease.

Finally, another organ model successfully developed using this technique is the eye-on-chip system reported by Achberger et al. (Figure 4Ei).[81] This device replicates key anatomical and functional features of the human ocular surface, including the corneal epithelium, tear film dynamics, and blinking-like mechanical stimulation (Figure 4Eii). The platform integrates human corneal epithelial cells cultured within a microfluidic chamber and uses a programmable eyelid-like mechanism to reproduce shear forces generated during blinking (Figure 4Eiii). This dynamic model enabled the investigation of tear film stability, mucin secretion, and epithelial barrier function under physiological and pathological conditions, offering a powerful tool for studying dry eye disease, ocular drug delivery (Figure 4Eiv), and surface disorders that cannot be accurately recapitulated in static culture systems.

Despite its many advantages, soft lithography is not without limitations. A primary drawback lies in its reliance on elastomeric materials, which restricts applicability to certain device types and complicates scale-up for large-scale production.[125] Almost all PDMS-based OOC platforms discussed above retain a separating membrane between compartments, preventing direct tissue-tissue contact and limiting intercellular cross-talk (e.g., Figures 4B and 4C, and 4E). Moreover, PDMS's high gas permeability, typically an asset, becomes problematic when modeling hypoxic or anaerobic conditions—such as necrosis or the oxygen-sensitive environments required in certain intestinal inflammation models—rendering it unsuitable for such applications. The material's hydrophobicity, coupled with its porosity, leads to the absorption of small hydrophobic molecules and leaching of uncured oligomers, interfering with drug dosing, analytical accuracy, and long-term culture integrity.[126,127] This limitation can be partially addressed by surface modification techniques, such as oxygen plasma treatment or coating with hydrophilic polymers, which improve surface wettability and reduce molecule absorption.[128–130] Additionally, multilayer "sandwich" fabrication using PDMS frequently encounters alignment challenges, particularly for laboratories without access to precision masking tools. Studies have demonstrated that material shrinkage in PDMS soft lithography often lead to layer misalignment, with errors reaching tens of microns, particularly when curing thick PDMS layers at elevated temperatures. Misalignment due to rotation and translation is typically observed unless one employs dedicated aligners or compensates for shrinkage, which requires specialized desktop aligners or layer-specific scaling during fabrication.[131,132]

### *Hot embossing*

In the case of "hot molding," the microfluidic circuit is obtained by molding a thermoplastic polymer with the desired microstructure under controlled conditions of heat and pressure. This process relies on heating the substrate above the polymer's glass transition temperature and applying pressure to imprint the desired microstructure using a mold.[133] Detailing the manufacturing process (Figure 5A), the substrate is initially heated above its glass transition temperature, and a predetermined force is applied to shape the material. Once the molding is complete, the temperature is reduced below the glass transition point

observation throughout the membrane. L&D scale bar is 100 μm. ZO-1 scale bar is 50 μm. (Eiv) Confocal microscope HUVEC's images (4×, 20×) and immunofluorescence images (40×) on I-M chip with 3 μm pore size. Adapted from Lee et al.,[87] under CC BY 4.0 license.

(F) Vascularized OOC. (Fi) Schematic of the microfluidic chip with central hydrogel channel (blue) flanked by parallel media channels (red). (Fii) Fluorescence images showing freshly seeded endothelial cells (Vybrant DiD, magenta) and supporting cells (Vybrant DiO, yellow; pericytes or stromal cells) in two setups for vasculogenesis (left) and angiogenesis (right). White arrows indicate the hydrogel-media interface. Scale bars, 500 μm. (Fiii) Confocal images of stromal-endothelial co-cultures treated with control media or fresh media supplemented with EVs from pericytes/stromal cells. Scale bars, 200 μm. Adapted from Gonzalez-Rubio,[88] under CC BY (https://creativecommons.org/licenses/by/).

to allow the material to solidify. During the final stage, the master is separated from the mold, a critical phase where improper handling can damage the replicated microstructure. Reducing this force and achieving a smooth separation between the mold and substrate is crucial for producing a high-quality microstructure.[134]

The stresses generated in components fabricated through hot embossing are considerably lower than those produced by alternative methods, due to the localized stretching of the polymer over a short distance from the bulk substrate. Furthermore, the narrower operating temperature range reduces shrinkage during cooling and minimizes frictional forces during de-embossing.[135] This technique is compatible with a range of thermoplastics and thermoplastic elastomers (TPEs), which combine elasticity with manufacturability, making them attractive alternatives to PDMS in OOC fabrication. Hot embossing allows reproducible replication of microscale features with improved scalability, lower absorption of small hydrophobic molecules, and the possibility of bonding to other polymer or glass layers—properties that are leveraged in the following OOC examples.

Schneider et al. developed a tailored hot embossing process for a polycarbonate/TPE hybrid material, combining the flexibility and bonding capacity of TPE with the rigidity and optical clarity of polycarbonate (Figure 5B).[85] Microstructures were first patterned in SU-8 on silicon wafers, then transferred via a PDMS negative to an epoxy master mold. The final hybrid chips were produced by pressing the epoxy mold into the TPE layer while simultaneously thermally fusing it to a polycarbonate backing (Figure 5Bi). This resulted in stiffer, easier-to-handle chips with precise channel geometries. The authors demonstrated the device's applicability to OOC models by seeding human umbilical vein endothelial cells (HUVECs) within the microchannels coated with collagen type I. After 3 days of culture under static conditions, the endothelial layer formed a confluent monolayer, confirming the material's biocompatibility and the system's suitability for creating vessel-on-chip platforms (Figure 5Bii).

Moon et al. employed a similar hot embossing approach to fabricate TPE microchannels, which were reversibly bonded to polystyrene (PS) substrates (Figure 5C).[86] This reversible assembly enabled the straightforward removal of the channel layer without damaging the cultured tissue—an advantage for downstream analysis or transplantation. Their OOC platform supported the co-culture of GFP-expressing HUVECs and RFP-labeled fibroblasts within a fibrin gel, leading to the self-assembly of interconnected 3D microvessel networks over 8 days. Quantitative analysis showed progressive increases in vessel coverage, junction number, and total length. Importantly, one of the presented configurations was designed to model angiogenesis, allowing the study of sprouting, branching, and network maturation within a controlled microenvironment (Figures 5Ci and 5Cii). After culture, the TPE slab could be removed and the intact vascular networks harvested for further analysis or potential therapeutic applications.

Despite its versatility, hot embossing presents some drawbacks. The method is inherently restricted to thermoplastic substrates, which may not always provide the optimal surface properties for certain biological applications without additional treatments. The process also requires elevated temperatures and pressures to achieve adequate pattern transfer, which can complicate fabrication when working with temperature-sensitive materials or integrated components.[133] Furthermore, the technique is less suited for producing nanoscale features, where high-precision lithographic approaches remain superior. The process involves sequential heating and cooling cycles for both the polymer and the mold, extending cycle times significantly longer than injection molding. Non-uniform temperature distribution across the mold can induce residual stresses or dimensional distortions, affecting pattern fidelity and device functionality.[136,137] These factors, coupled with the need for high-tolerance alignment in multi-layer designs, pose additional challenges for large-scale production.[138]

Certain application-specific limitations were also observed in the OOC examples described above. In the PC/TPE-hybrid device by Schneider et al., while the hybrid material exhibits lower small-molecule absorption than PDMS, it is not completely resistant to hydrophobic compound adsorption, which could affect the accuracy of drug assays conducted over extended periods. In the reversible TPE-PS platform by Moon et al., the microchannel geometry included micropillar arrays separating compartments. While these structures provide physical stability to the fibrin matrix and facilitate media perfusion, they also act as inert barriers that prevent full tissue-to-tissue contact across channels, potentially limiting the physiological relevance of inter-compartmental interactions.

### *Microinjection molding*

Injection molding is a manufacturing process in which a polymer is heated and injected into a mold cavity to obtain the desired pattern. Microinjection, a more precise version of this process, involves transferring thermoplastic material in granular form from a hopper into a heated barrel. Once the material becomes molten and pliable, it is injected under pressure into a mold cavity and held under pressure for a set duration to compensate for shrinkage. As the mold temperature is lowered below the polymer's glass transition temperature, the material solidifies. After sufficient time, it freezes into the shape of the mold and is ejected, allowing the cycle to repeat. Each cycle typically lasts from several seconds to a few minutes (Figure 5D).[139,140]

This process offers numerous advantages, making it commercially viable and promising for future advancements. These benefits include the potential for full automation with short cycle times, and cost-efficiency for mass production, particularly for disposable products. More importantly, unlike most conventional microfabrication techniques, microinjection molding inherently supports scale-up and process standardization, enabling the production of large numbers of highly reproducible chips under controlled industrial manufacturing conditions. Additionally, micro-injection molding ensures highly accurate shape replication, precise dimension control, and lower maintenance costs for capital equipment compared to methods like lithography. Furthermore, it benefits from the wealth of industrial expertise and knowledge derived from conventional injection molding processes.[141,142] Then, several OOC models were developed using it.[87–91]

One example is the tubule-on-chip developed by Lee et al., in which a two-layer microfluidic platform was fabricated via microinjection molding to enable the culture and perfusion of

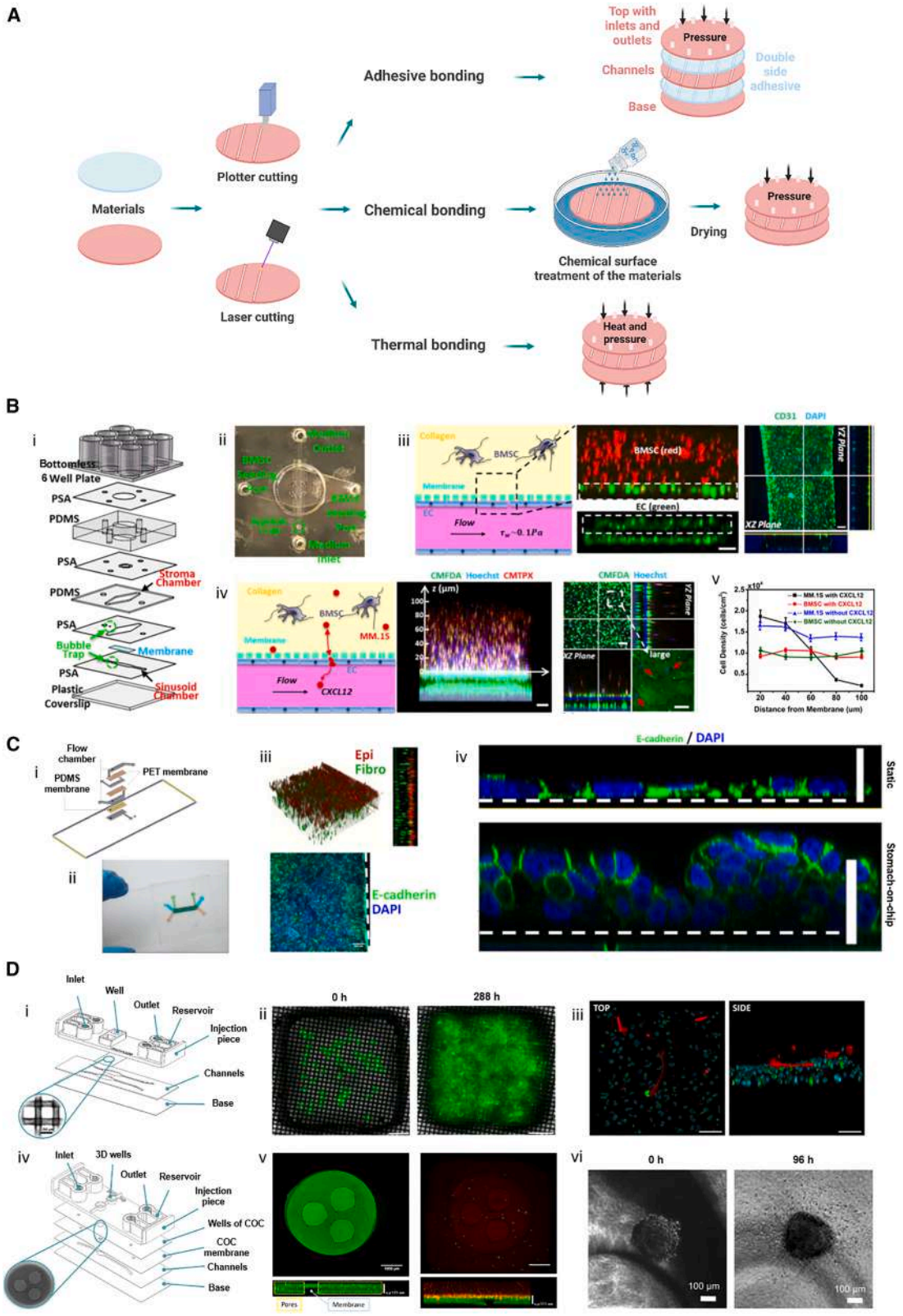


*(legend on next page)*

renal epithelial cells (Figure 5E).[87] The design incorporated parallel microchannels separated by a porous membrane, allowing selective filtration and directional flow to mimic kidney tubular physiology (Figures 5Ei and 5Eii). By culturing human kidney proximal tubule epithelial cells within the channel, the device successfully reproduced key tubular functions such as vectorial transport, barrier integrity, and biomarker secretion under physiologically relevant shear stress (Figures 5Eiii and 5Eiv). This approach provided a robust, high-throughput platform for modeling renal physiology and screening nephrotoxic compounds with enhanced reproducibility compared to soft-lithography-fabricated chips.

Another example is the vascularized OOC system developed by Gonzalez-Rubio et al., using a commercially available AIM Biotech three-channel microfluidic device produced via microinjection molding (Figure 5Fi).[88] In this model, the central hydrogel channel enabled the co-culture of endothelial cells with either adipose-derived CD146+ pericytes or unselected stromal cells to study vasculogenesis and angiogenesis in a controlled microenvironment (Figure 5Eii). The study demonstrated that pericytes promoted the formation of longer, more interconnected, and more branched microvascular networks than stromal cells, largely through an interleukin-6-dependent mechanism. Moreover, pericyte-derived conditioned media and extracellular vesicles were sufficient to enhance vessel formation in stromal cell co-cultures, confirming the paracrine contribution of pericytes (Figure 5Eiii). This work not only elucidated the distinct roles of pericytes in vascular network maturation and stability but also highlighted the value of microinjection-molded chips in generating reproducible, optically clear, and structurally precise platforms for advanced vascular biology research.

Despite its clear benefits for scale and reproducibility, microinjection molding presents certain drawbacks. First, capital expenditure is high: precision presses and temperature-controlled tooling are costly, and making or iterating steel or nickel molds carries long lead times and significant expense. Second, material choice is constrained to thermoplastics that are both biocompatible and processable under high shear and temperature; many research-grade polymers and surface-engineered substrates are therefore excluded.[143] Third, faithful replication of high-aspect-ratio or sub-micrometric features can be limited by melt viscosity, gate design, and demolding forces, which also necessitate draft angles that may slightly alter channel cross-sections.[144] Fourth, residual stresses, shrinkage, weld lines, and gate vestiges can distort microchannels, degrade optical performance, or compromise bonding.[145] Finally, enclosure of channels typically requires thermal or solvent bonding, which can deform shallow features, limit solvent compatibility downstream, and introduce variability relative to monolithic processes.[146,147] Moreover, some application-specific limitations have been reported: for instance, in the injection-molded tubule-on-chip, the separable insert design and use of rigid polycarbonate facilitated mass production but imposed fixed membrane geometries and bonding constraints that could limit adaptation to other organ models or more complex 3D architectures. Similarly, in the vascularized model by Gonzalez-Rubio et al., the commercial AIM Biotech chip allowed reproducible vasculogenesis assays, yet its predefined channel and gel compartment dimensions, coupled with challenges in extracting intact hydrogels for downstream high-resolution analyses, restricted flexibility for alternative tissue layouts or post-culture structural characterization.

## Xurography

Xurography-based techniques involve bonding layers of adhesives, polymers, or glass together under pressure to create the device. The process involves cutting each layer separately and then aligning and bonding the layers to form the complete device (Figure 6). This method employs rapid and cost-effective microfabrication using a cutting plotter—an automated device equipped with a precision knife blade capable of directly patterning microstructures in polymer films. The resolution of cutting plotters can reach approximately 10 μm, enabling the fabrication of microfeatures without resorting to photolithography or chemical etching processes. Positive and negative features, primarily microchannels, are typically patterned in films ranging from 25 to 1,000 μm in thickness. These structures can be organized into single-layer or multilayer 3D configurations for applications including microfluidic networks, micromolds, shadow masks, sensors, and electroplated elements. Previous studies have proposed models to estimate the minimum feature size achievable based on material properties and cutting conditions.[148,149] In addition to mechanical cutting, laser micromachining is

**Figure 6. Xurography fabrication technique possibilities and its application to fabricate and create OOC models**

(A) Scheme of the fabrication method and its options: different material pattern definitions: plotter and laser cutting and multiple bonding methods: adhesive, chemical, and thermal.

(B) Microfluidic culture device fabricated using adhesive bonding designed to mimic the trafficking of cancer cells through the sinusoidal niche of bone marrow. (Bi) Schematic of the layer-by-layer assembly of the microfluidic device. (Bii) Photograph of the device prior to assembly onto a bottomless 96-well plate. (Biii) ECs (green, CMFDA) and BMSCs (red, CMTPX) cultured in sinusoid and stroma chambers; confocal images show cross-sections after 12 h and ECs (CD31, green; DAPI, blue) after 24 days (Biv) CXCL12-induced migration of MM.1S cells from stroma to sinusoid chamber: confocal cross-sections and z-projection images (ECs green, BMSCs red, MM.1S blue). Scale bars, 20–200 μm. (Bv) Quantification of Hoechst-stained MM.1S cells in six z-locations ($n = 6$). Adapted from Sui et al.,[92] under CC BY 4.0 license (https://creativecommons.org/licenses/by/4.0/).

(C) Stomach-on-chip fabricated using chemical bonding. (Ci) Exploded view showing fluidic and microactuator structures. (Cii) Final device. (Ciii) 3D projection of epithelial barrier (red) over fibroblasts in collagen I matrix (green); lower panel shows tightly knit epithelium. Scale bar: 200 μm. (Civ) Comparison of static vs. SOC conditions after 6 days: MKN74 cells in Transwell display flattened morphology (top, 20 μm); SOC epithelium forms globular, polarized structures with basolateral E-cadherin (bottom, 50 μm). Adapted from Ferreira et al.,[93] RSC, under CC BY 3.0 (https://creativecommons.org/licenses/by/3.0/).

(D) Microfluidic devices fabricated for epithelium generation and GBM invasion fabricated using thermal bonding. (Di) Mesh device: COP injection part, nylon membrane (150 × 150 μm), COC Flex channels, COP base. (Dii) Epithelium formation over 288 h; insets show cell spreading. Scale bars, 1,000 μm. (Diii) z stack of U-87 MG spheroids (red) interacting with endothelium (green, nuclei cyan). Scale bars, 100 μm. (Div) Macropore device design: COP injection, COC Flex wells, tripore membrane, channels, base. (Dv) Validation with collagen gel and fluospheres (green/red). Scale bars, 1,000 μm. (Dvi) Invasion assay showing spheroid (U-87 cells) expansion and migration at 96 h. Scale bars, 100 μm. Adapted from Olaizola-Rodrigo et al.,[94] under CC BY 4.0 license.

increasingly used as a complementary or alternative technique. Laser cutting utilizes a focused laser beam—typically from a $CO_2$ or fiber laser source—to locally melt, burn, or vaporize material in a controlled manner, thus allowing the creation of precise microfeatures without physical contact.[150,151] This cutting method offers enhanced versatility by enabling precise ablation of rigid or brittle substrates such as PMMA, polycarbonate, or certain composite films that are not easily processed using a plotter blade. The selection between plotter-based and laser-based cutting methods depends primarily on the mechanical properties of the substrate, the required resolution, and the available technical and financial resources of the research facility or institution.

Once the individual layers have been patterned, the final assembly of xurography-based microfluidic devices can be achieved through various bonding strategies, including adhesive bonding, chemical bonding, and thermal bonding, each selected based on the substrate material and the performance requirements of the device (Figure 6A). In adhesive bonding, a pressure-sensitive double-sided adhesive film is placed between the layers, followed by uniform pressure application to ensure proper contact and sealing of microchannels.[152,153] This method is frequently employed due to its simplicity, compatibility with a wide range of thermoplastics (such as PET, PC, or PMMA), and suitability for rapid prototyping with minimal equipment. Chemical bonding, in contrast, involves surface modification—typically via a chemical treatment that induces functional groups capable of forming strong covalent or hydrogen bonds between layers.[154] In practice, this method is often preceded by a physical surface activation step, such as oxygen plasma, UV/ozone, or corona discharge, which introduces reactive functionalities (e.g., hydroxyl or carboxyl groups) on the polymer surface. Although this form of surface activation is not explicitly illustrated in the xurography workflow, it has been described earlier in the soft lithography section and is represented as the final bonding steps in Figure 4A, where it was used for PDMS-PDMS or PDMS-glass bonding. The integration of physical and chemical treatment enhances bond strength and enables permanent bonding for PDMS and certain thermoplastics like PMMA or COC.[146,155] In thermal (fusion) bonding, heat and pressure are applied simultaneously to thermoplastic layers, raising the temperature of one or both materials to, or slightly above, their glass-transition temperature (Tg). At this stage, the polymer surfaces undergo partial softening, enabling the interdiffusion of polymer chains across the interface. Upon cooling, this molecular entanglement solidifies into a permanent, high-integrity bond. However, this method requires careful control of temperature to avoid deformation of microstructures and is most effective with materials that possess sufficient thermal stability.[156] The choice among these techniques depends on factors such as material compatibility, thermal tolerance, required mechanical strength, device complexity, and available fabrication resources.

Within the field of OOC development, numerous devices fabricated through xurography and employing various bonding techniques have been reported. Regarding models created in devices assembled using adhesive bonding, several examples exist in the literature.[92,157] As a representative case, the platform developed by Sui et al. was designed to investigate the trafficking of multiple myeloma (MM) cells through the sinusoidal niche of the bone marrow (Figure 6B).[92] In this work, the authors fabricated a microfluidic platform through plotter cutting of thermoplastic layers and subsequent application of a double-sided pressure-sensitive adhesive, enabling rapid prototyping and microchannel sealing under modest pressure (Figures 6Bi and 6Bii). The device recapitulates key aspects of the bone marrow sinusoidal niche: endothelial and stromal compartments are co-cultured in close spatial proximity (Figure 6Biii), and CXCL12 gradients effectively induce the directed migration of MM.1S multiple myeloma cells, thus capturing chemokine-mediated trafficking dynamics within the marrow microenvironment (Figures 6Biv and 6Bv).

Chemically bonded xurographic devices have also enabled the development of advanced OOC models.[93,154] One such example is the stomach-on-chip introduced by Ferreira et al. (Figure 6C), which was constructed by cutting pre-cured PDMS layers and PET membranes using xurography, followed by sequential bonding of the layers through oxygen plasma surface activation and chemical treatment with bis[3-(trimethoxysilyl)propyl]amine, a bis-amino silane.[93] This combined approach enabled robust, long-term adhesion between dissimilar materials, resulting in a perfusable, multi-layered gastric model (Figures 6Ci and 6Cii) in which a fibronectin-coated basement membrane supports epithelial cell growth, while adjacent chambers host lamina propria analogues and ensure sustained nutrient perfusion (Figure 6Ciii). Under dynamic culture, epithelial cells adopted a polarized, columnar morphology with organized junctional markers—contrasting with the flattened, undifferentiated phenotype observed under static Transwell conditions—thus demonstrating the importance of controlled surface chemistry and mechanical stimulation for tissue maturation (Figure 6Civ).

OOC models fabricated using thermal bonding in xurography have also demonstrated significant potential.[94,158,159] The study explained here presents two microfluidic platforms—the Mesh and Macropore devices—fabricated by plotter cutting COP/COC components and applying heat and pressure to create permanent bonds without the use of solvents (Figure 6D).[94] The Mesh device combines a fine porous membrane (Figure 6Di) with microchannels to facilitate epithelial monolayer formation and tumor-endothelium interactions (Figures 6Dii and 6Diii). The Macropore design (Figures 6Div and 6Dv) enhances three-dimensional invasion assays by incorporating large pores through which spheroids can invade surrounding matrices (Figure 6Dvi). In both cases, the thermal bonding strategy yields robust structural integrity and supports complex 3D culture and invasion studies.

Xurography is valued for its simplicity, speed, and low cost, requiring only basic equipment such as a cutting plotter and readily available substrates. It allows for rapid prototyping and short fabrication times, enabling efficient iteration of design modifications.[160] However, its 2D nature imposes constraints on the fabrication of complex or high-aspect-ratio geometries, and limited cutting resolution can hinder the creation of fine features. Moreover, material selection is restricted to thin, flexible layers—typically thermoplastics or elastomers—compatible with the cutting process. In some cases, incomplete cuts or

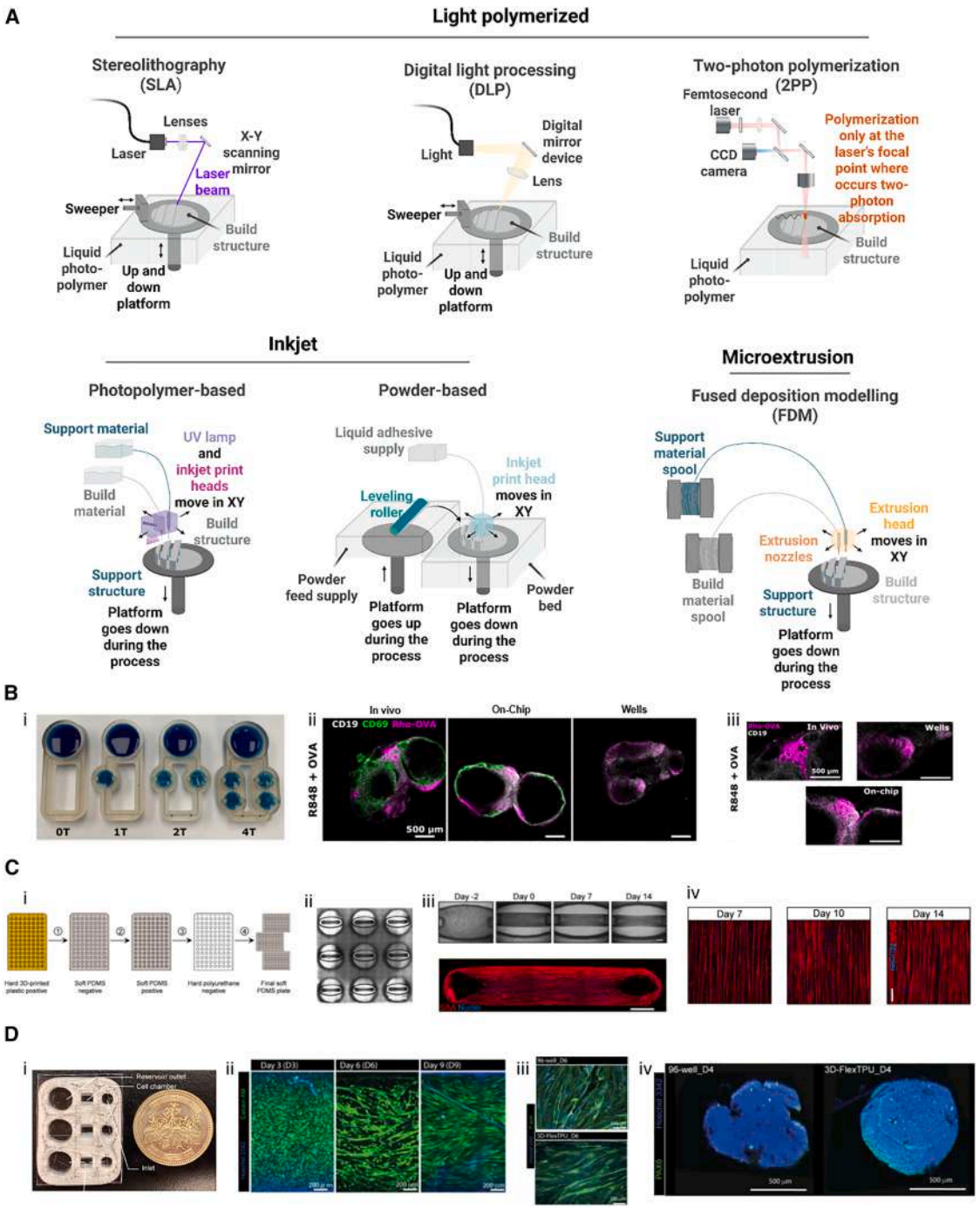


**Figure 7. 3D printing fabrication methods**

(A) Light polymerized techniques: SLA, DPL, and 2PP. Inkjet 3D printing techniques: photopolymer-based and powder-based. Microextrusion printing, in particular, FDM technique.

(B) Multi-organ-on-chip for lymph node communication fabricated by DPL. (Bi) Photograph of four ITX-PEGDA devices with 0, 1, 2, or 4 wells filled with blue dye to visualize channels. (Bii) Representative LN slices cultured with R848 + Rho-OVA or PBS *in vivo*, on-chip, or in well plates; B cells (CD19, gray), CD69 (green), Rho-OVA (magenta). (Biii) Distribution of Rho-OVA (magenta) across conditions with B cells (gray). Adapted from Cook et al.,[95] RSC, under CC BY 3.0 (https://creativecommons.org/licenses/by/3.0/).

(C) MyoTACTIC platform for analyze human skeletal muscle microtissue. (Ci) Fabrication workflow: 3D CAD design printed in 3D, PDMS negative mold, soft replica, rigid polyurethane mold, and final PDMS plates. (Cii) Phase-contrast stitched image of nine wells containing remodeled hMMTs 10 days post-seeding. Scale bars, 5 mm. (Ciii) hMMTs form aligned myotubes with ECM remodeling; top: phase-contrast images over time, bottom: confocal of 2-week hMMT

*(legend continued on next page)*

edge burrs can affect channel fidelity and bonding quality. The bonding technique used in combination with xurography also significantly influences device performance. Adhesive bonding, while straightforward and effective for rapid assembly, may introduce challenges such as air bubble entrapment, autofluorescence, and unintended cell adhesion to the adhesive interface, which can compromise optical imaging and biological reproducibility.[146,153] Chemical bonding, particularly when using silane coupling agents, enables the formation of robust and biocompatible seals. However, it requires meticulous surface activation and rapid layer alignment, as the transient reactivity of plasma-treated surfaces demands immediate bonding. Moreover, the process is sensitive to air entrapment during assembly and may involve labor-intensive protocols that limit scalability.[161] In contrast, thermal bonding, though capable of generating strong, solvent-free interfaces, is susceptible to feature deformation and bubble formation due to heat-induced warping.[162] Small but measurable structural distortions have been observed following thermal processing, particularly in microscale features.[163]

In addition to these general considerations, each reported xurography-based OOC model reveals case-specific constraints. In the bone-marrow sinusoidal trafficking device, the reliance on pressure-sensitive adhesive and manual layer alignment may introduce variability in channel dimensions and shear flow patterns, potentially affecting reproducibility of CXCL12-mediated cell migration studies. In the stomach-on-chip model, the integration of flexible gastric organoids and peristaltic actuation via chemically bonded layers could introduce challenges in maintaining long-term mechanical stability under dynamic deformation, risking delamination or mechanical failure during extended culture periods. Finally, in approaches aimed at reducing inert materials to improve cell-cell and cell-matrix interactions, the xurography-based reduction strategies may inadvertently compromise structural durability or fluid-tight integrity due to the thinner or softer materials used in lieu of conventional rigid barriers, increasing the risk of leakage or deformation under flow. In summary, while xurography offers an accessible and scalable route for the fabrication of OOC devices, its precision, material constraints, and compatibility with bonding methods must be critically evaluated during device design to ensure functional integrity and biological relevance.

## 3D printing

3D printing encompasses a range of additive manufacturing methods that construct solid three-dimensional objects by sequentially adding material layer by layer, all under precise digital control.[164] The most commonly employed 3D printing techniques relevant to microfluidics include light-polymerized 3D printing, inject printing, and (micro)extrusion printing, represented in Figure 7. All these 3D printing techniques have two distinct modes of operation: a direct printing mode, which is a one-step manufacturing process, and an indirect printing mode, which is based on a mold. This is similar to the soft lithography technique, which was discussed in previous sections. Within the indirect printing techniques, there is a further distinction to be made between the use of a sacrificial mold, which is designed for a single use, and a non-sacrificial mold, which is intended for multiple uses.[100,165–169]

### *Light-polymerized 3D printing*

Light-polymerized 3D printing relies on the selective solidification of photosensitive resins through controlled light exposure, enabling the creation of structures with high resolution and fine feature detail. The most prevalent techniques within this category are stereolithography (SLA), digital light processing (DLP), and two-photon polymerization (2PP). These methods are also known as vat photopolymerization microfabrication techniques.

SLA employs UV lasers to selectively illuminate a liquid photopolymer, thereby inducing its polymerization and crosslinking, facilitating the formation of three-dimensional structures. This technique employs a layer-by-layer fabrication methodology, relying on high-precision photopolymers, including epoxies and acrylic-based photoresins, to achieve the desired outcome (Figure 7A). It is necessary to subject the components manufactured by SLA to a post-processing and post-curing procedure in order to complete the curing of the partially cured parts of the object. The capacity to create structures of considerable intricacy, adaptability, and scalability is possible by using digital micromirror arrays, which facilitate the precise patterning process and a resolution around 20–100 μm. This technique offers several advantages, including the capacity to create intricate structures, high precision, surface finishing, and compatibility with a wide range of materials, including those with biocompatible properties. However, it also presents certain limitations, such as the high cost of resins and the limited availability of biocompatible photopolymers.[167,170,171]

DLP technology is based on the same fundamental principle as SLA, but instead of exposing the layer in a series of discrete dots, a sequence of digital micromirror devices is employed to project the entire optical pattern of the predefined layer (Figure 7A). This technique allows to produce a printed object in a shorter time than SLA. Furthermore, it offers high precision (resolution down to 10 μm) and favorable material properties. It should be noted that the technology has certain limitations in terms of the types of materials that can be used for printing, like SLA, and that its projection capabilities are not as advanced as those of other production lines.[172]

2PP represents an advanced stereolithographic technique capable of producing three-dimensional structures with nanoscale resolution, thereby surpassing the diffraction limit (Figure 7A). The exceptional precision of this technique, which can achieve feature sizes below 100 nm, makes it particularly

immunostained for sarcomeric α-actinin (red) and nuclei (blue). Scale bars, 500 μm. (Civ) Confocal images of myotubes at 7, 10, and 14 days (SAA red, nuclei blue). Scale bars, 50 μm. Adapted from Afshar et al.,[101] under CC BY 4.0 license (https://creativecommons.org/licenses/by/4.0/).
(D) FDM-based 3D-FlexTPU-MFD device for OOC applications. (Di) Fully assembled device. (Dii) Myoblast differentiation, maturation, and alignment over D3, D6, and D9; Calcein AM (green) and Hoechst 33342 (blue). (Diii) F-actin staining of myoblasts on D6 in device versus 96-well plate. Scale bars, 200 μm. (Div) iPSC-derived optic vesicle organoids attachment and differentiation; PAX6 expression compared between 96-well plate and 3D-FlexTPU-MFD at D4. Adapted from Kado Abdalkader et al.,[102] under CC BY 4.0 license.

suited for applications such as the fabrication of microfluidic systems and the *in vitro* replication of physiological microenvironments. Nevertheless, the extended fabrication times associated with its high resolution restrict its utility for the generation of larger-scale tissue analogues. Moreover, the technique is constrained by its reliance on photosensitive polymers originating from the microelectronics sector, which are often characterized by limited biocompatibility. This technique offers precise nanometer-level control but is also associated with slower processing times and the need for expensive equipment.[171]

Recent studies have shown that these photopolymerization techniques are increasingly used to fabricate complete OOC platforms. For example, a DLP-printed PEGDA/ITX resin device enabled the construction of a multi-organ platform to investigate lymph node communication (Figure 7B).[95] In this approach, the high-resolution capabilities of DLP printing allowed the fabrication of microfluidic channels and chamber geometries tailored to support viable lymph-node tissue (Figure 7Bi). The system successfully sustained murine lymph node slices on-chip and reproduced antigen uptake and activation profiles comparable to *in vivo* conditions (Figures 7Bii and 7Biii). These results not only demonstrate that DLP can yield directly biocompatible OOC devices when combined with appropriate post-processing treatments but also highlight the potential of photopolymerization-based methods to create immunologically relevant models that integrate multiple organ functions. Likewise, SLA and 2PP approaches have been applied to fabricate BBB-on-chip, placenta-on-chip, or vessel-on-chip platforms, highlighting their ability to reproduce barrier functions and physiological microenvironments at high resolution.[96–99]

### *Inkjet printing*

Inkjet-based 3D printing is founded on the precise deposition of small droplets of liquid material, allowing for the construction of complex geometries in a layer-by-layer manner. Here, two principal categories may be distinguished: photopolymer-based and powder-based.

Inkjet-photopolymer-based 3D printing involves the deposition of photocurable resins in a selective manner, with each drop deposited individually continuously. Once the first layer has been deposited, it is cured by UV light. The platform on which the layers are placed is then lowered, and the next layer is formed, repeating this process until the final piece is formed (Figure 7A). One of the most significant advantages of this technology is its capacity to fabricate structures with exceptional precision and resolution. This capability is attributed to the precise control of the printhead, which enables the deposition of minimum quantities of material at designated locations on the substrate. Consequently, this approach enables the fabrication of layers with a thickness of approximately 10 μm. This technology is further distinguished by its capacity to process a diverse range of polymeric materials, enabling the smooth integration of multiple materials within a single component.[166,171]

Powder-based inkjet 3D printing entails the binding of solid powder particles through the utilization of a polymeric adhesive solution, which is applied via an inkjet print head. The initial stage of the process entails the application of a thin, uniform layer of powder by a roller across the build platform (Figure 7A). Subsequently, the inkjet print head meticulously dispenses adhesive droplets on a selective basis, thereby creating the desired pattern on specific regions of the powder bed. This process is repeated until the final piece is formed, which is the result of the aforementioned process. The powder exhibits a size range of approximately 50–100 μm, with 2–4 particles forming a layer, thereby limiting the achievable Z resolution to 200 μm.[173]

Inkjet-based three-dimensional printing provides an exceptional degree of versatility in the fabrication of highly functional and customized objects. Furthermore, the superior resolution and high printing speeds associated with this process make it an extremely attractive methodology for the construction of intricate microfluidic devices, particularly those designed for droplet generation and cell culture applications.[100]

Despite these advantages, inkjet photopolymer printing is seldom used as a final culture substrate in OOC applications due to challenges with biocompatibility and the removal of support materials. Instead, it is frequently employed in an indirect mode, where the printed part serves as a mold for the fabrication of PDMS-based devices. A representative example is the MyoTACTIC platform (Figure 7C), in which a photopolymer-based inkjet print was used to produce molds that were subsequently replicated into PDMS plates (Figure 7Ci). These plates enabled the reproducible generation of engineered human skeletal muscle microtissues (hMMTs) that showed alignment, maturation, and quantifiable contractile strength over time (Figures 7Ciii and 7Civ). This approach illustrates how inkjet printing accelerates prototyping and mold production, while the final biological culture is carried out in a more biocompatible material.

To date, no published reports describe the fabrication of functional OOC microfluidic chips directly by powder-based inkjet printing, mainly due to its limited resolution and challenges in producing leak-tight enclosed channels. Instead, its use in bioengineering has focused on bone scaffolds and tissue engineering constructs where porosity is advantageous.

### *Microextrusion printing*

The extrusion printing technique is commonly known as fused deposition modeling (FDM) or fused filament fabrication (FFF). The FDM technique is based on a filament roller from which filament is fed to both rollers and subsequently transformed into a semi-liquid substance before transferal to an item. Thus, a thermoplastic material is extruded through a nozzle that has been subjected to high temperatures.[174,175] The molten material, upon exiting the nozzle, undergoes an immediate solidification process within the desired area. Once a layer has been formed, the platform descends and the nozzle deposits another layer, and this sequence of operations is repeated until the entire object has been created (Figure 7A). The resolution and performance of FDM methods are influenced by a number of parameters, including temperature, viscosity of extruded filament, layer height, layer density, shear strength, the size of the nozzle, printing speed, and the specific material type being used.[176] A notable advantage of fused deposition modeling is its capacity to process a diverse range of thermoplastic polymers. This capability is of particular value in that thermoplastics are widely employed in large-scale manufacturing processes, including injection molding and hot embossing. Consequently, the components produced via FDM may be manufactured using

materials that are compatible with the established methods of mass production. As a result, they can be integrated effectively into industrial manufacturing workflows. The technique has certain disadvantages, including a low resolution, surface finishing, and a lack of suitability for highly detailed designs or complex microstructures.[177]

Nevertheless, several reports have demonstrated that with careful material choice, FDM can directly yield microfluidic devices suitable for OOC models.[103–105] A recent example is the 3D-FlexTPU-MFD (Figure 7D), fabricated in one step by combining thermoplastic polyurethane (TPU) and PVC (Figure 7Di).[102] This device successfully supported the differentiation of human myoblasts into aligned myotubes (Figure 7Dii) and also sustained the culture of iPSC-derived optic vesicle organoids (Figure 7Diii). Such studies confirm that FDM, although traditionally considered low resolution, can be adapted to generate robust OOC devices for muscle and neural tissues.

3D printing techniques are becoming more widely used as a consequence of the multiplicity of advantages proffered by this technique. The advantages include a low cost of prototyping, flexibility of design, a reduction in waste, and the ability to produce complex devices in a single piece, obviating the need for assembly of multiple components.[178] Nevertheless, it encounters several challenges when compared to traditional manufacturing techniques. A notable limitation is the lack of consistency in resolution across different printing techniques. While techniques such as SLA can achieve high levels of detail, others, such as FDM, often lack the precision required for specific microfluidic applications. This can impede the fabrication of intricate microchannels or features that are crucial for intricate designs. Moreover, the opacity of numerous printable materials presents a challenge in visualizing cell cultures or fluid dynamics within the device, which is crucial for biological studies. An additional concern is the cost. High-resolution printers and the specialized materials required for advanced applications can be prohibitively expensive, which limits access for researchers or those working on small-scale projects. Furthermore, scalability remains a significant challenge, as 3D printing is often a time-consuming process, and the cost per unit increases with production volume. This renders the technique less practical for mass production in comparison to methods such as injection molding. Moreover, the surface quality of 3D-printed devices frequently fails to meet the standards of a polished finish achieved through traditional techniques, which may impact both the aesthetics and functionality of microfluidic platforms.

In addition to these general considerations, case-specific drawbacks are evident in reported OOC applications. For example, the DLP-printed multi-organ-on-chip designed to model lymph node communication still depends on specialized custom resins and surface coatings to mitigate cytotoxicity, adding complexity to device preparation and limiting immediate translation. This challenge reflects a broader issue in photopolymer-based 3D printing techniques: incomplete polymerization of photopolymer resins can result in leaching of residual monomers or oligomers, which may compromise biocompatibility if post-curing is insufficient. Regarding inkjet-based approaches, the MyoTACTIC platform, although powerful for longitudinal skeletal muscle studies, requires multi-step mold replication and PDMS casting, which limits throughput and direct biocompatibility. In the case of the FDM-based 3D-FlexTPU-MFD, while the flexible TPU-PVC bonding strategy improves robustness, challenges remain with optical clarity and printing fidelity at the smallest channel scales, which may restrict detailed imaging and microenvironmental control. A further limitation shared across these platforms is the absence of integrated perfusion systems, as none of the reported devices incorporate functional flow connections. This omission constrains their ability to recapitulate dynamic fluid exchange and shear forces, which are central to physiologically faithful OOC models. Taken together, while 3D printing is enabling increasingly sophisticated OOC platforms, the drawbacks tied to each method underscore the need for continued refinement of both materials and fabrication protocols to fully unlock its potential.

## MATERIALS IN ORGAN-ON-CHIP TECHNOLOGY: EVOLUTION AND APPLICATIONS

Since the advent of microfabrication of microsystems, the materials employed have constituted a primary focus of investigation, undergoing a process of evolution to meet the demands of the applications in question. The initial microsystems were manufactured using materials that could be classified into two main groups: rigid materials and elastomers.[179]

The first group included silicon (in both crystalline and amorphous forms), quartz, metals, glass, and organic polymers, which were subjected to study and subsequent utilization. Focusing on medical applications, rigid materials were reduced to silicon and glass as they are biocompatible, highly resistant to chemicals and high temperatures, and in the case of glass, also transparent (Table 2). These rigid materials frequently serve as structural substrates or outer supports in OOC devices, although in many designs they can also constitute the base layer in direct contact with the microenvironment of interest.[2,185] Nevertheless, they are costly, which became a significant factor when soft lithography with elastomers began to be used.

At that time, as mentioned in previous sections, the PDMS elastomer revolutionized the field of microfluidics, offering numerous advantages. It was optically transparent, cost-effective, biocompatible, thermally stable, impermeable to water, and easy to work with.[11,186–188] Moreover, its permeability to gases can be particularly beneficial in applications where gas exchange is required, such as in the maintenance of cell cultures under oxygenated conditions. However, its tendency to absorb certain organic compounds can limit its suitability for specific uses.[189] In addition, incomplete curing can result in the leaching of uncrosslinked oligomers, which may interfere with cellular assays unless properly treated. Other elastomers, including SU-8 resin, polyurethane (PU), and poly(lactic-co-glycolic) acid (PLGA), among others, are employed, albeit on a smaller scale (Table 3). SU-8-negative photoresist has been extensively employed in the microfluidic domain due to its transparency, high structural resolution, reproducibility, stiffness, and chemical resistance.[77,195,206,207] Nevertheless, cytotoxic effects have been reported when unpolymerized photoresist residues remain, highlighting the importance of complete crosslinking and solvent extraction. On the other hand, polyurethane has

**Table 2. Classification of the most commonly used rigid materials used in OOC technology**

| Family | Material | Fabrication methods | Advantages | Disadvantages | Applications |
|---|---|---|---|---|---|
| Rigid materials | glass | photolithography, laser micromachining, thermal bonding, powder blasting, 3-day glass printing | highly resistant to chemicals, resistant to high temperatures, transparency | costly production (machines and materials) | monolithic membrane valves,[180] cell culture,[181] drug testing and delivery,[181] liver-on-chip,[182] |
| | silicon | photolithography, laser micromachining, wet and dry etching, anodic and fusion bonding, nanoimprint lithography, physical and chemical vapor deposition[183] | highly resistant to chemicals, resistant to high temperatures | costly production (machines and materials), opacity | oxygen-sensor-based microphysiological system,[26] single- and multi-organ models[184] |

several advantageous properties, including flexibility, good mechanical strength, and chemical inertness. However, it should be noted that it can emit odors and toxic gases. Furthermore, both SU-8 and polyurethane are employed in the fabrication of the molds used to create the final OOC devices, which are produced through soft lithography.[61,65,196,197] Another material that is extensively utilized in this field, particularly in the domains of drug delivery and tissue engineering, is PLGA.[192,199–201] This material is highly reproducible and can be easily replicated. The field of elastomeric materials has witnessed a notable expansion in recent years, with the emergence of novel materials such as poly(octamethylene maleate (anhydride) citrate) (POMaC) and poly(itaconate-co-citrate-co-octanediol) (PICO). Both are non-toxic and low-cost. POMaC is biodegradable, its mechanical properties can be modified according to requirements, and its manufacture is straightforward.[202] PICO can be readily functionalized at the surface and exhibits good mechanical strength. POMaC has been used to fabricate some OOC devices, but both POMaC and PICO are mainly used for tissue engineering, an area that is often integrated into OOC devices.[202–205]

Over the past decade, thermoplastic materials have been employed extensively in the development of microfluidic OOC devices. These materials offer several advantages, including low cost, ease of fabrication, biocompatibility, and transparency (Table 4). Furthermore, they are particularly promising for mass production in biomedical and clinical applications, given their high reproducibility and low production costs. The production of these thermoplastic materials is generally carried out through injection molding or hot embossing. Among thermoplastic materials, the most commonly used in this field are polymethyl methacrylate (PMMA), polystyrene (PS), cyclic olefin polymer and copolymer (COP/COC), polycarbonate (PC), polyethylene terephthalate (PET), and polylactic acid (PLA).

PMMA and PS are extensively employed in the domain of OOC technology due to their formidable advantages, including the expediency with which highly stable molds and prototypes can be created, the non-absorption of small molecules, the low cost (PMMA), and its remarkable durability.[71,209,226–228] Indeed, PMMA can be combined with PDMS to create devices through the process of xurography.[210,211] Cyclic olefin polymers also possess a number of advantageous characteristics, including reduced impurity content, limited permeability to gases, minimal water absorption, and favorable machining properties. Their limited gas permeability, while restricting oxygen exchange, can be advantageous in applications that aim to reproduce hypoxic microenvironments. Furthermore, the material exhibits favorable electrical insulating properties and is biologically inert, which enhances its utility in the domain of OOC research.[154,212,215,216,229–233] Polycarbonate, on the other hand, is employed in this field as a porous membrane, particularly in on-chip technology.[63,217,234–236] It is rigid and can be easily fabricated (using techniques such as thermal bonding or microwave hot press) and exhibits only moderate hydrophobicity. This material can be used alone or in combination with PDMS to produce OOC devices.[218–220] Furthermore, polyethylene terephthalate (PET) is a common material used in the construction of porous membranes that separate the compartments of OOC devices.[91,223,224] The PLA is also a thermoplastic with noteworthy characteristics, including its origin from renewable sources, which renders it environmentally friendly, as well as its ease and speed of workability. Nevertheless, there is currently a relatively limited number of examples on the market, although it seems likely that this will change in the future.[225]

The utilization of polymers, both natural and synthetic, has become essential in the progression of microfluidics and OOC technologies, thereby facilitating integration between biological systems and engineering methodologies. Natural polymers used in OOC include fibrin, collagen, matrigel, gellan gum (GG), and alginate, among others[237–247] (Table 5).

Fibrin is a biopolymer comprising the monomer fibrinogen, which is itself composed of two sets of three polypeptide chains. The most commonly utilized forms of fibrin scaffolds are fibrin hydrogels, fibrin glue, and fibrin microbeads (FMB).[250] Collagen represents approximately a quarter of the proteins in the human body, is the dominant element of the extracellular matrix, and, due to its physicochemical characteristics, is responsible for the integrity, strength, and elasticity of tissues. The characteristics of collagen fibers make it a biopolymer compatible with the human body, which is why it is widely used in biomedical and biomaterials research.[251] Matrigel is an extract derived from a mouse tumor. It contains all of the major components known to be present in many tissue basement membranes.[249] Gellan gum is a water-soluble microbial polysaccharide that forms

**Table 3. Classification of elastomers used in OOC technology**

| Family | Material | Fabrication methods | Advantages | Disadvantages | Applications |
|---|---|---|---|---|---|
| Elastomers | polydimethylsiloxane (PDMS) | soft lithography, plasma and laser etching, 3D printing | transparency, flexibility, cost-effective, thermally stable, impermeable to water, easy to work with, low auto-fluorescence | absorption of small hydrophobic molecules, hydrophobicity | lung-on-chip,[10,28,190] blood vessels-on-chip,[59,60] gut-on-chip,[55,61] liver-on-chip,[40,57] brain-on-chip,[66] cartilage-on-chip,[72] placenta-on-chip,[73] bone regeneration,[191] drug testing,[74,192] tissue engineering[193,194] |
| | SU-8 | photolithography, xurography, plasma etching | transparency, high structural resolution (3 days), high reproducibility, high stiffness, high resistance to solvents, chemically stable | medium cost-effective, adhesion selectivity, cytotoxicity if not properly processed, high auto-fluorescence | tumor-on-chip,[77] biosensing applications,[195] molds used to create final OOCs[61,65,196] |
| | Polyurethane (PU) | photolithography, 3D printing (FDM and SLA), xurography, laser micromachining | flexibility, good mechanical strength, chemically inert | emit odors and toxic gases | molds used to create final OOC,[197] tissue engineering[198] |
| | Poly(lactic-co-glycolic) acid (PLGA) | 3D printing (extrusion-based) | highly reproducible, easy replicated | toxicity from residual stabilizing molecules, limited capacity to carry high concentration of drugs | tissue engineering,[192,199] drug testing[200,201] |
| | Poly(octamethylene maleate (anhydride) citrate) (POMaC) | soft lithography, hot embossing, injection molding | low-cost material, biodegradable, modifiable mechanical properties, easy manufacturing | high viscosity, slow crosslinking | tissue engineering[202–204] |
| | Poly(itaconate-co-citrate-co-octanediol) (PICO) | soft lithography, 3D printing | low-cost material, good mechanical strength, easy surface functionalization | rapid degradation | tissue engineering[205] |

strong, stable hydrogels when interacting with divalent cations like calcium. These hydrogels, created through ionotropic cross-linking, are more robust and less penetrable than alginate-based gels.[245,252] Alginate is a water-soluble polysaccharide composed of β-D-mannuronic acid and α-L-guluronic acid, commonly used in medicine, pharmaceuticals, and various industries due to its biocompatibility and mild ionic gelation properties. Recent research highlights microfluidics as a valuable tool for cell manipulation and encapsulation within alginate-based microgels.[253]

These polymers are widely recognized for their flexibility, excellent biocompatibility, and effective gas permeability. These characteristics render them highly suitable for applications such as drug delivery systems, tissue engineering, biosensor fabrication, and the development of OOC devices.[245] Despite the aforementioned advantages, natural polymers do, however, present certain limitations. These materials require sterilization and purification, which increases the process complexity. Furthermore, their intrinsic characteristics are fixed and cannot be readily modified to meet specific requirements.

Synthetic biomaterials could overcome some of the limitations of naturally occurring biomaterials. One of their main advantages is that the physical and chemical properties of these materials appear to be more tunable than those of natural materials (Table 6).

The materials in question comprise gelatin methacryloyl (GelMA) and poly(ethylene glycol) diacrylate (PEGDA).[260] These materials are also employed in other manufacturing techniques, in addition to 3D printing, such as photopatterning. GelMA is a gelatin derivative comprising predominantly methacrylamide groups and a lesser amount of methacrylate groups.[261] The material is broadly recognized as a key component in biofabrication

**Table 4. Classification of thermoplastic materials used in OOC technology**

| Family | Material | Fabrication methods | Advantages | Disadvantages | Applications |
|---|---|---|---|---|---|
| Thermoplastic materials | polymethyl methacrylate (PMMA) | xurography, photolithography, injection molding, hot embossing | low-cost material, non-absorption of biomolecules, transparency, durability, reusable, transparency, low auto-fluorescence | post-processing, high cost of the molds, residual monomer toxicity | molds used to create final OOC,[208] drug testing,[71] blood vessels-on-chip,[209] metastasis-on-chip,[210] liver-on-chip[211] |
| | polystyrene (PS) | soft lithography, injection molding, hot embossing, 3D printing | low-cost material, non-absorption of biomolecules, durability, transparency | post-processing, high cost of the molds, low solvent resistance, high auto-fluorescence | drug delivery[75] |
| | cyclic olefin polymer and copolymer (COP/COC) | injection molding, hot embossing, xurography | low auto-fluorescence, non-absorption of biomolecules, high heat resistance, low water absorption, low impurity, good machining properties, biologically inert, electrical insulating properties, transparency | post-processing, high cost of the molds | blood-brain barrier-on-chip,[212] tumor-on-chip,[213,214] immune-tumor-on-chip,[70] liver-on-chip,[215] drug testing[216] |
| | polycarbonate (PC) | hot embossing, injection molding, xurography, 3D printing | easy manufacturing, moderate hydrophobicity, durability, transparency | post-processing, high cost of the molds, low resistance to organic solvents, high auto-fluorescence | tissue engineering (integrated scaffold in OOC),[62,63,217] cell culture platform,[218] gastrointestinal human-microbe-on-chip,[219] lung-on-chip[220] liver-on-chip,[221] vessel-on-chip[222] |
| | polyethylene terephthalate (PET) | laser micromachining, hot embossing, injection molding | high solvent resistance, high acid/base resistance, transparency | post-processing, high cost of the molds, low transparency | tissue engineering (integrated scaffold in OOC)[91,223,224] |
| | polylactic acid (PLA) | hot embossing, 3D printing, injection molding | environmentally friendly, biodegradable, easy to work with, low absorption | high degradation rate | cell culture[225] |

and tissue engineering applications. As with other photocrosslinkable hydrogels, residual methacrylate groups and photoinitiator by-products may induce cytotoxicity if washing and curing steps are not adequately optimized. PEGDA is a synthetic polymer that was created by the functionalization of polyethylene glycol (PEG) with the addition of acrylate groups at both ends.[262] This material offers excellent tunability and optical clarity. Yet, unreacted acrylate groups or photoinitiator residues can leach out if polymerization or post-curing is insufficient, potentially compromising cell viability. Both materials have been extensively employed within the context of OOC technology, predominantly in the field of tissue engineering.[254–256,258,259,262]

## INNOVATIVE APPROACHES TO BARRIER-FREE ORGAN-ON-CHIP DESIGNS

There are numerous designs for OOC devices, as discussed in previous sections. The primary goal of these devices is to replicate organ and tissue functions as accurately as possible, mimicking *in vivo* conditions. Achieving this requires the elimination of inert materials between compartments, enhancing direct cell-cell and cell-extracellular matrix interactions. Many devices currently incorporate membranes[10,61,62,263–265] or micropillars[53,213,266–268] to separate compartments, each presenting distinct challenges. Membranes, often made from materials

**Table 5. Classification of natural polymers used in used in OOC technology**

| Family | Material | Fabrication methods | Advantages | Disadvantages | Applications |
|---|---|---|---|---|---|
| Natural polymers | fibrin | 3D printing, soft lithography, and photopatterning if chemically modified before the fabrication processes | flexible, high bioactivity | required purification, fixed characteristics | BBB-on-chip, tissue engineering (skin) |
| | collagen | 3D printing (extrusion-based, i3Dp, drop-on-demand), soft lithography, and photopatterning if chemically modified before the fabrication processes | flexible, high bioactivity | required purification, fixed characteristics | tissue engineering (integrated membrane in OOC)[240,241,246,248] |
| | matrigel | 3D printing, soft lithography, and photopatterning if chemically modified before the fabrication processes | flexible, very high bioactivity, low immunogenicity, transparency | composition can vary (biological origin), without chemical modification, it is not photopolymerizable | tissue engineering[249] |
| | gellan gum | 3D printing, soft lithography, and photopatterning if chemically modified before the fabrication processes | flexible, cost-effectiveness and scalability, transparency | required purification, fixed characteristics | tissue engineering[244] |
| | alginate | 3D printing (extrusion-based), soft lithography, and photopatterning if chemically modified before the fabrication processes | flexible, biodegradable, mechanical stability, transparency | required purification, fixed characteristics | tissue engineering[239] |

like PC, PET, or PDMS, typically have pores no larger than 10 μm,[269] limiting the contact area between compartments. Pillars, on the other hand, can disrupt shear stress and trap cells, introducing additional complications.[212] As a result, recent research is increasingly focused on "barrier-free" strategies—approaches that eliminate these structures to allow direct tissue-tissue contact without inert interfaces (Table 7). Various innovative techniques are being explored to overcome the limitations of traditional compartmentalized systems and improve OOC performance.

## Laminar flow patterning

Laminar flow patterns result from the channels of small microfluidic devices where laminar flow conditions prevail. The Reynolds number (Re) is a dimensionless quantity that characterizes a fluid's propensity to transition between laminar (non-turbulent) and turbulent flow.[279,280]

$$Re = \frac{vl\rho}{\mu}$$

Here, all quantities are expressed in SI units: ρ in kg·m$^{-3}$, μ in kg·(m·s)$^{-1}$, l in meters (m), and v in m/s. Specifically, Re depends on the fluid's density (ρ), measured in kilograms per cubic meter, its viscosity (μ) in kilograms per meter-second, the diameter of the channel or capillary (L) in meters, and the flow velocity (v) in meters per second. The critical Re value at which flow transitions from laminar to turbulent varies with channel geometry. In a straight pipe, this shift typically occurs at approximately Re ≈ 2100. However, at lower Reynolds numbers, around Re ≈ 40–300, turbulence may emerge when flow passes an object or when the channel geometry varies. In capillaries (where l ranges around 50–100 μm), fluid flows usually maintain low Re values and thus exhibit laminar flow, even at higher flow velocities, up to approximately 0.5 m s$^{-1}$. Consequently, in narrow channels, multiple fluid streams can merge and flow in parallel without turbulent mixing, maintaining a steady, laminar profile.

This principle has led to the development of microfluidic devices capable of maintaining continuous parallel flows, permitting full contact between two or more different reagents and the formation of different protein microstrips on a glass surface[281] or quantification of the microbial electrochemical activity.[282] In both cases, the device was manufactured using soft lithography, and the material used was PDMS. In the first, polyelectrolyte and proteins were introduced, and microarrays were created in the central area using laminar flow patterning and the Y-type geometry required for their creation (Figure 8A). Precise

**Table 6. Classification of synthetic biomaterials used in OOC technology**

| Family | Material | Fabrication methods | Advantages | Disadvantages | Applications |
|---|---|---|---|---|---|
| Synthetic biomaterials | gelatin methacryloyl (GelMA) | 3D printing, soft lithography, photopatterning | photopolymerizable transparent | fast degradation, photoinitiator residuals | tissue engineering,[254–256] blood-vessel-on-chip[257] |
| | poly(ethylene glycol) diacrylate (PEGDA) | 3D printing (extrusion-based), soft lithography, photopatterning | photopolymerizable, transparent, low fluorescence non-absorption of biomolecules, good (variable) mechanical properties, non-degradable | poor cell adhesion without functionalization, cytotoxicity unless adequate post-processing | tissue engineering,[258,259] tumor-on-chip[52] |

synchronization of flow initiation through both channels was critical to ensure proper patterning. Similarly, the second system employed the same Y-shaped geometry, with reagents introduced at equal flow rates.

With a focus on OOC technology, several models were developed, such as a cardiomyocyte culture device using gels to coat the channels to the surface for cell adhesion.[270] This device contains 15 parallel channels. The mold was initially produced by photolithography, and the final PDMS device was obtained by soft lithography. The hydrogel was then introduced through the channels and polymerized. PBS was next introduced through the channels, creating two strips of polymerized gel at the sides of each channel. The cardiomyocytes attached to the gel were then inserted, and the medium was perfused (Figure 8B). After seeding and culture within the patterned microchannels, cardiomyocytes exhibited remarkable functional and structural behavior. Cardiomyocytes cultured in 5% (w/v) MeTro-coated microchannels aligned along the flow direction, forming contractile fibers reminiscent of native myocardium and exhibiting synchronous beating as early as day 4, reaching up to ~138 beats/min—significantly higher and better coordinated than in GelMA-coated channels (Figure 8Bi). The successful culture was further confirmed by the expression of cardiac-specific markers such as troponin I, sarcomeric α-actinin, and connexin-43 (Figure 8Bii), indicating proper structural organization and intercellular connectivity, thereby validating the physiological relevance of the OOC model.

A lymph-node-on-chip to study the intracellular dynamics of T cells and dendritic cells is another example.[68] To achieve the final PDMS device, the above process was employed, but with a glass substrate. The channels were then coated with fibronectin or collagen. PBS was later added to wash the channels, and culture medium was included, to ensure optimal conditions for cell seeding. In this case, dendritic cells formed a monolayer in the central channel and $CD4^+/CD8^+$ T cells were introduced through side channels under controlled laminar flow. T cells exhibited random migration and stable contacts with antigen-presenting DCs, with $CD4^+$ cells showing long dwell times (~12.8 min, ~6 μm/min) and $CD8^+$ cells displaying more transient interactions under varying shear stresses (0.01–100 dyn/cm$^2$). Importantly, antigen-specific T cells adhered selectively to DCs and could be detached at defined shear thresholds (~12 dyn/cm$^2$), demonstrating a functional, mechanically tunable immune synapse within an OOC platform.

A more recent approach involves introducing a chemical to make the desired channel hydrophilic.[271] By simultaneously introducing other liquids and utilizing laminar flow, this technique creates a mix of hydrophilic and hydrophobic channels, effectively preventing the reagents in each channel from mixing (Figure 8C). As in the previous examples, the hydrophilic channel was then coated to improve cell adhesion. Notably, this design achieves a three-channel device with a hydrophilic central channel with the option of changing patterns (Figure 8Ci). Following cell adhesion in the hydrophilic central channel, human endothelial cells (HUVECs) were seeded and cultured. By day 5, cells were confined by the patterned gel geometry and exhibited normal F-actin and nuclear staining, with some migrating into the gel in straight, hourglass, or meandering channel designs (Figure 8Cii). Moreover, under *trans*-gel flow conditions, GFP-expressing HUVECs showed significantly enhanced migration into the patterned gels compared to static culture, as confirmed quantitatively ($p < 0.05$) (Figure 8Ciii), demonstrating functional endothelial interaction with the three-channel OOC design. This configuration enables a wide range of applications, including the generation of diffusion-based, chemical, or biological gradients.

Laminar flow patterning has been effectively applied across diverse OOC models to achieve spatially defined hydrogel architectures and functional tissue organization. Initially as Li et al. and Shchukin et al. demonstrated as a fabrication strategy, it enabled the generation of adjacent hydrogel lanes within microchannels using parallel laminar streams and photopolymerization, allowing precise spatial control over scaffold composition and geometry—laying the groundwork for later biological applications.[281,282] In a cardiac platform, controlled prepolymer flow and UV crosslinking were employed to deposit hydrogel coatings of tunable thickness and elasticity along channel walls, thereby optimizing mechanical cues for cardiomyocyte adhesion, alignment, contractility, and synchronous beating, while maintaining perfusable lumens.[270] In the last example, the combination of laminar flow with chemohydrophilic modification permitted the definition of hydrophilic and hydrophobic regions within a simple three-channel layout, enabling the

**Table 7. Comparative analysis of barrier-free microfluidic patterning techniques for OOC fabrication**

| Method | Feature size (resolution) | Scalability/ commercial readiness | Material compatibility | Strengths | Limitations | Relevance for OOC |
|---|---|---|---|---|---|---|
| Laminar flow patterning | feature-dependent (~50–100 μm interfaces) | low/ research-level | hydrogels, PDMS, thermoplastics | creates total contact fluidic interfaces without solid barriers | limited to co-planar interface geometries, control depends on flow stability | cardiomyocytes-on-chip,[270] vessels-on-chip[271] |
| Phaseguides | ~50 μm ridge sets boundary, gel lanes typically ≥100 μm | medium-high (plate-based)/ commercially established by MIMETAS (OrganoPlate®) | thermoplastics, hydrogels | highly scalable, enables parallel culture in multiwell plates | fixed geometry, still requires precise molds | mammalian cells-on-chip,[272] chemotaxis in lipid bilayers study on-chip,[273] liver-on-chip,[221] vessel-on-chip[222,274] |
| Hydrogel photopatterning | <10–50 μm (light-defined) | low (serial/ optics steps)/ research-level | photocrosslinkable hydrogels | spatial control of 3D microenvironments, sub-cellular resolution possible | hydrogel fragility, light penetration limits, requires expensive optics/light sources | tumor-on-chip,[275] vessels-on-chip,[276] intestine-on-chip[277] |
| Surface treatment patterning | feature-independent (chemical boundary, limited by plotter typically ≥300 μm) | medium-high/ implemented commercially by Beonchip (Be-Gradient) | thermoplastics, glass, PDMS, hydrogels | patterning of any geometry/design possible, stable and universal flow connection | plotter resolution-dependent | BBB-on-chip,[212] GBM-on-chip,[214] colon-on-chip,[214] tumor-immune-on-chip[278] |

straightforward creation of multi-patterned geometries such as straight, hourglass, or meandering channels. This spatial control not only guided endothelial confinement but also induced their directional migration into adjacent gels under flow, thereby reproducing angiogenic behavior and providing a modular platform for investigating cell-matrix interactions, mechano-transduction, and geometry-dependent endothelial function in OOC systems.[271] Across all cases, this technique proved to be a robust method for engineering complex, biomimetic microenvironments with high spatial resolution.

## Phaseguides

The phaseguide structure is widely employed to eliminate inert materials between compartments in microfluidic systems, enabling clean fluid interface control within open channels. This concept was first introduced by Vulto et al.,[283] who developed passive liquid routing mechanisms based on phaseguides—microscale geometries designed to control the advancement of the air-liquid interface without requiring physical barriers or active pumping. Since then, phaseguides have been fabricated in various materials and shapes, offering versatility across numerous device architectures. One notable fabrication approach involves the use of dry film resist (DFR) technologies.[283–285] In particular, Phurimsak et al. later demonstrated the use of Ordyl SY 330 resin, a commercially available DFR, to construct the entire microfluidic device, including the phaseguide structures.[286] This method provided high patterning resolution and chemical resistance, making it suitable for integrating liquid lamination, magnetic immunoassays, and compartmentalized assays into robust lab-on-chip platforms.

In contrast to resin-based approaches, phaseguides can also involve a series of integrated techniques.[272] First, deep reactive ion etching (DRIE) was used to create channels in thick silicon. This was followed by the patterning of titanium nitride and gold onto two borosilicate glass wafers. Afterward, one of the glass wafers was anodically bonded to the silicon wafer. Inlets were then created on the second glass wafer through powder jetting, which was subsequently bonded via anodic bonding. Finally, the process concludes with the gold coating using octadecanethiol (ODT) and the creation of agarose membranes (Figure 9A). In this approach, the phaseguides were composed of titanium nitride (TiN), gold (Au), and ODT. Final device inserted in a holder could be seen in Figure 9Ai. Following this fabrication sequence, MDCK cells were seeded into the chambers, exhibiting normal proliferation and on-chip growth. At t = 24 h, cells had expanded throughout the chamber, while a brief TrypLE incubation (~12 min) at t = 24 h led to localized cell detachment. Subsequent on-chip and off-chip culture confirmed the viability and re-growth of cells over the next 24 h. These results demonstrate effective epithelial culture and dynamic cell behavior within a compartmentalized system, while enabling *in situ* passaging and harvest without mechanical disruption or the need for physical barriers between compartments.

Devices featuring PDMS-based phaseguides were also available,[273] where poly-D-lysine (PDL), a synthetic compound that improves cell adhesion and enhances protein adsorption by altering the surface charge of the culture substrate, was applied to form gel barriers in the same area (Figure 9B). To manufacture this device, the process begins with milling a mold from polycarbonate (Figure 9Bi), followed by soft lithography to produce the

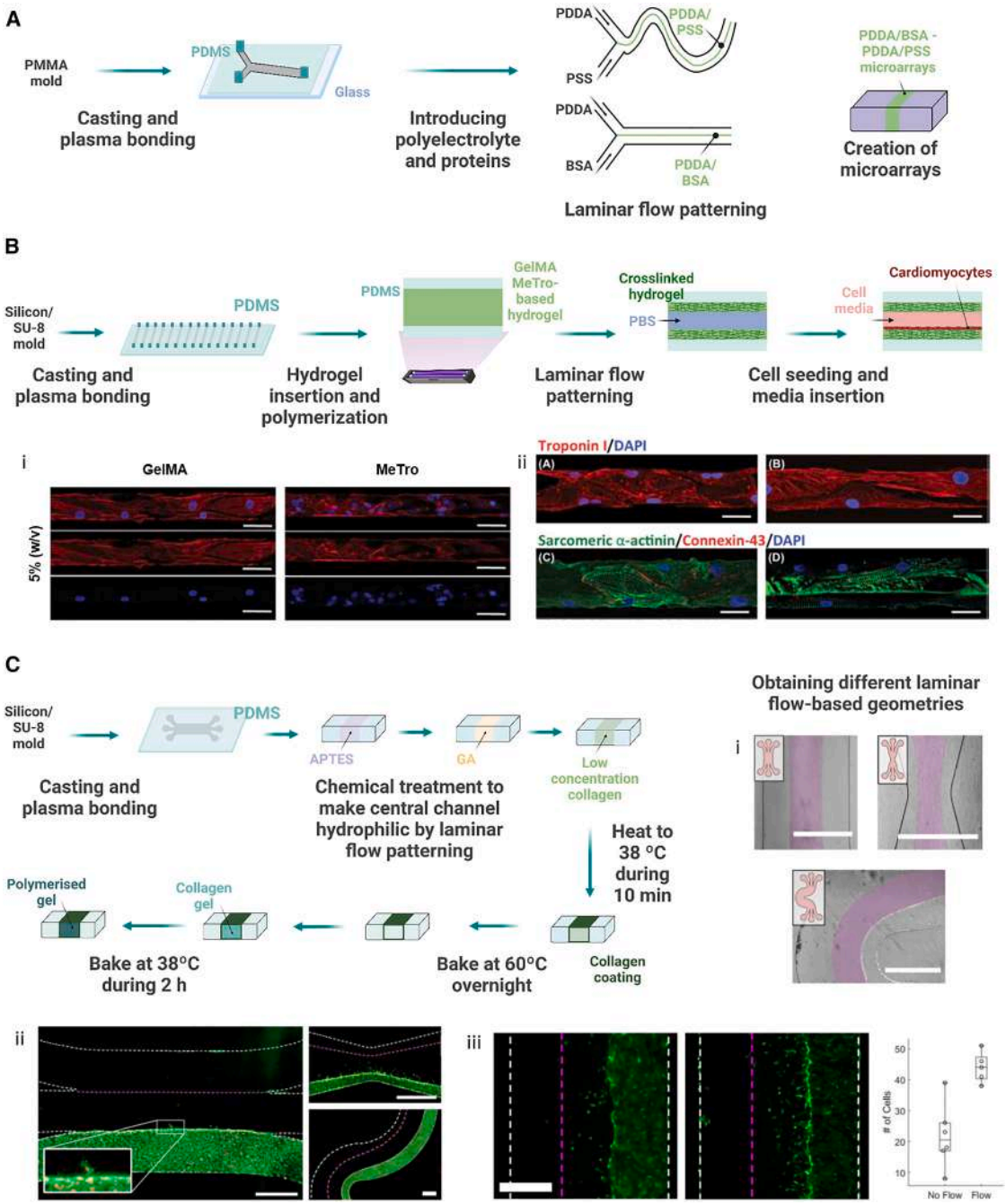


**Figure 8. Laminar flow patterning technique processes and OOC examples**

(A) Representation of polyelectrolyte micropatterning using laminar flow patterning adapted with permission from Shchukin et al.,[281] Wiley.

(B) Using laminar flow patterning for cardiomyocyte culture. (Bi) CM elongation and alignment inside MeTro- and GelMA-coated microchannels on day 6; stained with rhodamine-phalloidin/DAPI. Scale bars, 50 μm. (Bii) Confocal immunostaining on day 6: troponin (red)/nuclei (blue) and sarcomeric α-actinin (green)/connexin-43 (red)/nuclei (blue) in MeTro- or GelMA-coated channels. Scale bars, 50 μm. Adapted from Annabi et al.,[270] RSC, under CC BY 3.0 (https://creativecommons.org/licenses/by/3.0/).

(C) Patterning gels by surface treatments using laminar flow patterning. (Ci) Various gel geometries obtained via laminar flow; gel regions shown in pink. Scale bars, 1 mm. (Cii) HUVEC migration into patterned gels after 5 days; F-actin (green) and nuclei (red). Examples: simple channel, hourglass, and meandering channel. Scale bars, 500 μm. (Ciii) GFP-HUVECs show limited migration without cues (left), enhanced migration with *trans*-gel flow (right). The right-hand graph quantifies cell displacement; individual data points are shown, and box-and-whisker plots indicate quartiles. A significant difference is detected between conditions ($p < 0.05$). Scale bars, 500 μm. Adapted from Loessberg-Zahl et al.,[271] under CC BY 4.0 license (https://creativecommons.org/licenses/by/4.0/).

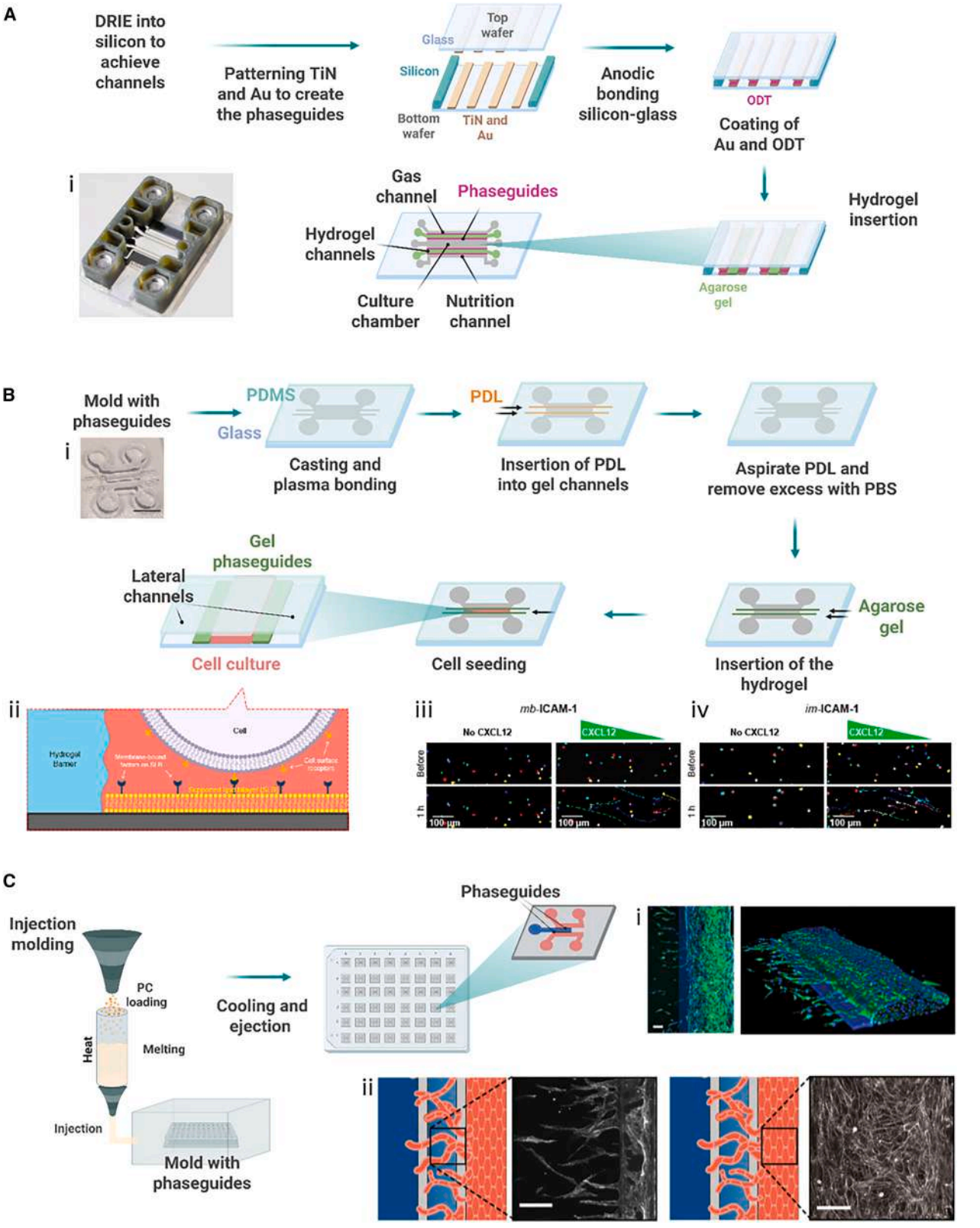


*(legend on next page)*

final PDMS device.[287] Before cell seeding, the device was treated with a 0.01% PDL solution to promote agarose anchoring; excess PDL was removed after 2 h of incubation. Subsequently, low-melting agarose was introduced to form physical gel barriers between compartments, defining stable diffusion zones within the channels. This platform was specifically designed for studying chemotaxis on supported lipid bilayers under controlled gradient conditions, with the cell culture chamber distributed appropriately as shown in Figure 9Bii. To this end, Jurkat T cells were exposed to a CXCL12 gradient in the presence of either membrane-bound ICAM-1 (mb-ICAM-1) or immobilized ICAM-1 (im-ICAM-1). Within 1 h, Jurkat cells exhibited directed migration toward the chemokine source on mb-ICAM-1 (Figure 9Biii), while movement on im-ICAM-1 remained largely undirected (Figure 9Biv)—demonstrating that the mode of adhesion molecule presentation significantly influences T cell guidance.

Devices featuring phaseguide architecture were also realized via injection molding in polycarbonate,[221,222,274,288] exemplified by the OrganoPlate 3-lane 64 (Mimetas) (Figure 9C). In the angiogenesis model developed by Soragni et al., endothelial vessels were cultured against a collagen type I matrix and exposed to pro- and anti-angiogenic conditions. The images shown (Figures 9Ci and 9Cii) illustrate sprout formation, lumenization, and actin remodeling, enabling quantification of angiogenic parameters such as sprout number, length, and barrier integrity. Beyond this application, the platform has supported large-scale phenotypic screening of ~1,537 kinase inhibitors across thousands of microvessels to evaluate angiogenic responses and compound toxicity. These injection-molded phaseguide-contained devices have been employed for a multitude of applications, including the long-term culture of mammalian cells,[272] the study of chemotaxis in lipid bilayers,[273] and the development of liver-on-chip[221] or vessel-on-chip models.[222]

Phaseguide-enabled systems have demonstrated considerable versatility in OOC applications by allowing precise fluid partitioning without physical membranes. Across diverse fabrication approaches, from high-precision DRIE-glass integration to accessible PDMS molding and scalable injection-molded platforms, phaseguides have enabled the formation of stable gel interfaces and reproducible compartmentalization. These technical features have supported a wide range of biological models, including dynamic epithelial culture with *in situ* passaging, immune cell chemotaxis on lipid substrates, and perfused angiogenic microvessels. Collectively, these studies highlight the potential of phaseguide-based devices to replicate complex microenvironments while supporting high-resolution cellular readouts and experimental throughput, advancing their value as modular, functional OOC platforms.

## Hydrogel photopatterning

Photolithography allows a photocrosslinkable culture 3D matrix to be patterned using a photomask. This technology for the development of engineered hydrogels suitable for cell culture has been under development for some time.[289–292] Nowadays, photopatterning has been applied to form hydrogel monolayers for subsequent cell seeding, generate free-floating microstructures that can be collected for further processing, produce cell-loaded micropillar arrays, and create structured tumor-on-chip or organ-on-chip culture systems.[275,277,293–295] These latter examples represent the innovative aspects comparable to the other technologies discussed in this section: OOC devices that demonstrate substantial advancements achieved by eliminating intervening materials between tissues *in vitro*. However, it should be taken into consideration that to replicate complex tissue structures in 3D cultures on-chip, it is essential to crosslink cell-laden hydrogels in a way that avoids cytotoxic effects while maintaining biomimetic mechanical properties and stability under fluid flow.

In this context, Ortiz-Cárdenas et al. developed a versatile *in situ* photopatterning method for generating spatially organized cell-laden hydrogels within a microfluidic platform (Figure 10A).[296] The device consisted of a PDMS layer bonded to glass by soft lithography and functionalized to allow covalent anchoring of photocrosslinked gels. Precursor solutions of gelatin-based hydrogels—either methacryloyl-modified gelatin (GelMA) or thiol-modified gelatin (GelSH) crosslinked with norbornene—together with a biocompatible photoinitiator were introduced into the chamber and exposed to collimated violet-blue light through a photomask. This process yielded free-standing hydrogel structures of various shapes, which could be altered simply by changing the mask. Sequential exposures enabled the creation of complex architectures such as concentric features or adjacent multi-region constructs (Figure 10Ai). Importantly, while GelMA hydrogels tended to swell and degrade under flow, GelSH provided accurate feature definition and robust mechanical stability during perfusion. The system was validated biologically using primary human $CD4^+$ T lymphocytes. High-density suspensions ($>10^7$ cells $mL^{-1}$) were encapsulated without impairing gelation, and patterned regions showed uniform cell distribution in three dimensions with minimal adhesion outside the targeted features. Viability remained high (>85%) after 12 h of continuous flow, confirming cytocompatibility. Furthermore, multi-population geometries could be generated, with distinct but contiguous regions containing different fluorescently labeled cell groups

**Figure 9. Examples of fabrication processes for phaseguide-based devices**

(A) Microfluidic device based on phaseguides for on-chip cultivation of mammalian cells. Fabrication process step by step. (Ai) Assembly of a microfluidic chip clamped between 3D-printed holders and sealed with O-rings. Adapted from Bunge et al.,[272] under CC BY 4.0 license (https://creativecommons.org/licenses/by/4.0/).

(B) Phaseguide devices were manufactured through soft lithography and injection molding using polycarbonate as a substrate. (Bi) Polycarbonate mold. (Bii) Enlarged view of culture chamber. (Biii–Biv) Jurkat chemotaxis toward CXCL12 in diffusion microdevice on mb-ICAM-1 vs. im-ICAM-1; trajectories recorded after 1 h. Adapted from Hao et al.,[273] under CC BY 4.0 license.

(C) Angiogenesis assay in the phaseguide-based OrganoPlate 3-lane 64 fabricated by injection molding. (Ci) Confocal z stack max projection and 3D reconstruction (DNA, blue and F-actin, green). (Cii) Angiogenesis inhibition quantified in gel region; toxicity assessed via vessel morphology. Scale bars, 100 μm. Adapted from Soragni et al.,[274] under CC BY 4.0 license.

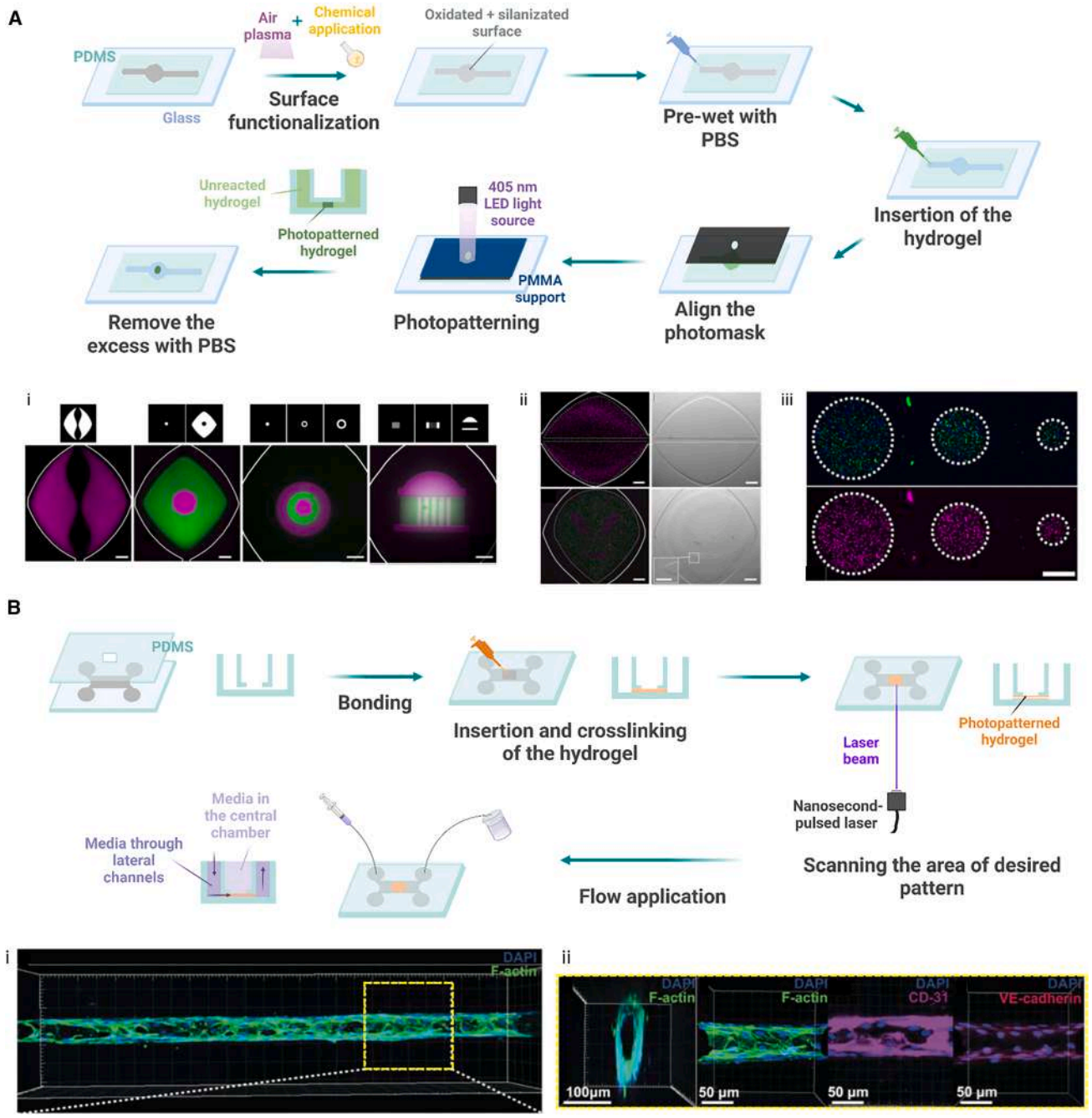


**Figure 10. Hydrogel photopatterning processes and biomimetic on-chip applications**

(A) T cells hydrogels photopatterned on-chip. (Ai) On-chip photo-patterning of GelSH hydrogels enables diverse geometries. From left to right: NHS-rhodamine-labeled hydrogel (magenta) forming a curved channel; a central island (magenta) surrounded by NHS-fluorescein-labeled GelSH (green); concentric circles produced in three steps with alternating labels; and a three-step UVA Rotunda pattern. Photomasks are shown above each panel. Scale bars, 500 μm. (Aii) Photo-patterned, cell-laden hydrogel constructs. Top: fluorescence/brightfield images of a 3D culture (magenta cells) arranged into two lobes, with a straight channel between and a curved channel around them for media distribution. Bottom: two cell populations patterned into a lobular geometry (magenta NHS-rhodamine vs. green CFSE). Inset: enlarged view of the interface. Scale bars, 500 μm; inset 250 μm. Dashed lines outline hydrogels; white lines mark chamber edges. (Aiii) On-chip microarray of human $CD4^+$ T cells after overnight culture. Top: circular GelSH arrays with NHS-rhodamine-prelabeled cells. Bottom: viability staining with Calcein-AM (green) and DAPI (blue). Scale bars, 250 μm. Adapted from Ortiz-Cárdenas et al.,[296] under CC BY 4.0 license (https://creativecommons.org/licenses/by/4.0/).

(B) Networks in 3D hydrogels photopatterning. (Bi) Confocal 3D reconstruction of hollow HUVEC tube in collagen I. (Bii) Transversal and frontal planes showing CD31 and VE-cadherin immunostaining. Adapted with permission from Brandenberg Lutolf,[276] Wiley.

(Figures 10Aii and 10Aiii). This work demonstrated that photopatterning enables precise spatial organization of fragile immune cells within perfused 3D constructs.

An alternative method for producing these gels involves a sequence adapted from techniques used in the fabrication of mini intestines-on-chip,[277] with the background of previously developed technology (Figure 10B).[276] Here, soft lithography was first used to build the microfluidic device. The extracellular matrix was then prepared by combining type I collagen from bovine dermis with Matrigel, which was introduced into the chamber and polymerized. Micropatterns were subsequently inscribed using a nanosecond laser system programmed with the desired design. Laser power and etching speed were calibrated to define channel height and architecture. With this method, researchers produced perfusable, biomimetic vascular networks within collagen matrices, enabling endothelial cells to self-assemble into hollow tubular structures resembling native microvessels (Figure 10Bi). The functional integrity of these constructs was verified by immunostaining for endothelial markers CD31 and VE-cadherin, confirming junction formation and vascular polarization (Figure 10Bii).

Hydrogel photopatterning enables the spatial definition of soft, cell-laden matrices within microfluidic environments, offering both geometric precision and physiological relevance. The first study demonstrated its application to organize primary human lymphocytes into well-defined 3D geometries under flow, confirming its suitability for immunologically relevant models.[296] A tumor-on-chip platform employing similar principles further highlighted the capacity of photopatterning to investigate immune-cancer interactions by enabling selective T cell infiltration into tumor spheroids in response to chemokine cues.[275] In the other previously exposed application, laser-based micropatterning within collagen matrices allowed the generation of perfusable microvascular networks, where endothelial cells self-assembled into lumenized tubular structures.[276] A comparable fabrication workflow was also applied to intestine-on-chip systems, emphasizing the adaptability of this method across diverse tissue types.[277] Collectively, these examples illustrate how hydrogel photopatterning can be harnessed to reproduce architecturally and functionally relevant microtissues, thereby expanding the capabilities of OOC technology.

### Surface treatment patterning

Recently, a versatile fabrication technique was introduced that enables full contact between adjacent compartments while allowing customizable channel geometries depending on the desired microenvironment.[212] The fabrication process of the device comprises three main stages (Figure 11A). Initially, the material that constitutes the channels and base was cut using a cutting plotter. Subsequently, a surface treatment was applied to the unmasked area, rendering it hydrophilic and thereby creating the desired design. Finally, a thermal bonding process assembles all the device's components. In this instance, a thermoplastic material, COP, was used. This technique allows the generation of devices featuring a central chamber (Be-Gradient) and three connected compartments (Multicompartment), each tailored to distinct biological applications (Figure 11B).[212,278]

In the Be-Gradient configuration (Figure 11C), the central chamber design is highly flexible and can be photopatterned into shapes such as waves, hammers, or diamonds, as demonstrated using rhodamine flow assays (Figure 11Ci). This device was applied to develop a blood-brain barrier (BBB) model by seeding neurovascular components in a spatially defined manner. The chip supported the co-culture of endothelial (hCMEC/D3) (Figure 11Cii), astrocytic, and pericytic cells, with evidence of tight junction formation (ZO-1 and VE-cadherin staining), cell viability, and polarization under flow (Figure 11Ciii). This setup enabled the study of cell-cell interactions across the BBB and confirmed the ability of this platform to replicate essential features of the neurovascular interface, validating it as a robust OOC system. Furthermore, the same Be-Gradient platform was adapted for the detection of volatile organic compounds (VOCs) released by cancer cells, offering a novel, non-invasive approach to monitor tumor progression in real time through VOC diffusion dynamics and sensor integration, thereby broadening its potential utility in cancer diagnostics and metabolic profiling.[214]

The same fabrication technique was adapted to create a Multicompartment device where plasma treatment defined three gel-seeding regions, enabling total hydrogel confinement and full interface contact between adjacent ECM compartments (Figure 11D). By tuning the hydrophilic mask design and bonding strategy, the overlap between compartments and channels could be adjusted, offering controllable tissue-tissue connectivity (Figure 11Di). This was exploited to model the glioblastoma (GBM) tumor microenvironment by integrating a tumor chamber, adjacent ECM compartments, and immune-access channels. The platform supported stiffness-dependent changes in tumor cell morphology (Figure 11Dii), real-time immune cell infiltration, and anti-cancer drug testing. For instance, immune cell migration toward tumor spheroids was modulated by ECM stiffness (2 mg $mL^{-1}$ vs. 4 mg $mL^{-1}$ collagen) (Figure 11Diii) and significantly suppressed upon treatment with temozolomide (TMZ), with quantitative cell tracking performed via time-lapse imaging (Figure 11Div).

The surface treatment patterning technique offers precise and flexible control over microfluidic chamber geometries and compartmentalization without the need for physical barriers. This fabrication approach enables rapid prototyping of sterilizable thermoplastic devices adaptable to a variety of experimental designs. Biologically, the Be-Gradient platform facilitates the development of a physiologically relevant BBB model, characterized by endothelial tight junction formation and compatibility with perfusion flow. Meanwhile, the Multicompartment system supports the co-culture of tumor and immune cells within tunable extracellular matrix environments, providing a robust and versatile OOC model to investigate tumor microenvironment dynamics and therapeutic efficacy. Collectively, these advances demonstrate the technique's significant potential to produce customizable, biologically faithful platforms for complex *in vitro* modeling in OOC research.

## COMMERCIAL PREVALENCE OF FABRICATION METHODS AND MATERIALS

Building on the fabrication strategies described above, it is essential to contextualize how these techniques translate into

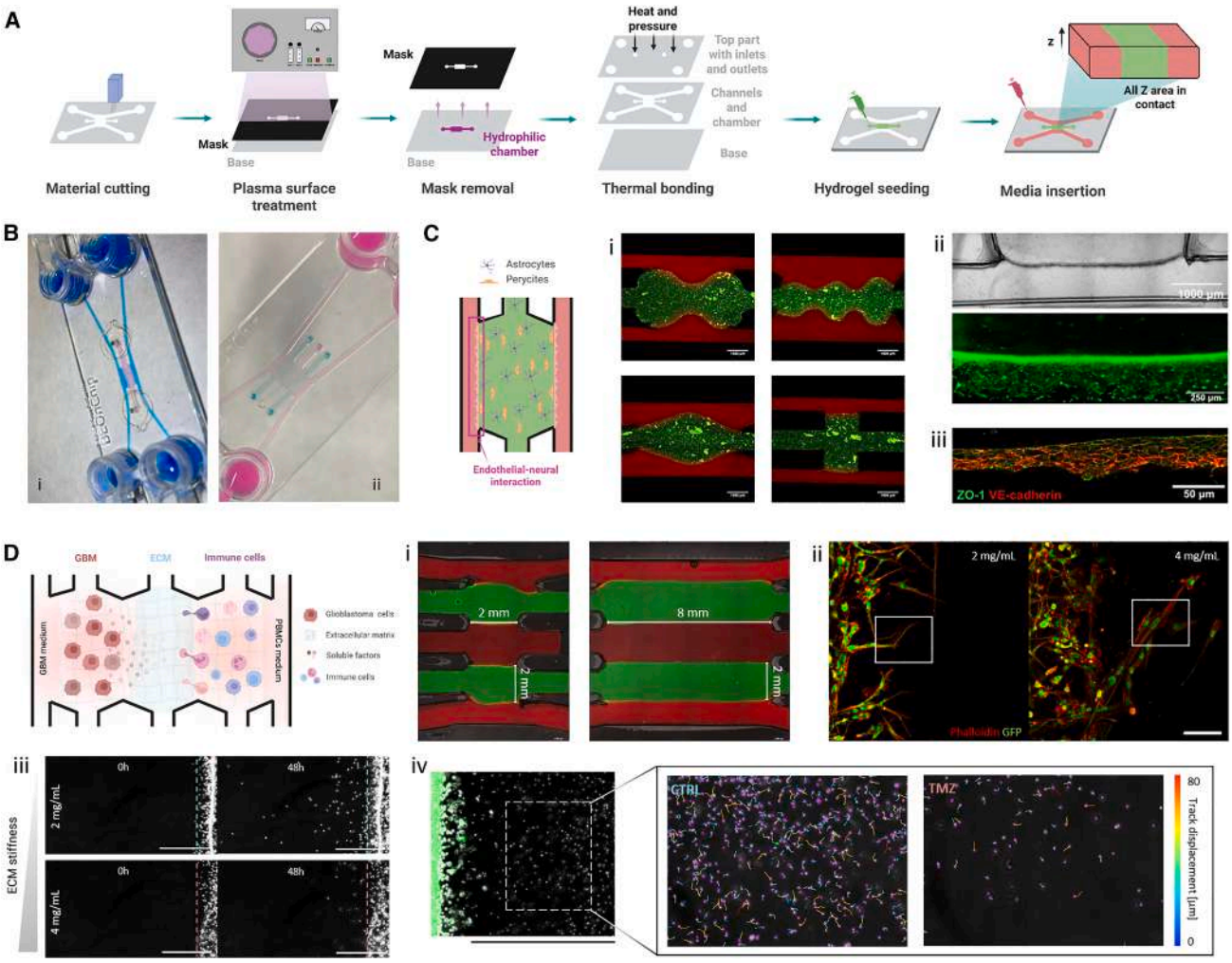


**Figure 11. Surface treatment patterning**

(A) Fabrication technique steps.

(B) Both devices. (Bi) Be-Gradient and (Bii) Multicompartment.

(C) BBB-assembly in the Be-Gradient; schematic representation of the neurovascular cell arrangement in the microdevice. (Ci) Customizable design: patterns of the central chamber: guitar, waves, diamond, and hammer during the flow validation in the devices by perfusing a rhodamine solution through the side channels. Scale bars, 1,000 µm. (Cii) Bright-field and fluorescence images of BBB with live cell marker. Scale bars, 1,000 µm (bright-field), 250 µm (fluorescence). (Ciii) Immunofluorescence of tight-junction markers in hCMEC/D3. Scale bars, 50 µm. (Bi and C) adapted from Olaizola-Rodrigo et al.,[212] RSC, under CC BY 3.0 (https://creativecommons.org/licenses/by/3.0/).

(D) GBM tumor microenvironment in the Multicompartment device; schematic representation of the model. (Di) Device design customs. Smaller and larger interconnection areas; chambers seeded with hydrogel/fluorospheres and lateral channels perfused with rhodamine. (Dii) Fluorescence images of F-actin (red) in U-251 MG GFP+ cells at different ECM stiffness (2 vs. 4 mg $mL^{-1}$). Scale bars, 100 µm. (Diii) Phase-contrast images of immune cell infiltration into 2 vs. 4 mg $mL^{-1}$ ECM toward GBM cells. Scale bars, 500 µm. (Div) TMZ reduces immune cell infiltration; time-lapse trajectories color-coded by displacement (red = long, blue = short). Scale bars, 1,000 µm. (Bii and D) adapted from Bayona et al.,[278] under CC BY 4.0 license (https://creativecommons.org/licenses/by/4.0/).

commercially available OOC products. Although precise market share values per material or fabrication methods are rarely disclosed, converging evidence from vendor documentation, industrial reports, and recent reviews indicates a clear transition trend from academic-scale prototyping to scalable thermoplastic-based manufacturing.[297,298]

PDMS-based systems remain widely used in research and commercial fields. Some examples of commercial platforms include Emulate, Inc.'s Organ-Chip systems, whose multilayer PDMS architecture has been discussed earlier in this review, and TissUse GmbH's HUMIMIC devices, which integrate elastomeric microfluidic layers with rigid supporting components and reusable perfusion instruments. These chips are typically intended for single use to ensure sterility and consistent surface properties, whereas the associated fluidic modules or control units are designed for repeated use. PDMS allows precise microfluidic feature fabrication, yet its inherent limitations have prompted exploration of thermoplastic materials to facilitate larger-scale and standardized manufacturing.[2,121,126,299]

Thermoplastic-based platforms are increasingly adopted for commercial use due to their scalability, chemical stability, cost-effectiveness, and compatibility with automated fabrication. Companies such as MIMETAS, Beonchip S.L., AIM Biotech, CN Bio Innovation, and InSphero, exemplify this trend. Their products are typically injection-molded or hot-embossed thermoplastic consumables, while associated perfusion instruments or holders are reusable. Publicly available product information from several vendors confirms the use of COC, COP, or PS families of thermoplastics, chosen for their optical transparency, low non-specific adsorption, and regulatory acceptance. These devices are compatible with either active perfusion systems (as in Beonchip or AIM Biotech) or passive flow by gravitational rocking (as in MIMETAS OrganoPlate), highlighting the diversity of design strategies across manufacturers.[3,300–304] Beyond these design aspects, injected molded thermoplastics can be mass-produced under cleanroom-independent conditions, sterilized through established processes such as gamma irradiation or ethylene oxide treatment, and integrated within Good Manufacturing Practice (GMP)-compatible workflows, which together ensure product consistency and quality for pharmaceutical and diagnostic applications.[144,305–308]

As with PDMS-based devices, most thermoplastic platforms are designed for single use, whereas associated instruments, pumps, and perfusion controllers are reusable. Vendor and distributor listings consulted show that integrated kits including reusable components are marketed at higher bundled prices, while standalone thermoplastic chip packs are listed at significantly lower per-unit costs, consistent with high-throughput thermoplastic production.[301,302,309–312] While absolute pricing varies, the general trend supports a lower cost per unit for thermoplastic chips compared with PDMS prototypes.

Sustainability and device life cycle management are also becoming important design considerations. Current strategies include the use of recyclable thermoplastics compatible with injection molding, modular device architectures that separate the biological compartment from reusable mechanical housings, and design miniaturization to reduce material and reagent consumption.[313,314] Such approaches align with circular-economy principles and contribute to lowering the environmental footprint of OOC technologies.

In brief, the commercial OOC field currently exhibits a dual structure: PDMS-based systems dominate academic research and early validation stages, while injection-molded thermoplastic platforms underpin the expanding industrial and preclinical market.[315] Emerging methods—such as additive manufacturing, advanced surface modifications, and barrier-free designs—are being incorporated for specialized applications, further diversifying the technological landscape. Ultimately, material choice remains central not only to biological performance but also to economic feasibility, sustainability, and regulatory translation.

## Conclusions and future perspectives

The evolution of fabrication techniques and materials for OOC devices has markedly enhanced our capacity to reproduce physiological environments *in vitro*. Conventional approaches, beginning with photolithography, enabled the first microchannel networks with high precision, but the reliance on cleanroom infrastructure and rigid substrates restricted accessibility and biological versatility. As discussed above, photolithography is now predominantly employed for the fabrication of molds and membranes rather than complete devices. Replication-based methods—including soft lithography, hot embossing, and microinjection molding—lowered prototyping barriers and improved reproducibility, though each entails trade-offs. Soft lithography remains the most widely used method due to its accessibility and ease of fabrication for a broad range of users. However, advances in alternative materials and techniques are gradually expanding the range of options beyond PDMS. Hot embossing is increasingly explored with novel thermoplastics, but tooling costs and thermal stresses continue to limit its versatility. Injection molding remains the principal method for large-scale production, which is critical for commercial applications, though it is constrained by limited material choices and potential thermal damage. Xurography offers low-cost, user-friendly fabrication accessible to non-specialists but lacks the resolution and durability required for complex designs. Furthermore, the achievable resolution is constrained by the cutting plotter or laser, and material choice often dictates the suitable cutting method. Its effectiveness also depends on the bonding strategy: adhesive bonding may introduce auto-fluorescence or trap cells, while adhesive, thermal, or chemical bonding can produce bubbles if sealing is incomplete. 3D printing, through vat polymerization, inkjet, or extrusion, delivers unmatched design freedom and on-demand customization, yet printable materials rarely combine optical transparency, biocompatibility, and surface smoothness without post-processing. Nonetheless, 3D printing has become particularly influential over the past decade by democratizing access to device fabrication. While the drawbacks of producing entire microfluidic systems remain, it has proven highly valuable for manufacturing individual components or for the direct bioprinting of tissues, where ongoing advances in printable biomaterials are greatly expanding its relevance. Together, these methods have provided a versatile toolkit for OOC fabrication but using them individually often introduce inert barriers—membranes, micropillars, or other interfaces—that restrict the physiological relevance of tissue-tissue interactions.

Building upon this foundation, recent barrier-free strategies represent not a complete departure, but rather an integration and refinement of traditional methods. Techniques such as laminar flow patterning, phaseguide technology, hydrogel photopatterning, and surface treatment patterning draw directly on principles from lithography, replication, or additive manufacturing while adapting them to remove non-physiological interfaces. Laminar flow patterning enables full contact between hydrogels and tissues, creating seamless laminar structures while simultaneously validating the establishment of fluid flow—an essential yet still evolving aspect of OOC devices. Phaseguide technology ensures that each compartment remains precisely confined to its intended compounds, gels, or cells, while also creating zones of maximal interfacial contact between them. Hydrogel photopatterning allows the recreation of micro- and nanoscale cellular geometries, emulating human biological organization with unprecedented fidelity. Surface treatment patterning further expand the design space by enabling the creation of virtually any geometry without compromising cell-cell or

tissue-tissue interactions, ensuring complete continuity across compartments. By leveraging the strengths of established fabrication while addressing their shortcomings, these approaches enable devices that are more physiologically faithful than earlier generations. They open the way to reproducing direct physiological interactions, more accurate paracrine signaling, and complex microenvironmental cues. Nonetheless, their implementation remains technically demanding. Each strategy presents specific obstacles to broader adoption: laminar flow patterning suffers from sensitivity to flow stability and diffusion; phaseguide technology requires precise molding and offers limited geometric flexibility; hydrogel photopatterning is constrained by light penetration, hydrogel fragility, and cell viability under exposure; and surface treatment patterning, while geometry-agnostic, depends on the resolution and reproducibility of the technique tools. These aspects represent key areas for refinement toward substantial improvement of OOC devices and their closest approximation to *in vivo* models.

Looking ahead, several bottlenecks must be addressed. The development of new biomaterials that combine thermoplastic processability with low absorption, tunable permeability, and regulatory acceptance is essential. Bonding and integration technologies must evolve to ensure robust sealing without compromising structural fidelity. Embedding multimodal sensing—optical, electrical, or biochemical—into fabrication workflows will provide real-time monitoring and expand analytical potential. Above all, standardization and scale-up are needed: academic prototypes must transition into reproducible, manufacturable devices aligned with industrial quality control and regulatory standards.

Beyond these manufacturing and standardization requirements, the regulatory integration of OOC technologies has become a decisive step for their preclinical and industrial translation. Ongoing initiatives by the FDA through its Innovative Science and Technology Approaches for New Drugs (ISTAND) pilot program, the European Medicines Agency (EMA) on NAMs, and European efforts as the CEN-CENELEC Focus Group on OOC standardization are defining evidentiary and reporting criteria for regulatory qualification.[298,316–319] These frameworks highlight reproducibility, well-defined contexts of use, transparent data sharing, and cross-laboratory validation as prerequisites for building scientific confidence.[319,320] Importantly, standardization runs in parallel to, but does not coincide with, formal device regulation: the former harmonizes performance and reporting, while the latter governs manufacturing quality and safety. Continued coordination among developers, regulators, and industry stakeholders will therefore be essential to transform OOC platforms from exploratory research tools into qualified, human-relevant systems capable of informing regulatory decision-making.

As regulatory confidence and technical maturity advance in parallel, the next stage will involve integrating barrier-free fabrication within multi-organ architectures, advancing toward body-on-chip systems. Whether by connecting separate OOC units through fluidic circuits or consolidating multiple organ models into unified platforms, success will depend on solving challenges such as mechanical stimulation, nutrient gradients, and inter-organ communication. These advances will be decisive for the clinical and industrial translation of OOCs, particularly in drug development, personalized medicine, and regenerative therapies.

In summary, the trajectory of OOC fabrication reflects a progressive layering of methods: from photolithography and replication to xurography and 3D printing, each generation has introduced capabilities while revealing limitations. The most recent barrier-free strategies arise from combining and adapting these established methods, exploiting their strengths to achieve higher biomimicry. By critically integrating traditional and emerging fabrication within scalable frameworks, the field is poised to deliver OOC platforms that are not only physiologically predictive but also practical for widespread adoption in research, industry, and medicine.

## ACKNOWLEDGMENTS

Claudia Olaizola-Rodrigo would like to acknowledge the financial support received from the Spanish Government through a research grant provided by the MINECO fellowship (DIN 2020-011544). We also thank BioRender for providing the platform to create the figures used in this study.

## AUTHOR CONTRIBUTIONS

C.O.-R., conceptualization, investigation, visualization, writing—original draft, and writing—review & editing. C.B., writing—review & editing. S.O., supervision, funding acquisition, and writing—review & editing. R.M., supervision, funding acquisition, and writing—review & editing.

## DECLARATION OF INTERESTS

R.M. and S.O. are promoters and consultants for Beonchip S.L. Beonchip S.L. does not benefit or take part in any economic decisions of this work.

## REFERENCES

1. Bhatia, S.N., and Ingber, D.E. (2014). Microfluidic organs-on-chips. Nat. Biotechnol. *32*, 760–772. https://doi.org/10.1038/nbt.2989.
2. Leung, C.M., De Haan, P., Ronaldson-Bouchard, K., Kim, G.-A., Ko, J., Rho, H.S., Chen, Z., Habibovic, P., Jeon, N.L., Takayama, S., et al. (2022). A guide to the organ-on-a-chip. Nat. Rev. Methods Primers *2*, 33. https://doi.org/10.1038/s43586-022-00118-6.
3. Nahak, B.K., Mishra, A., Preetam, S., and Tiwari, A. (2022). Advances in Organ-on-a-Chip Materials and Devices. ACS Appl. Bio Mater. *5*, 3576–3607. https://doi.org/10.1021/acsabm.2c00041.
4. Chen, X., Zhang, Y.S., Zhang, X., and Liu, C. (2021). Organ-on-a-chip platforms for accelerating the evaluation of nanomedicine. Bioact. Mater. *6*, 1012–1027. https://doi.org/10.1016/j.bioactmat.2020.09.022.
5. Reyes, D.R., Esch, M.B., Ewart, L., Nasiri, R., Herland, A., Sung, K., Piergiovanni, M., Lucchesi, C., Shoemaker, J.T., Vukasinovic, J., et al. (2024). From animal testing to *in vitro* systems: advancing standardization in microphysiological systems. Lab Chip *24*, 1076–1087. https://doi.org/10.1039/D3LC00994G.
6. Van Berlo, D., Van De Steeg, E., Amirabadi, H.E., and Masereeuw, R. (2021). The potential of multi-organ-on-chip models for assessment of drug disposition as alternative to animal testing. Curr. Opin. Toxicol. *27*, 8–17. https://doi.org/10.1016/j.cotox.2021.05.001.
7. Shinha, K., Nihei, W., Ono, T., Nakazato, R., and Kimura, H. (2020). A pharmacokinetic–pharmacodynamic model based on multi-organ-on-a-chip for drug–drug interaction studies. Biomicrofluidics *14*, 044108. https://doi.org/10.1063/5.0011545.
8. Donkers, J.M., Van Der Vaart, J.I., and Van De Steeg, E. (2023). Gut-on-a-Chip Research for Drug Development: Implications of Chip Design on

Preclinical Oral Bioavailability or Intestinal Disease Studies. Biomimetics *8*, 226. https://doi.org/10.3390/biomimetics8020226.

9. Picollet-D'hahan, N., Zuchowska, A., Lemeunier, I., and Le Gac, S. (2021). Multiorgan-on-a-Chip: A Systemic Approach To Model and Decipher Inter-Organ Communication. Trends Biotechnol. *39*, 788–810. https://doi.org/10.1016/j.tibtech.2020.11.014.
10. Huh, D., Matthews, B.D., Mammoto, A., Montoya-Zavala, M., Hsin, H.Y., and Ingber, D.E. (2010). Reconstituting Organ-Level Lung Functions on a Chip. Science *328*, 1662–1668. https://doi.org/10.1126/science.1188302.
11. Miranda, I., Souza, A., Sousa, P., Ribeiro, J., Castanheira, E.M.S., Lima, R., and Minas, G. (2021). Properties and Applications of PDMS for Biomedical Engineering: A Review. J. Forensic Biomech. *13*, 2. https://doi.org/10.3390/jfb13010002.
12. U.S. Food and Drug Administration (2025). FDA Announces Plan to Phase Out Animal Testing Requirement for Monoclonal Antibodies and Other Drugs (FDA News Release). https://www.fda.gov/news-events/press-announcements/fda-announces-plan-phase-out-animal-testing-requirement-monoclonal-antibodies-and-other-drugs?.
13. Grand View Research (2025). Organ-on-a-Chip Market Size, Share & Trends Analysis Report. https://www.grandviewresearch.com/industry-analysis/organ-on-a-chip-market-report.
14. Kochhar, J.S., Chan, S.Y., Ong, P.S., Lee, W.G., and Kang, L. (2013). Microfluidic devices for drug discovery and analysis. In Microfluidic Devices for Biomedical Applications (Elsevier), pp. 231–280. https://doi.org/10.1533/9780857097040.2.231.
15. Weibel, D.B., and Whitesides, G.M. (2006). Applications of microfluidics in chemical biology. Curr. Opin. Chem. Biol. *10*, 584–591. https://doi.org/10.1016/j.cbpa.2006.10.016.
16. El-Ali, J., Sorger, P.K., and Jensen, K.F. (2006). Cells on chips. Nature *442*, 403–411. https://doi.org/10.1038/nature05063.
17. deMello, A.J. (2006). Control and detection of chemical reactions in microfluidic systems. Nature *442*, 394–402. https://doi.org/10.1038/nature05062.
18. Whitesides, G.M. (2006). The origins and the future of microfluidics. Nature *442*, 368–373. https://doi.org/10.1038/nature05058.
19. Zhang, M., Gong, X., and Wen, W. (2009). Manipulation of microfluidic droplets by electrorheological fluid. Electrophoresis *30*, 3116–3123. https://doi.org/10.1002/elps.200900119.
20. Nathanson, H.C., and Wickstrom, R.A. (1965). A resonant gate surface transistor with high-q bandpass properties. IEEE Trans. Electron Devices *12*, 507. https://doi.org/10.1109/T-ED.1965.15583.
21. Nathanson, H.C., Newell, W.E., Wickstrom, R.A., and Davis, J.R. (1967). The resonant gate transistor. IEEE Trans. Electron Devices *14*, 117–133. https://doi.org/10.1109/T-ED.1967.15912.
22. Grayson, A.C.R., Shawgo, R.S., Johnson, A.M., Flynn, N.T., Li, Y., Cima, M.J., and Langer, R. (2004). A BioMEMS Review: MEMS Technology for Physiologically Integrated Devices. Proc. IEEE *92*, 6–21. https://doi.org/10.1109/JPROC.2003.820534.
23. Goldstein, Y., Grover, N.B., Chang, C., Jelli, A., Andre, J., Mark, P., Goodwin, A., and Mark, P. (1979). A Gas Chromatographic Air Analyzer Fabricated (IEEE), pp. 1880–1886.
24. Jurina, T., Sokač Cvetnić, T., Šalić, A., Benković, M., Valinger, D., Gajdoš Kljusurić, J., Zelić, B., and Jurinjak Tušek, A. (2023). Application of Spectroscopy Techniques for Monitoring (Bio)Catalytic Processes in Continuously Operated Microreactor Systems. Catalysts *13*, 690. https://doi.org/10.3390/catal13040690.
25. Duffy, D.C., McDonald, J.C., Schueller, O.J., and Whitesides, G.M. (1998). Rapid Prototyping of Microfluidic Systems in Poly(dimethylsiloxane). Anal. Chem. *70*, 4974–4984. https://doi.org/10.1021/ac980656z.
26. Sin, A., Chin, K.C., Jamil, M.F., Kostov, Y., Rao, G., and Shuler, M.L. (2004). The Design and Fabrication of Three-Chamber Microscale Cell Culture Analog Devices with Integrated Dissolved Oxygen Sensors. Biotechnol. Prog. *20*, 338–345. https://doi.org/10.1021/bp034077d.
27. Martinez, A.W., Phillips, S.T., Butte, M.J., and Whitesides, G.M. (2007). Patterned Paper as a Platform for Inexpensive, Low-Volume, Portable Bioassays. Angew. Chem. Int. Ed. *46*, 1318–1320. https://doi.org/10.1002/anie.200603817.
28. Huh, D., Fujioka, H., Tung, Y.C., Futai, N., Paine, R., 3rd, Grotberg, J.B., and Takayama, S. (2007). Acoustically detectable cellular-level lung injury induced by fluid mechanical stresses in microfluidic airway systems. Proc. Natl. Acad. Sci. USA *104*, 18886–18891. https://doi.org/10.1073/pnas.0610868104.
29. Manz, A., Graber, N., and Widmer, H.M. (1990). Miniaturized total chemical analysis systems: A novel concept for chemical sensing. Sensor. Actuator. B Chem. *1*, 244–248. https://doi.org/10.1016/0925-4005(90)80209-I.
30. Vilkner, T., Janasek, D., and Manz, A. (2004). Micro Total Analysis Systems. Recent Developments. Anal. Chem. *76*, 3373–3385. https://doi.org/10.1021/ac040063q.
31. Erickson, D., and Li, D. (2004). Integrated microfluidic devices. Anal. Chim. Acta *507*, 11–26. https://doi.org/10.1016/j.aca.2003.09.019.
32. Convery, N., and Gadegaard, N. (2019). 30 years of microfluidics. Micro Nano Eng. *2*, 76–91. https://doi.org/10.1016/j.mne.2019.01.003.
33. Widmer, H.M. (1990). Miniaturized Total Chemical Analysis Systems : a Novel Concept for Chemical Sensing. Sensor. Actuator. B Chem. *1*, 244–248.
34. Fan, Z., Ludi, H., and Widmers, H.M. (1992). Capillary Electrophoresis and Sample Injection Systems Integrated on a Planar Glass Chip. Anal. Chem. *64*, 1926–1932.
35. Manz, A., Harrison, D.J., Verpoorte, E.M.J., Fettinger, J.C., Paulus, A., Lüdi, H., and Widmer, H.M. (1992). Planar chips technology for miniaturization and integration of separation techniques into monitoring systems: Capillary electrophoresis on a chip. J. Chromatogr. A *593*, 253–258. https://doi.org/10.1016/0021-9673(92)80293-4.
36. Xia, Y., and Whitesides, G.M. (1998). Soft Lithography. Angew. Chem. Int. Ed. Engl. *37*, 550–575. https://doi.org/10.1002/(SICI)1521-3773(19980316)37:5%253C550::AID-ANIE550%253E3.0.CO;2-G.
37. Alexandre-Franco, M.F., Kouider, R., Kassir Al-Karany, R., Cuerda-Correa, E.M., and Al-Kassir, A. (2024). Recent Advances in Polymer Science and Fabrication Processes for Enhanced Microfluidic Applications: An Overview. Micromachines *15*, 1137. https://doi.org/10.3390/mi15091137.
38. Zhang, J.X.J., and Hoshino, K. (2014). Microfluidics and Micro Total Analytical Systems. Mol. Sens. Nanodevices, 103–168. https://doi.org/10.1016/b978-1-4557-7631-3.00003-x.
39. Manz, A., Harrison, D.J., Verpoorte, E.M.J., Fettinger, J.C., Paulus, A., Lüdi, H., and Widmer, H.M. (1992). Planar chips technology for miniaturization and integration of separation techniques into monitoring systems Capillary electrophoresis on a chip. J. Chromatogr. A *593*, 253–258.
40. Ho, C.T., Lin, R.Z., Chang, W.Y., Chang, H.Y., and Liu, C.H. (2006). Rapid heterogeneous liver-cell on-chip patterning via the enhanced field-induced dielectrophoresis trap. Lab Chip *6*, 724–734. https://doi.org/10.1039/b602036d.
41. Kimura, H., Yamamoto, T., Sakai, H., Sakai, Y., and Fujii, T. (2008). An integrated microfluidic system for long-term perfusion culture and on-line monitoring of intestinal tissue models. Lab Chip *8*, 741–746. https://doi.org/10.1039/b717091b.
42. Boyden, S. (1962). The chemotactic effect of mixtures of antibody and antigen on polymorphonuclear leucocytes. J. Exp. Med. *115*, 453–466. https://doi.org/10.1084/jem.115.3.453.
43. Martinez, A.W., Phillips, S.T., and Whitesides, G.M. (2008). Three-dimensional microfluidic devices fabricated in layered paper and tape. Proc. Natl. Acad. Sci. USA *105*, 19606–19611. https://doi.org/10.1073/pnas.0810903105.

44. Martinez, A.W., Phillips, S.T., Whitesides, G.M., and Carrilho, E. (2010). Diagnostics for the Developing World: Microfluidic Paper-Based Analytical Devices. Anal. Chem. *82*, 3–10. https://doi.org/10.1021/ac9013989.

45. Yager, P., Domingo, G.J., and Gerdes, J. (2008). Point-of-Care Diagnostics for Global Health. Annu. Rev. Biomed. Eng. *10*, 107–144. https://doi.org/10.1146/annurev.bioeng.10.061807.160524.

46. Connelly, J.T., Rolland, J.P., and Whitesides, G.M. (2015). "Paper Machine" for Molecular Diagnostics. Anal. Chem. *87*, 7595–7601. https://doi.org/10.1021/acs.analchem.5b00411.

47. Kumar, A.A., Hennek, J.W., Smith, B.S., Kumar, S., Beattie, P., Jain, S., Rolland, J.P., Stossel, T.P., Chunda-Liyoka, C., and Whitesides, G.M. (2015). From the Bench to the Field in Low-Cost Diagnostics: Two Case Studies. Angew. Chem. Int. Ed. *54*, 5836–5853. https://doi.org/10.1002/anie.201411741.

48. Heidt, B., Siqueira, W.F., Eersels, K., Diliën, H., Van Grinsven, B., Fujiwara, R.T., and Cleij, T.J. (2020). Point of Care Diagnostics in Resource-Limited Settings: A Review of the Present and Future of PoC in Its Most Needed Environment. Biosensors *10*, 133. https://doi.org/10.3390/bios10100133.

49. Singh, G., Mishra, A., Mathur, A., Shastri, S., Nizam, A., Rizwan, A., Dadial, A.S., Firdous, A., and Hassan, H. (2024). Biosensors and Bioelectronics : X Advancement of organ-on-chip towards next generation medical technology. Biosens. Bioelectron. X *18*, 100480. https://doi.org/10.1016/j.biosx.2024.100480.

50. Nakao, Y., Kimura, H., Sakai, Y., and Fujii, T. (2011). Bile canaliculi formation by aligning rat primary hepatocytes in a microfluidic device. Biomicrofluidics *5*, 022212. https://doi.org/10.1063/1.3580753.

51. Mathur, A., Loskill, P., Shao, K., Huebsch, N., Hong, S., Marcus, S.G., Marks, N., Mandegar, M., Conklin, B.R., Lee, L.P., et al. (2015). Human iPSC-based Cardiac Microphysiological System For Drug Screening Applications. Sci. Rep. *5*, 8883. https://doi.org/10.1038/srep08883.

52. Fan, Y., Nguyen, D.T., Akay, Y., Xu, F., and Akay, M. (2016). Engineering a Brain Cancer Chip for High-throughput Drug Screening. Sci. Rep. *6*, 25062. https://doi.org/10.1038/srep25062.

53. Uwamori, H., Higuchi, T., Arai, K., and Sudo, R. (2017). Integration of neurogenesis and angiogenesis models for constructing a neurovascular tissue. Sci. Rep. *7*, 17349. https://doi.org/10.1038/s41598-017-17411-0.

54. Skardal, A., Murphy, S.V., Devarasetty, M., Mead, I., Kang, H.-W., Seol, Y.-J., Shrike Zhang, Y., Shin, S.-R., Zhao, L., Aleman, J., et al. (2017). Multi-tissue interactions in an integrated three-tissue organ-on-a-chip platform. Sci. Rep. *7*, 8837. https://doi.org/10.1038/s41598-017-08879-x.

55. Kasendra, M., Tovaglieri, A., Sontheimer-Phelps, A., Jalili-Firoozinezhad, S., Bein, A., Chalkiadaki, A., Scholl, W., Zhang, C., Rickner, H., Richmond, C.A., et al. (2018). Development of a primary human Small Intestine-on-a-Chip using biopsy-derived organoids. Sci. Rep. *8*, 2871. https://doi.org/10.1038/s41598-018-21201-7.

56. Rogal, J., Binder, C., Kromidas, E., Roosz, J., Probst, C., Schneider, S., Schenke-Layland, K., and Loskill, P. (2020). WAT-on-a-chip integrating human mature white adipocytes for mechanistic research and pharmaceutical applications. Sci. Rep. *10*, 6666. https://doi.org/10.1038/s41598-020-63710-4.

57. Domansky, K., Inman, W., Serdy, J., Dash, A., Lim, M.H.M., and Griffith, L.G. (2010). Perfused multiwell plate for 3D liver tissue engineering. Lab Chip *10*, 51–58. https://doi.org/10.1039/b913221j.

58. Jang, K.J., Cho, H.S., Kang, D.H., Bae, W.G., Kwon, T.H., and Suh, K.Y. (2011). Fluid-shear-stress-induced translocation of aquaporin-2 and reorganization of actin cytoskeleton in renal tubular epithelial cells. Integr. Biol. *3*, 134–141. https://doi.org/10.1039/c0ib00018c.

59. Zheng, Y., Chen, J., Craven, M., Choi, N.W., Totorica, S., Diaz-santana, A., Kermani, P., Hempstead, B., Fischbach-Teschl, C., López, J.A., et al. (2012). In vitro microvessels for the study of angiogenesis and thrombosis. Proc. Natl. Acad. Sci. USA *109*, 9342–9347. https://doi.org/10.1073/pnas.1201240109.

60. Franco, C., and Gerhardt, H. (2012). Blood vessels on a chip phosphorus. 5–6. Nature *488*, 465–466.

61. Kim, H.J., Huh, D., Hamilton, G., and Ingber, D.E. (2012). Human gut-on-a-chip inhabited by microbial flora that experiences intestinal peristalsis-like motions and flow. Lab Chip *12*, 2165–2174. https://doi.org/10.1039/c2lc40074j.

62. Wei-xuan, L.I., Guang-tie, L., Wei, Y.A.N., Qiong, Z., Wei, W., Xiao-mian, Z., and Da-yu, L.I.U. (2013). Artificial Uterus on a Microfluidic Chip. Chin. J. Anal. Chem. *41*, 467–472. https://doi.org/10.1016/S1872-2040(13)60639-8.

63. Griep, L.M., Wolbers, F., Wagenaar, B.D., and Hall, W. (2013). BBB ON CHIP : microfluidic platform to mechanically and biochemically modulate blood-brain barrier function. Biomed. Microdevices *15*, 145–150. https://doi.org/10.1007/s10544-012-9699-7.

64. Ataç, B., Wagner, I., Horland, R., Lauster, R., Marx, U., Tonevitsky, A.G., Azar, R.P., and Lindner, G. (2013). Skin and hair on-a-chip: in vitro skin models versus ex vivo tissue maintenance with dynamic perfusion. Lab Chip *13*, 3555–3561. https://doi.org/10.1039/c3lc50227a.

65. Torisawa, Y.s., Spina, C.S., Mammoto, T., Mammoto, A., Weaver, J.C., Tat, T., Collins, J.J., and Ingber, D.E. (2014). Bone marrow – on – a – chip replicates hematopoietic niche physiology in vitro. Nat. Methods *11*, 663–669. https://doi.org/10.1038/nmeth.2938.

66. Park, J., Lee, B.K., Jeong, G.S., Hyun, J.K., Lee, C.J., and Lee, S.-H. (2015). Three-dimensional brain-on-a-chip with an interstitial level of flow and its application as an in vitro model of Alzheimer's disease. Lab Chip *15*, 141–150. https://doi.org/10.1039/C4LC00962B.

67. Nunes, S.S., Miklas, J.W., Liu, J., Aschar-Sobbi, R., Xiao, Y., Zhang, B., Jiang, J., Massé, S., Gagliardi, M., Hsieh, A., et al. (2013). Biowire: a platform for maturation of human pluripotent stem cell–derived cardiomyocytes. Nat. Methods *10*, 781–787. https://doi.org/10.1038/nmeth.2524.

68. Moura Rosa, P., Gopalakrishnan, N., Ibrahim, H., Haug, M., and Halaas, Ø. (2016). The intercell dynamics of T cells and dendritic cells in a lymph node-on-a-chip flow device. Lab Chip *16*, 3728–3740. https://doi.org/10.1039/C6LC00702C.

69. U.S. Food and Drug Administration (2017). FDA Researchers to Evaluate 'Organs-on-Chips' Technology. https://www.fda.gov/food/hfp-constituent-updates/fda-researchers-evaluate-organs-chips-technology?.

70. Moore, N., Doty, D., Zielstorff, M., Kariv, I., Moy, L.Y., Gimbel, A., Chevillet, J.R., Lowry, N., Santos, J., Mott, V., et al. (2018). A multiplexed microfluidic system for evaluation of dynamics of immune–tumor interactions. Lab Chip *18*, 1844–1858. https://doi.org/10.1039/C8LC00256H.

71. Nguyen, T., Jung, S.H., Lee, M.S., Park, T.-E., Ahn, S.K., and Kang, J.H. (2019). Robust chemical bonding of PMMA microfluidic devices to porous PETE membranes for reliable cytotoxicity testing of drugs. Lab Chip *19*, 3706–3713. https://doi.org/10.1039/C9LC00338J.

72. Occhetta, P., Mainardi, A., Votta, E., Vallmajo-Martin, Q., Ehrbar, M., Martin, I., Barbero, A., and Rasponi, M. (2019). Hyperphysiological compression of articular cartilage induces an osteoarthritic phenotype in a cartilage-on-a-chip model. Nat. Biomed. Eng. *3*, 545–557. https://doi.org/10.1038/s41551-019-0406-3.

73. Yin, F., Zhu, Y., Zhang, M., Yu, H., Chen, W., and Qin, J. (2019). A 3D human placenta-on-a-chip model to probe nanoparticle exposure at the placental barrier. Toxicol. Vitro *54*, 105–113. https://doi.org/10.1016/j.tiv.2018.08.014.

74. Herland, A., Maoz, B.M., Das, D., Somayaji, M.R., Prantil-Baun, R., Novak, R., Cronce, M., Huffstater, T., Jeanty, S.S.F., Ingram, M., et al. (2020). Quantitative prediction of human pharmacokinetic responses to drugs via fluidically coupled vascularized organ chips. Nat. Biomed. Eng. *4*, 421–436. https://doi.org/10.1038/s41551-019-0498-9.

75. Jia, Z., Guo, Z., Yang, C.-T., Prestidge, C., and Thierry, B. (2021). "Mucus-on-Chip": A new tool to study the dynamic penetration of nanoparticulate drug carriers into mucus. Int. J. Pharm. *598*, 120391. https://doi.org/10.1016/j.ijpharm.2021.120391.

76. Esteve, V., Berganzo, J., Monge, R., Martínez-Bisbal, M.C., Villa, R., Celda, B., and Fernandez, L. (2014). Development of a three-dimensional cell culture system based on microfluidics for nuclear magnetic resonance and optical monitoring. Biomicrofluidics *8*, 064105. https://doi.org/10.1063/1.4902002.

77. Ayuso, J.M., Monge, R., Martínez-González, A., Virumbrales-Muñoz, M., Llamazares, G.A., Berganzo, J., Hernández-Laín, A., Santolaria, J., Doblaré, M., Hubert, C., et al. (2017). Glioblastoma on a microfluidic chip: Generating pseudopalisades and enhancing aggressiveness through blood vessel obstruction events. Neuro Oncol. *19*, 503–513. https://doi.org/10.1093/neuonc/now230.

78. Plebani, R., Potla, R., Soong, M., Bai, H., Izadifar, Z., Jiang, A., Travis, R.N., Belgur, C., Dinis, A., Cartwright, M.J., et al. (2022). Modeling pulmonary cystic fibrosis in a human lung airway-on-a-chip. J. Cyst. Fibros. *21*, 606–615. https://doi.org/10.1016/j.jcf.2021.10.004.

79. Gnecco, J.S., Pensabene, V., Li, D.J., Ding, T., Hui, E.E., Bruner-Tran, K.L., and Osteen, K.G. (2017). Compartmentalized Culture of Perivascular Stroma and Endothelial Cells in a Microfluidic Model of the Human Endometrium. Ann. Biomed. Eng. *45*, 1758–1769. https://doi.org/10.1007/s10439-017-1797-5.

80. Cho, M., and Park, J.-K. (2021). Modular 3D In Vitro Artery-Mimicking Multichannel System for Recapitulating Vascular Stenosis and Inflammation. Micromachines *12*, 1528. https://doi.org/10.3390/mi12121528.

81. Achberger, K., Probst, C., Haderspeck, J., Bolz, S., Rogal, J., Chuchuy, J., Nikolova, M., Cora, V., Antkowiak, L., Haq, W., et al. (2019). Merging organoid and organ-on-a-chip technology to generate complex multilayer tissue models in a human retina-on-a-chip platform. eLife *8*, e46188. https://doi.org/10.7554/eLife.46188.

82. Ingber, D., Ozkan, A., Merry, G., Posey, R., Calderon, K., Stejskalova, A., Sperry, M., Horvath, V., Goyal, G., Carlotti, E., et al. (2025). Human Organ Chips Reveal New Inflammatory Bowel Disease Drivers. Preprint at medRxiv. https://doi.org/10.21203/rs.3.rs-5627712/v1.

83. Jang, K.-J., Otieno, M.A., Ronxhi, J., Lim, H.-K., Ewart, L., Kodella, K.R., Petropolis, D.B., Kulkarni, G., Rubins, J.E., Conegliano, D., et al. (2019). Reproducing human and cross-species drug toxicities using a Liver-Chip. Sci. Transl. Med. *11*, eaax5516. https://doi.org/10.1126/scitranslmed.aax5516.

84. Park, T.-E., Mustafaoglu, N., Herland, A., Hasselkus, R., Mannix, R., FitzGerald, E.A., Prantil-Baun, R., Watters, A., Henry, O., Benz, M., et al. (2019). Hypoxia-enhanced Blood-Brain Barrier Chip recapitulates human barrier function and shuttling of drugs and antibodies. Nat. Commun. *10*, 2621. https://doi.org/10.1038/s41467-019-10588-0.

85. Schneider, S., Brás, E.J.S., Schneider, O., Schlünder, K., and Loskill, P. (2021). Facile Patterning of Thermoplastic Elastomers and Robust Bonding to Glass and Thermoplastics for Microfluidic Cell Culture and Organ-on-Chip. Micromachines *12*, 575. https://doi.org/10.3390/mi12050575.

86. Moon, B.-U., Li, K., Malic, L., Morton, K., Shao, H., Banh, L., Viswanathan, S., Young, E.W.K., and Veres, T. (2024). Reversible bonding in thermoplastic elastomer microfluidic platforms for harvestable 3D microvessel networks. Lab Chip *24*, 4948–4961. https://doi.org/10.1039/D4LC00530A.

87. Lee, J.-B., Kim, H., Kim, S., and Sung, G.Y. (2022). Fabrication and Evaluation of Tubule-on-a-Chip with RPTEC/HUVEC Co-Culture Using Injection-Molded Polycarbonate Chips. Micromachines *13*, 1932. https://doi.org/10.3390/mi13111932.

88. Gonzalez-Rubio, J., Kubiza, H., Xu, Y., Koenigs-Werner, H., Schmitz, M.S., Schedel, M., Apel, C., Jockenhoevel, S., Cornelissen, C.G., and Thiebes, A.L. (2025). Pericytes Promote More Vascularization than Stromal Cells via an Interleukin-6-Dependent Mechanism in Microfluidic Chips. Adv. Sci. *12*, 2408131. https://doi.org/10.1002/advs.202408131.

89. Rivera-Burgos, D., Sarkar, U., Lever, A.R., Avram, M.J., Coppeta, J.R., Wishnok, J.S., Borenstein, J.T., and Tannenbaum, S.R. (2016). Glucocorticoid Clearance and Metabolite Profiling in an In Vitro Human Airway Epithelium Lung Model. Drug Metab. Dispos. *44*, 220–226. https://doi.org/10.1124/dmd.115.066365.

90. Glieberman, A.L., Pope, B.D., Zimmerman, J.F., Liu, Q., Ferrier, J.P., Kenty, J.H.R., Schrell, A.M., Mukhitov, N., Shores, K.L., Tepole, A.B., et al. (2019). Synchronized stimulation and continuous insulin sensing in a microfluidic human Islet on a Chip designed for scalable manufacturing. Lab Chip *19*, 2993–3010. https://doi.org/10.1039/C9LC00253G.

91. Zhang, J., Chen, Z., Zhang, Y., Wang, X., Ouyang, J., Zhu, J., Yan, Y., Sun, X., Wang, F., Li, X., et al. (2021). Construction of a high fidelity epidermis-on-a-chip for scalable *in vitro* irritation evaluation. Lab Chip *21*, 3804–3818. https://doi.org/10.1039/D1LC00099C.

92. Sui, C., Zilberberg, J., and Lee, W. (2022). Microfluidic device engineered to study the trafficking of multiple myeloma cancer cells through the sinusoidal niche of bone marrow. Sci. Rep. *12*, 1439. https://doi.org/10.1038/s41598-022-05520-4.

93. Ferreira, D.A., Conde, J.P., Rothbauer, M., Ertl, P., Granja, P.L., and Oliveira, C. (2023). Bioinspired human stomach-on-a-chip with *in vivo* like function and architecture. Lab Chip *23*, 495–510. https://doi.org/10.1039/D2LC01132H.

94. Olaizola-Rodrigo, C., Castro-Abril, H., Perisé-Badía, I., Pancorbo, L., Ochoa, I., Monge, R., and Oliván, S. (2024). Reducing Inert Materials for Optimal Cell–Cell and Cell–Matrix Interactions within Microphysiological Systems. Biomimetics *9*, 262. https://doi.org/10.3390/biomimetics9050262.

95. Cook, S.R., Ball, A.G., Mohammad, A., and Pompano, R.R. (2025). A 3D-printed multi-compartment organ-on-chip platform with a tubing-free pump models communication with the lymph node. Lab Chip *25*, 155–174. https://doi.org/10.1039/D4LC00489B.

96. Mandt, D., Gruber, P., Markovic, M., Tromayer, M., Rothbauer, M., Kratz, S.R.A., Ali, S.F., Hoorick, J.V., Holnthoner, W., Mühleder, S., et al. (2018). Fabrication of biomimetic placental barrier structures within a microfluidic device utilizing two-photon polymerization. IJB *4*, 144. https://doi.org/10.18063/ijb.v4i2.144.

97. Marino, A., Tricinci, O., Battaglini, M., Filippeschi, C., Mattoli, V., Sinibaldi, E., and Ciofani, G. (2018). A 3D Real-Scale, Biomimetic, and Biohybrid Model of the Blood-Brain Barrier Fabricated through Two-Photon Lithography. Small *14*, 1702959. https://doi.org/10.1002/smll.201702959.

98. Zhang, R., and Larsen, N.B. (2017). Stereolithographic hydrogel printing of 3D culture chips with biofunctionalized complex 3D perfusion networks. Lab Chip *17*, 4273–4282. https://doi.org/10.1039/C7LC00926G.

99. Dobos, A., Gantner, F., Markovic, M., Van Hoorick, J., Tytgat, L., Van Vlierberghe, S., and Ovsianikov, A. (2021). On-chip high-definition bioprinting of microvascular structures. Biofabrication *13*, 015016. https://doi.org/10.1088/1758-5090/abb063.

100. Gonzalez, G., Roppolo, I., Pirri, C.F., and Chiappone, A. (2022). Current and emerging trends in polymeric 3D printed microfluidic devices. Addit. Manuf. *55*, 102867. https://doi.org/10.1016/j.addma.2022.102867.

101. Afshar, M.E., Abraha, H.Y., Bakooshli, M.A., Davoudi, S., Thavandiran, N., Tung, K., Ahn, H., Ginsberg, H.J., Zandstra, P.W., and Gilbert, P.M. (2020). A 96-well culture platform enables longitudinal analyses of engineered human skeletal muscle microtissue strength. Sci. Rep. *10*, 6918. https://doi.org/10.1038/s41598-020-62837-8.

102. Kado Abdalkader, R., Konishi, S., and Fujita, T. (2025). Development of a flexible 3D printed TPU-PVC microfluidic devices for organ-on-a-chip applications. Sci. Rep. *15*, 6125. https://doi.org/10.1038/s41598-025-90470-w.

103. Mader, M., Rein, C., Konrat, E., Meermeyer, S.L., Lee-Thedieck, C., Kotz-Helmer, F., and Rapp, B.E. (2021). Fused Deposition Modeling of Microfluidic Chips in Transparent Polystyrene. Micromachines *12*, 1348. https://doi.org/10.3390/mi12111348.

104. Riester, O., Laufer, S., and Deigner, H.-P. (2022). Direct 3D printed biocompatible microfluidics: assessment of human mesenchymal stem cell differentiation and cytotoxic drug screening in a dynamic culture system. J. Nanobiotechnol. *20*, 540. https://doi.org/10.1186/s12951-022-01737-7.

105. Abdalkader, R., Konishi, S., and Fujita, T. (2021). The Development of Biomimetic Aligned Skeletal Muscles in a Fully 3D Printed Microfluidic Device. Biomimetics *7*, 2. https://doi.org/10.3390/biomimetics7010002.

106. Schena, M., Shalon, D., Davis, R.W., and Brown, P.O. (1995). Quantitative Monitoring of Gene Expression Patterns with a Complementary DNA Microarray. Science *270*, 467–470. https://doi.org/10.1126/science.270.5235.467.

107. Chee, M., Yang, R., Hubbell, E., Berno, A., Huang, X.C., Stern, D., Winkler, J., Lockhart, D.J., Morris, M.S., and Fodor, S.P. (1996). Accessing Genetic Information with High-Density DNA Arrays. Science *274*, 610–614. https://doi.org/10.1126/science.274.5287.610.

108. Fodor, S.P., Rava, R.P., Huang, X.C., Pease, A.C., Holmes, C.P., and Adams, C.L. (1993). Multiplexed biochemical assays with biological chips. Nature *364*, 555–556.

109. Lockhart, D.J., Dong, H., Byrne, M.C., Follettie, M.T., Gallo, M.V., Chee, M.S., Mittmann, M., Wang, C., Kobayashi, M., Horton, H., and Brown, E.L. (1996). Expression monitoring by hybridization to high-density oligonucleotide arrays. Nat. Biotechnol. *14*, 1675–1680.

110. Monge, R. (2017). Development and application of microtechnologies in the design and fabrication of cell culture biomimetic systems. https://zaguan.unizar.es/record/61705.

111. Martinez-Duarte, R., and Madou, M.J. (2010). SU-8 Photolithography and Its Impact on Microfluidics. In Microfluidics and Nanofluidics Handbook: Fabrication, Implementation and Applications, 1, C. Suman and K.M. Sushanta, eds. (CRC Press), pp. 231–268.

112. Despont, M., Lorenz, H., Fahrni, N., Brugger, J., Renaud, P., and Vettiger, P. (1997). High-aspect-ratio, ultrathick, negative-tone near-uv photoresist for MEMS applications. In Proceedings IEEE The Tenth Annual International Workshop on Micro Electro Mechanical Systems. An Investigation of Micro Structures, Sensors, Actuators, Machines and Robots (IEEE), pp. 518–522. https://doi.org/10.1109/MEMSYS.1997.581916.

113. Lin, C.-H., Lee, G.-B., Chang, B.-W., and Chang, G.-L. (2002). A new fabrication process for ultra-thick microfluidic microstructures utilizing SU-8 photoresist. J. Micromech. Microeng. *12*, 590–597. https://doi.org/10.1088/0960-1317/12/5/312.

114. Blanco, F.J., Agirregabiria, M., Garcia, J., Berganzo, J., Tijero, M., Arroyo, M.T., Ruano, J.M., Aramburu, I., and Mayora, K. (2004). Novel three-dimensional embedded SU-8 microchannels fabricated using a low temperature full wafer adhesive bonding. J. Micromech. Microeng. *14*, 1047–1056. https://doi.org/10.1088/0960-1317/14/7/027.

115. Hudecz, D., Khire, T., Chung, H.L., Adumeau, L., Glavin, D., Luke, E., Nielsen, M.S., Dawson, K.A., McGrath, J.L., and Yan, Y. (2020). Ultrathin Silicon Membranes for *in Situ* Optical Analysis of Nanoparticle Translocation across a Human Blood–Brain Barrier Model. ACS Nano *14*, 1111–1122. https://doi.org/10.1021/acsnano.9b08870.

116. Tang, B., Bendas, S., Krajka, V., May, T., Moritz, A., Constantinou, I., Reichl, S., and Dietzel, A. (2022). Self-loading microfluidic platform with ultra-thin nanoporous membrane for organ-on-chip by wafer-level processing. Front. Sens. *3*, 974895. https://doi.org/10.3389/fsens.2022.974895.

117. Hudecz, D., McCloskey, M.C., Vergo, S., Christensen, S., McGrath, J.L., and Nielsen, M.S. (2023). Modelling a Human Blood-Brain Barrier Co-Culture Using an Ultrathin Silicon Nitride Membrane-Based Microfluidic Device. IJMS *24*, 5624. https://doi.org/10.3390/ijms24065624.

118. St. John, P.M., Davis, R., Cady, N., Czajka, J., Batt, C.A., and Craighead, H.G. (1998). Diffraction-Based Cell Detection Using a Microcontact Printed Antibody Grating. Anal. Chem. *70*, 1108–1111. https://doi.org/10.1021/ac9711302.

119. James, C.D., Davis, R.C., Kam, L., Craighead, H.G., Isaacson, M., Turner, J.N., and Shain, W. (1998). Patterned Protein Layers on Solid Substrates by Thin Stamp Microcontact Printing. Langmuir *14*, 741–744. https://doi.org/10.1021/la9710482.

120. Chen, C.S., Mrksich, M., Huang, S., Whitesides, G.M., and Ingber, D.E. (1997). Geometric Control of Cell Life and Death. Science *276*, 1425–1428. https://doi.org/10.1126/science.276.5317.1425.

121. Emulate (2025). The future of drug development is human.The FDA and NIH are prioritizing human-based testing. https://emulatebio.com/.

122. Mata, A., Fleischman, A.J., and Roy, S. (2005). Characterization of Polydimethylsiloxane (PDMS) Properties for Biomedical Micro/Nanosystems. Biomed. Microdevices *7*, 281–293. https://doi.org/10.1007/s10544-005-6070-2.

123. Benam, K.H., Villenave, R., Lucchesi, C., Varone, A., Hubeau, C., Lee, H.-H., Alves, S.E., Salmon, M., Ferrante, T.C., Weaver, J.C., et al. (2016). Small airway-on-a-chip enables analysis of human lung inflammation and drug responses in vitro. Nat. Methods *13*, 151–157. https://doi.org/10.1038/nmeth.3697.

124. Si, L., Bai, H., Rodas, M., Cao, W., Oh, C.Y., Jiang, A., Moller, R., Hoagland, D., Oishi, K., Horiuchi, S., et al. (2021). A human-airway-on-a-chip for the rapid identification of candidate antiviral therapeutics and prophylactics. Nat. Biomed. Eng. *5*, 815–829. https://doi.org/10.1038/s41551-021-00718-9.

125. Alver, C.G., Drabbe, E., Ishahak, M., and Agarwal, A. (2024). Roadblocks confronting widespread dissemination and deployment of Organs on Chips. Nat. Commun. *15*, 5118. https://doi.org/10.1038/s41467-024-48864-3.

126. Toepke, M.W., and Beebe, D.J. (2006). PDMS absorption of small molecules and consequences in microfluidic applications. Lab Chip *6*, 1484–1486. https://doi.org/10.1039/b612140c.

127. Van Meer, B.J., De Vries, H., Firth, K.S.A., Van Weerd, J., Tertoolen, L.G.J., Karperien, H.B.J., Jonkheijm, P., Denning, C., IJzerman, A.P., and Mummery, C.L. (2017). Small molecule absorption by PDMS in the context of drug response bioassays. Biochem. Biophys. Res. Commun. *482*, 323–328. https://doi.org/10.1016/j.bbrc.2016.11.062.

128. Sutthiwanjampa, C., Hong, S., Kim, W.J., Kang, S.H., and Park, H. (2023). Hydrophilic Modification Strategies to Enhance the Surface Biocompatibility of Poly(dimethylsiloxane)-Based Biomaterials for Medical Applications. Adv Materials Inter *10*, 2202333. https://doi.org/10.1002/admi.202202333.

129. Al-Ali, A., Waheed, W., Dawaymeh, F., Alamoodi, N., and Alazzam, A. (2023). A surface treatment method for improving the attachment of PDMS: acoustofluidics as a case study. Sci. Rep. *13*, 18141. https://doi.org/10.1038/s41598-023-45429-0.

130. Gonçalves, M., Gonçalves, I.M., Borges, J., Faustino, V., Soares, D., Vaz, F., Minas, G., Lima, R., and Pinho, D. (2024). Polydimethylsiloxane Surface Modification of Microfluidic Devices for Blood Plasma Separation. Polymers *16*, 1416. https://doi.org/10.3390/polym16101416.

131. Moraes, C., Sun, Y., and Simmons, C.A. (2009). Solving the shrinkage-induced PDMS alignment registration issue in multilayer soft lithography. J. Micromech. Microeng. *19*, 065015. https://doi.org/10.1088/0960-1317/19/6/065015.

132. Cottet, J., Vaillier, C., Buret, F., Frénéa-Robin, M., and Renaud, P. (2017). A reproducible method for $\mu$ m precision alignment of PDMS microchannels with on-chip electrodes using a mask aligner. Biomicrofluidics *11*, 064111. https://doi.org/10.1063/1.5001145.

133. Deshmukh, S.S., and Goswami, A. (2021). Recent developments in hot embossing – a review. Mater. Manuf. Process. *36*, 501–543. https://doi.org/10.1080/10426914.2020.1832691.

134. He, Y., Fu, J.-Z., and Chen, Z.-C. (2007). Research on optimization of the hot embossing process. J. Micromech. Microeng. *17*, 2420–2425. https://doi.org/10.1088/0960-1317/17/12/005.

135. Becker, H., and Heim, U. (2000). Hot embossing as a method for the fabrication of polymer high aspect ratio structures. Sensor Actuator Phys. *83*, 130–135. https://doi.org/10.1016/S0924-4247(00)00296-X.

136. Scott, S.M., and Ali, Z. (2021). Fabrication Methods for Microfluidic Devices: An Overview. Micromachines *12*, 319. https://doi.org/10.3390/mi12030319.

137. Shen, T., Han, S., He, W., Yang, W., Tang, X., Zhao, X., Liu, X., Shao, Z., Cheng, L., Zhao, Y., and Fan, J. (2025). Advances in Microfluidic Cochlea-On-A-Chip. Adv. Sci. *12*, 2406077. https://doi.org/10.1002/advs.202406077.

138. Ng, S.H., Wang, Z.F., Tjeung, R.T., and Rooij, N.D. (2006). Process issues for a multi-layer microelectrofluidic platform. Preprint at arXiv. https://doi.org/10.48550/arXiv.0711.3333.

139. Attia, U.M., Marson, S., and Alcock, J.R. (2009). Micro-injection moulding of polymer microfluidic devices. Microfluid Nanofluid *7*, 1–28. https://doi.org/10.1007/s10404-009-0421-x.

140. Chen, C.-S., Chen, S.-C., Liao, W.-H., Chien, R.-D., and Lin, S.-H. (2010). Micro injection molding of a micro-fluidic platform. Int. Commun. Heat Mass Tran. *37*, 1290–1294. https://doi.org/10.1016/j.icheatmasstransfer.2010.06.032.

141. Yao, D., and Kim, B. (2001). Injection Molding High-Aspect-Ratio Microstructures for Lab-On-A-Chip Applications. In Micro Total Analysis Systems 2001, J.M. Ramsey and A. Van Den Berg, eds. (Springer Dordrecht), pp. 413–414. https://doi.org/10.1007/978-94-010-1015-3_182.

142. De Mello, A. (2002). Focus: Plastic fantastic? Lab Chip *2*, 31N–36N. https://doi.org/10.1039/b203828p.

143. Lee, U.N., Su, X., Guckenberger, D.J., Dostie, A.M., Zhang, T., Berthier, E., and Theberge, A.B. (2018). Fundamentals of rapid injection molding for microfluidic cell-based assays. Lab Chip *18*, 496–504. https://doi.org/10.1039/C7LC01052D.

144. Zhang, H., Liu, H., and Zhang, N. (2022). A Review of Microinjection Moulding of Polymeric Micro Devices. Micromachines *13*, 1530. https://doi.org/10.3390/mi13091530.

145. Bian, Z., Xie, P.C., Ding, Y.M., and Yang, W.M. (2012). Effect of Processing Conditions on the Shrinkage and Warpage of Glass Fiber Reinforced PP Using Microcellular Injection Molding. Key Eng. Mater. *501*, 294–299. https://doi.org/10.4028/www.scientific.net/KEM.501.294.

146. Giri, K., and Tsao, C.-W. (2022). Recent Advances in Thermoplastic Microfluidic Bonding. Micromachines *13*, 486. https://doi.org/10.3390/mi13030486.

147. Trinh, K.T.L., Thai, D.A., and Lee, N.Y. (2022). Bonding Strategies for Thermoplastics Applicable for Bioanalysis and Diagnostics. Micromachines *13*, 1503. https://doi.org/10.3390/mi13091503.

148. Martínez-López, J.I., Mojica, M., Rodríguez, C.A., and Siller, H.R. (2016). Xurography as a Rapid Fabrication Alternative for Point-of-Care Devices: Assessment of Passive Micromixers. Sensors *16*, 705. https://doi.org/10.3390/s16050705.

149. Bartholomeusz, D.A., Boutte, R.W., and Andrade, J.D. (2005). Xurography: rapid prototyping of microstructures using a cutting plotter. J. Microelectromech. Syst. *14*, 1364–1374. https://doi.org/10.1109/JMEMS.2005.859087.

150. Klank, H., Kutter, J.P., and Geschke, O. (2002). CO2-laser micromachining and back-end processing for rapid production of PMMA-based microfluidic systems. Lab Chip *2*, 242–246. https://doi.org/10.1039/b206409j.

151. Konari, P.R., Clayton, Y.-D., Vaughan, M.B., Khandaker, M., and Hossan, M.R. (2021). Experimental Analysis of Laser Micromachining of Microchannels in Common Microfluidic Substrates. Micromachines *12*, 138. https://doi.org/10.3390/mi12020138.

152. Wang, Y., and Seidel, M. (2021). Strategy for fast manufacturing of 3D hydrodynamic focusing multilayer microfluidic chips and its application for flow-based synthesis of gold nanoparticles. Microfluid Nanofluid *25*, 64. https://doi.org/10.1007/s10404-021-02463-6.

153. Smith, S., Sypabekova, M., and Kim, S. (2024). Double-Sided Tape in Microfluidics: A Cost-Effective Method in Device Fabrication. Biosensors *14*, 249. https://doi.org/10.3390/bios14050249.

154. Paoli, R., Di Giuseppe, D., Badiola-Mateos, M., Martinelli, E., Lopez-Martinez, M.J., and Samitier, J. (2021). Rapid Manufacturing of Multilayered Microfluidic Devices for Organ on a Chip Applications. Sensors *21*, 1382. https://doi.org/10.3390/s21041382.

155. Sivakumar, R., Trinh, K.T.L., and Lee, N.Y. (2020). Heat and pressure-resistant room temperature irreversible sealing of hybrid PDMS–thermoplastic microfluidic devices *via* carbon–nitrogen covalent bonding and its application in a continuous-flow polymerase chain reaction. RSC Adv. *10*, 16502–16509. https://doi.org/10.1039/D0RA02332A.

156. Tsao, C.-W., and DeVoe, D.L. (2009). Bonding of thermoplastic polymer microfluidics. Microfluid Nanofluid *6*, 1–16. https://doi.org/10.1007/s10404-008-0361-x.

157. Dabaghi, M., Tiessen, N., Cao, Q., Chandiramohan, A., Saraei, N., Kim, Y., Gupta, T., Selvaganapathy, P.R., and Hirota, J.A. (2021). Adhesive-Based Fabrication Technique for Culture of Lung Airway Epithelial Cells with Applications in Cell Patterning and Microfluidics. ACS Biomater. Sci. Eng. *7*, 5301–5314. https://doi.org/10.1021/acsbiomaterials.1c01200.

158. Schlünder, K., Cipriano, M., Zbinden, A., Fuchs, S., Mayr, T., Schenke-Layland, K., and Loskill, P. (2024). Microphysiological pancreas-on-chip platform with integrated sensors to model endocrine function and metabolism. Lab Chip *24*, 2080–2093. https://doi.org/10.1039/D3LC00838J.

159. Kromidas, E., Geier, A., Weghofer, A., Liu, H.Y., Weiss, M., and Loskill, P. (2024). Immunocompetent PDMS-Free Organ-on-Chip Model of Cervical Cancer Integrating Patient-Specific Cervical Fibroblasts and Neutrophils. Adv. Healthc. Mater. *13*, 2302714. https://doi.org/10.1002/adhm.202302714.

160. Shahriari, S., Patel, V., and Selvaganapathy, P.R. (2023). Xurography as a tool for fabrication of microfluidic devices. J. Micromech. Microeng. *33*, 083002. https://doi.org/10.1088/1361-6439/ace05d.

161. Shiroma, L.S., Piazzetta, M.H.O., Duarte-Junior, G.F., Coltro, W.K.T., Carrilho, E., Gobbi, A.L., and Lima, R.S. (2016). Self-regenerating and hybrid irreversible/reversible PDMS microfluidic devices. Sci. Rep. *6*, 26032. https://doi.org/10.1038/srep26032.

162. Gale, B.K., Jafek, A.R., Lambert, C.J., Goenner, B.L., Moghimifam, H., Nze, U.C., and Kamarapu, S.K. (2018). A Review of Current Methods in Microfluidic Device Fabrication and Future Commercialization Prospects. Inventions *3*, 60. https://doi.org/10.3390/inventions3030060.

163. Cao, Y., Bontrager-Singer, J., and Zhu, L. (2015). A 3D microfluidic device fabrication method using thermopress bonding with multiple layers of polystyrene film. J. Micromech. Microeng. *25*, 065005. https://doi.org/10.1088/0960-1317/25/6/065005.

164. Bhattacharjee, N., Urrios, A., Kang, S., and Folch, A. (2016). The upcoming 3D-printing revolution in microfluidics. Lab Chip *16*, 1720–1742. https://doi.org/10.1039/C6LC00163G.

165. Yan, X., and Gu, P. (1996). A review of rapid prototyping technologies and systems. Computer-Aided Design *28*, 307–318.

166. Au, A.K., Huynh, W., Horowitz, L.F., and Folch, A. (2016). 3D-Printed Microfluidics. Angew. Chem. Int. Ed. *55*, 3862–3881. https://doi.org/10.1002/anie.201504382.

167. Amin, R., Knowlton, S., Hart, A., Yenilmez, B., Ghaderinezhad, F., Katebifar, S., Messina, M., Khademhosseini, A., and Tasoglu, S. (2016). 3D-printed microfluidic devices. Biofabrication *8*, 022001. https://doi.org/10.1088/1758-5090/8/2/022001.

168. Mehta, V., and Rath, S.N. (2021). 3D printed microfluidic devices: a review focused on four fundamental manufacturing approaches and implications on the field of healthcare. Bio-des. Manuf. *4*, 311–343. https://doi.org/10.1007/s42242-020-00112-5.

169. Duarte, L.C., Figueredo, F., Chagas, C.L.S., Cortón, E., and Coltro, W.K.T. (2024). A review of the recent achievements and future trends on 3D printed microfluidic devices for bioanalytical applications. Anal. Chim. Acta *1299*, 342429. https://doi.org/10.1016/j.aca.2024.342429.

170. Carnero, B., Bao-Varela, C., Gómez-Varela, A.I., Álvarez, E., and Flores-Arias, M.T. (2021). Microfluidic devices manufacturing with a stereolithographic printer for biological applications. Mater. Sci. Eng. C *129*, 112388. https://doi.org/10.1016/j.msec.2021.112388.

171. Rothbauer, M., Eilenberger, C., Spitz, S., Bachmann, B.E.M., Kratz, S.R.A., Reihs, E.I., Windhager, R., Toegel, S., and Ertl, P. (2022). Recent Advances in Additive Manufacturing and 3D Bioprinting for Organs-On-A-Chip and Microphysiological Systems. Front. Bioeng. Biotechnol. *10*, 837087. https://doi.org/10.3389/fbioe.2022.837087.

172. Luo, Z., Zhang, H., Chen, R., Li, H., Cheng, F., Zhang, L., Liu, J., Kong, T., Zhang, Y., and Wang, H. (2023). Digital light processing 3D printing for microfluidic chips with enhanced resolution via dosing- and zoning-controlled vat photopolymerization. Microsyst. Nanoeng. *9*, 103. https://doi.org/10.1038/s41378-023-00542-y.

173. Shirazi, S.F.S., Gharehkhani, S., Mehrali, M., Yarmand, H., Metselaar, H.S.C., Adib Kadri, N., and Osman, N.A.A. (2015). A review on powder-based additive manufacturing for tissue engineering: selective laser sintering and inkjet 3D printing. Sci. Technol. Adv. Mater. *16*, 033502. https://doi.org/10.1088/1468-6996/16/3/033502.

174. Thakar, C.M., Parkhe, S.S., Jain, A., Phasinam, K., Murugesan, G., and Ventayen, R.J.M. (2022). 3d Printing: Basic principles and applications. Mater. Today Proc. *51*, 842–849. https://doi.org/10.1016/j.matpr.2021.06.272.

175. Acierno, D., and Patti, A. (2023). Fused Deposition Modelling (FDM) of Thermoplastic-Based Filaments: Process and Rheological Properties—An Overview. Materials *16*, 7664. https://doi.org/10.3390/ma16247664.

176. Rajan, K., Samykano, M., Kadirgama, K., Harun, W.S.W., and Rahman, M.M. (2022). Fused deposition modeling: process, materials, parameters, properties, and applications. Int. J. Adv. Manuf. Technol. *120*, 1531–1570. https://doi.org/10.1007/s00170-022-08860-7.

177. Solomon, I.J., Sevvel, P., and Gunasekaran, J. (2021). A review on the various processing parameters in FDM. Mater. Today Proc. *37*, 509–514. https://doi.org/10.1016/j.matpr.2020.05.484.

178. Lu, B., Li, D., and Tian, X. (2015). Development Trends in Additive Manufacturing and 3D Printing. Engineering *1*, 85–89. https://doi.org/10.15302/J-ENG-2015012.

179. Qin, D., Xia, Y., Rogers, J.A., Jackman, R.J., Zhao, X.-M., and Whitesides, G.M. (1998). Microfabrication, Microstructures and Microsystems. In Microsystem Technology in Chemistry and Life Science. Topics in Current Chemistry, A. Manz and H. Becker, eds. (Springer, Berlin, Heidelberg). https://doi.org/10.1007/3-540-69544-3_1.

180. Grover, W.H., Skelley, A.M., Liu, C.N., Lagally, E.T., and Mathies, R.A. (2003). Monolithic membrane valves and diaphragm pumps for practical large-scale integration into glass microfluidic devices. Sensor. Actuator. B Chem. *89*, 315–323. https://doi.org/10.1016/S0925-4005(02)00468-9.

181. Aralekallu, S., Boddula, R., and Singh, V. (2023). Development of glass-based microfluidic devices: A review on its fabrication and biologic applications. Mater. Des. *225*, 111517. https://doi.org/10.1016/j.matdes.2022.111517.

182. Butkutė, A., Jurkšas, T., Baravykas, T., Leber, B., Merkininkaitė, G., Žilėnaitė, R., Čereška, D., Gulla, A., Kvietkauskas, M., Marcinkevičiūtė, K., et al. (2023). Combined Femtosecond Laser Glass Microprocessing for Liver-on-Chip Device Fabrication. Materials *16*, 2174. https://doi.org/10.3390/ma16062174.

183. Iliescu, C., Taylor, H., Avram, M., Miao, J., and Franssila, S. (2012). A practical guide for the fabrication of microfluidic devices using glass and silicon. Biomicrofluidics *6*, 16505–1650516. https://doi.org/10.1063/1.3689939.

184. Ramadan, Q., Gourikutty, S.B.N., and Zhang, Q.X. (2020). OOCHIP: Compartmentalized Microfluidic Perfusion System with Porous Barriers for Enhanced Cell–Cell Crosstalk in Organ-on-a-Chip. Micromachines *11*, 565. https://doi.org/10.3390/mi11060565.

185. Carvell, T., Burgoyne, P., Fraser, A.R., and Bridle, H. (2024). Categorising hybrid material microfluidic devices. Front. Lab Chip Technol. *3*, 1412290. https://doi.org/10.3389/frlct.2024.1412290.

186. Sia, S.K., and Whitesides, G.M. (2003). Microfluidic devices fabricated in Poly(dimethylsiloxane) for biological studies. Electrophoresis *24*, 3563–3576. https://doi.org/10.1002/elps.200305584.

187. Andrews, S., João, R., and Fernando da, S.A. (2019). Study of PDMS characterization and its applications in biomedicine: A review. JMEB *4*, 1–9. https://doi.org/10.24243/JMEB/4.1.163.

188. Raj M, K., and Chakraborty, S. (2020). PDMS microfluidics: A mini review. J. Appl. Polym. Sci. *137*, 48958. https://doi.org/10.1002/app.48958.

189. Mukhopadhyay, R. (2007). What are its weaknesses, and which other polymers can researchers add to their toolboxes? Anal Chem. *79*, 3248–3253.

190. Shrestha, J., Razavi Bazaz, S., Aboulkheyr Es, H., Yaghobian Azari, D., Thierry, B., Ebrahimi Warkiani, M., and Ghadiri, M. (2020). Lung-on-a-chip: the future of respiratory disease models and pharmacological studies. Crit. Rev. Biotechnol. *40*, 213–230. https://doi.org/10.1080/07388551.2019.1710458.

191. Carter, S.-S.D., Atif, A.-R., Kadekar, S., Lanekoff, I., Engqvist, H., Varghese, O.P., Tenje, M., and Mestres, G. (2020). PDMS leaching and its implications for on-chip studies focusing on bone regeneration applications. Organs-on-a-Chip *2*, 100004. https://doi.org/10.1016/j.ooc.2020.100004.

192. Li, W., Sun, X., Ji, B., Yang, X., Zhou, B., Lu, Z., and Gao, X. (2020). PLGA Nanofiber/PDMS Microporous Composite Membrane-Sandwiched Microchip for Drug Testing. Micromachines *11*, 1054. https://doi.org/10.3390/mi11121054.

193. Chen, J., Wright, K.E., and Birch, M.A. (2014). Nanoscale viscoelastic properties and adhesion of polydimethylsiloxane for tissue engineering. Acta Mech. Sin. *30*, 2–6. https://doi.org/10.1007/s10409-014-0022-0.

194. Drupitha, M.P., Bankoti, K., Pal, P., Das, B., Parameswar, R., Dhara, S., Nando, G.B., and Naskar, K. (2019). Morphology-induced physico-mechanical and biological characteristics of TPU–PDMS blend scaffolds for skin tissue engineering applications. J. Biomed. Mater. Res. *107*, 1634–1644. https://doi.org/10.1002/jbm.b.34256.

195. Chen, Z., and Lee, J.-B. (2021). Biocompatibility of SU-8 and Its Biomedical Device Applications. Micromachines *12*, 794. https://doi.org/10.3390/mi12070794.

196. Mitxelena-Iribarren, O., Olaizola, C., Arana, S., and Mujika, M. (2022). Versatile membrane-based microfluidic platform for in vitro drug diffusion testing mimicking in vivo environments. Nanomedicine. *39*, 102462. https://doi.org/10.1016/j.nano.2021.102462.

197. Liu, Y., Sakolish, C., Chen, Z., Phan, D.T.T., Bender, R.H.F., Hughes, C.C.W., and Rusyn, I. (2020). Human in vitro vascularized micro-organ and micro-tumor models are reproducible organ-on-a-chip platforms for studies of anticancer drugs. Toxicology *445*, 152601. https://doi.org/10.1016/j.tox.2020.152601.

198. Hammel, J.H., Cook, S.R., Belanger, M.C., Munson, J.M., and Pompano, R.R. (2021). Modeling Immunity In Vitro: Slices, Chips, and Engineered Tissues. Annu. Rev. Biomed. Eng. *23*, 461–491. https://doi.org/10.1146/annurev-bioeng-082420-124920.

199. Xu, G., Tan, Y., Xu, T., Yin, D., Wang, M., Shen, M., Chen, X., Shi, X., and Zhu, X. (2017). Hyaluronic acid-functionalized electrospun PLGA nanofibers embedded in a microfluidic chip for cancer cell

capture and culture. Biomater. Sci. *5*, 752–761. https://doi.org/10.1039/C6BM00933F.

200. Yang, X., Li, K., Zhang, X., Liu, C., Guo, B., Wen, W., and Gao, X. (2018). Nanofiber membrane supported lung-on-a-chip microdevice for anti-cancer drug testing. Lab Chip *18*, 486–495. https://doi.org/10.1039/C7LC01224A.

201. Operti, M.C., Dölen, Y., Keulen, J., Van Dinther, E.A.W., Figdor, C.G., and Tagit, O. (2019). Microfluidics-Assisted Size Tuning and Biological Evaluation of PLGA Particles. Pharmaceutics *11*, 590. https://doi.org/10.3390/pharmaceutics11110590.

202. Tran, R.T., Thevenot, P., Gyawali, D., Chiao, J.-C., Tang, L., and Yang, J. (2010). Synthesis and characterization of a biodegradable elastomer featuring a dual crosslinking mechanism. Soft Matter *6*, 2449–2461. https://doi.org/10.1039/c001605e.

203. Davenport Huyer, L., Zhang, B., Korolj, A., Montgomery, M., Drecun, S., Conant, G., Zhao, Y., Reis, L., and Radisic, M. (2016). Highly Elastic and Moldable Polyester Biomaterial for Cardiac Tissue Engineering Applications. ACS Biomater. Sci. Eng. *2*, 780–788. https://doi.org/10.1021/acsbiomaterials.5b00525.

204. Zhang, B., Montgomery, M., Chamberlain, M.D., Ogawa, S., Korolj, A., Pahnke, A., Wells, L.A., Massé, S., Kim, J., Reis, L., et al. (2016). Biodegradable scaffold with built-in vasculature for organ-on-a-chip engineering and direct surgical anastomosis. Nat. Mater. *15*, 669–678. https://doi.org/10.1038/nmat4570.

205. Davenport Huyer, L., Bannerman, A.D., Wang, Y., Savoji, H., Knee-Walden, E.J., Brissenden, A., Yee, B., Shoaib, M., Bobicki, E., Amsden, B.G., and Radisic, M. (2019). One-Pot Synthesis of Unsaturated Polyester Bioelastomer with Controllable Material Curing for Microscale Designs. Adv. Healthc. Mater. *8*, 1900245. https://doi.org/10.1002/adhm.201900245.

206. Sato, H., Matsumura, H., Keino, S., and Shoji, S. (2006). An all SU-8 microfluidic chip with built-in 3D fine microstructures. J. Micromech. Microeng. *16*, 2318–2322. https://doi.org/10.1088/0960-1317/16/11/010.

207. Hamid, Q., Wang, C., Snyder, J., and Sun, W. (2015). Surface modification of SU-8 for enhanced cell attachment and proliferation within microfluidic chips. J. Biomed. Mater. Res. *103*, 473–484. https://doi.org/10.1002/jbm.b.33223.

208. Arık, Y.B., Buijsman, W., Loessberg-Zahl, J., Cuartas-Vélez, C., Veenstra, C., Logtenberg, S., Grobbink, A.M., Bergveld, P., Gagliardi, G., Den Hollander, A.I., et al. (2021). Microfluidic organ-on-a-chip model of the outer blood–retinal barrier with clinically relevant read-outs for tissue permeability and vascular structure. Lab Chip *21*, 272–283. https://doi.org/10.1039/D0LC00639D.

209. Le, N.X.T., Trinh, K.T.L., and Lee, N.Y. (2021). Poly(acrylic acid) as an adhesion promoter for UV-assisted thermoplastic bonding: Application for the in vitro construction of human blood vessels. Mater. Sci. Eng. C Mater. Biol. Appl. *122*, 111874. https://doi.org/10.1016/j.msec.2021.111874.

210. Wang, Y., Wu, D., Wu, G., Wu, J., Lu, S., Lo, J., He, Y., Zhao, C., Zhao, X., Zhang, H., and Wang, S. (2020). Metastasis-on-a-chip mimicking the progression of kidney cancer in the liver for predicting treatment efficacy. Theranostics *10*, 300–311. https://doi.org/10.7150/thno.38736.

211. Bhise, N.S., Manoharan, V., Massa, S., Tamayol, A., Ghaderi, M., Miscuglio, M., Lang, Q., Shrike Zhang, Y., Shin, S.R., Calzone, G., et al. (2016). A liver-on-a-chip platform with bioprinted hepatic spheroids. Biofabrication *8*, 014101. https://doi.org/10.1088/1758-5090/8/1/014101.

212. Olaizola-Rodrigo, C., Palma-Florez, S., Ranđelović, T., Bayona, C., Ashrafi, M., Samitier, J., Lagunas, A., Mir, M., Doblaré, M., Ochoa, I., et al. (2024). Tuneable hydrogel patterns in pillarless microfluidic devices. Lab Chip *24*, 2094–2106. https://doi.org/10.1039/D3LC01082A.

213. Virumbrales-Muñoz, M., Ayuso, J.M., Lacueva, A., Randelovic, T., Livingston, M.K., Beebe, D.J., Oliván, S., Pereboom, D., Doblare, M., Fernández, L., and Ochoa, I. (2019). Enabling cell recovery from 3D cell culture microfluidic devices for tumour microenvironment biomarker profiling. Sci. Rep. *9*, 6199. https://doi.org/10.1038/s41598-019-42529-8.

214. Bayona, C., Wrona, M., Ranđelović, T., Nerín, C., Salafranca, J., and Ochoa, I. (2024). Development of an organ-on-chip model for the detection of volatile organic compounds as potential biomarkers of tumour progression. Biofabrication *16*, 045002. https://doi.org/10.1088/1758-5090/ad5764.

215. Wen, X., Yamanaka, M., Terada, S., and Kamei, K. (2020). In vitro nonalcoholic fatty liver disease model with cyclo-olefin-polymer-based microphysiological systems. Preprint at bioRxiv. https://doi.org/10.1101/2020.12.28.424535.

216. Azizgolshani, H., Coppeta, J.R., Vedula, E.M., Marr, E.E., Cain, B.P., Luu, R.J., Lech, M.P., Kann, S.H., Mulhern, T.J., Tandon, V., et al. (2021). High-throughput organ-on-chip platform with integrated programmable fluid flow and real-time sensing for complex tissue models in drug development workflows. Lab Chip *21*, 1454–1474. https://doi.org/10.1039/D1LC00067E.

217. Magno, M.H.R., Kim, J., Srinivasan, A., McBride, S., Bolikal, D., Darr, A., Hollinger, J.O., and Kohn, J. (2010). Synthesis, degradation and biocompatibility of tyrosine-derived polycarbonate scaffolds. J. Mater. Chem. *20*, 8885. https://doi.org/10.1039/c0jm00868k.

218. Mattern, K., Beißner, N., Reichl, S., and Dietzel, A. (2018). DynaMiTES – A dynamic cell culture platform for in vitro drug testing PART 1 – Engineering of microfluidic system and technical simulations. Eur. J. Pharm. Biopharm. *126*, 159–165. https://doi.org/10.1016/j.ejpb.2017.04.022.

219. Shah, P., Fritz, J.V., Glaab, E., Desai, M.S., Greenhalgh, K., Frachet, A., Niegowska, M., Estes, M., Jäger, C., Seguin-Devaux, C., et al. (2016). A microfluidics-based in vitro model of the gastrointestinal human–microbe interface. Nat. Commun. *7*, 11535. https://doi.org/10.1038/ncomms11535.

220. Zamprogno, P., Wüthrich, S., Achenbach, S., Thoma, G., Stucki, J.D., Hobi, N., Schneider-Daum, N., Lehr, C.-M., Huwer, H., Geiser, T., et al. (2021). Second-generation lung-on-a-chip with an array of stretchable alveoli made with a biological membrane. Commun. Biol. *4*, 168. https://doi.org/10.1038/s42003-021-01695-0.

221. Bircsak, K.M., DeBiasio, R., Miedel, M., Alsebahi, A., Reddinger, R., Saleh, A., Shun, T., Vernetti, L.A., and Gough, A. (2021). A 3D microfluidic liver model for high throughput compound toxicity screening in the OrganoPlate®. Toxicology *450*, 152667. https://doi.org/10.1016/j.tox.2020.152667.

222. Riddle, R.B., Jennbacken, K., Hansson, K.M., and Harper, M.T. (2024). A multicellular vessel-on-a-chip model reveals context-dependent roles for platelets in inflammation and inflammatory hemostasis. Blood Vessel. Thromb. Hemost. *1*, 100007. https://doi.org/10.1016/j.bvth.2024.100007.

223. Hegde, M., Jindal, R., Bhushan, A., Bale, S.S., McCarty, W.J., Golberg, I., Usta, O.B., and Yarmush, M.L. (2014). Dynamic interplay of flow and collagen stabilizes primary hepatocytes culture in a microfluidic platform. Lab Chip *14*, 2033–2039. https://doi.org/10.1039/C4LC00071D.

224. Walter, F.R., Valkai, S., Kincses, A., Petneházi, A., Czeller, T., Veszelka, S., Ormos, P., Deli, M.A., and Dér, A. (2016). A versatile lab-on-a-chip tool for modeling biological barriers. Sensor. Actuator. B Chem. *222*, 1209–1219. https://doi.org/10.1016/j.snb.2015.07.110.

225. Ongaro, A.E., Di Giuseppe, D., Kermanizadeh, A., Miguelez Crespo, A., Mencattini, A., Ghibelli, L., Mancini, V., Wlodarczyk, K.L., Hand, D.P., Martinelli, E., et al. (2020). Polylactic is a Sustainable, Low Absorption, Low Autofluorescence Alternative to Other Plastics for Microfluidic and Organ-on-Chip Applications. Anal. Chem. *92*, 6693–6701. https://doi.org/10.1021/acs.analchem.0c00651.

226. McKeen, L.W. (2017). Film Properties of Plastics and Elastomers (Elsevier).

227. Humayun, M., Chow, C.-W., and Young, E.W.K. (2018). Microfluidic lung airway-on-a-chip with arrayable suspended gels for studying epithelial

and smooth muscle cell interactions. Lab Chip *18*, 1298–1309. https://doi.org/10.1039/C7LC01357D.

228. Ma, X., Li, R., Jin, Z., Fan, Y., Zhou, X., and Zhang, Y. (2020). Injection molding and characterization of PMMA-based microfluidic devices. Microsyst. Technol. *26*, 1317–1324. https://doi.org/10.1007/s00542-019-04662-2.

229. Campbell, S.B., Wu, Q., Yazbeck, J., Liu, C., Okhovatian, S., and Radisic, M. (2021). Beyond Polydimethylsiloxane: Alternative Materials for Fabrication of Organ-on-a-Chip Devices and Microphysiological Systems. ACS Biomater. Sci. Eng. *7*, 2880–2899. https://doi.org/10.1021/acsbiomaterials.0c00640.

230. Agha, A., Waheed, W., Alamoodi, N., Mathew, B., Alnaimat, F., Abu-Nada, E., Abderrahmane, A., and Alazzam, A. (2022). A Review of Cyclic Olefin Copolymer Applications in Microfluidics and Microdevices. Macromol. Mater. Eng. *307*, 2200053. https://doi.org/10.1002/mame.202200053.

231. Rodrigues, R.G., Condelipes, P.G.M., Rosa, R.R., Chu, V., and Conde, J.P. (2023). Scalable Processing of Cyclic Olefin Copolymer (COC) Microfluidic Biochips. Micromachines *14*, 1837. https://doi.org/10.3390/mi14101837.

232. Bayona, C., Alza, L., Ranđelović, T., Sallán, M.C., Visa, A., Cantí, C., Ochoa, I., Oliván, S., and Herreros, J. (2024). Tetralol derivative NNC-55-0396 targets hypoxic cells in the glioblastoma microenvironment: an organ-on-chip approach. Cell Death Dis. *15*, 127. https://doi.org/10.1038/s41419-024-06492-1.

233. Grindulis, K., Matusevica, N.G., Kozlova, V., Rimsa, R., Klavins, K., and Mozolevskis, G. (2025). Sorption and release of small molecules in PDMS and COC for Organs on chip. Sci. Rep. *15*, 14012. https://doi.org/10.1038/s41598-025-97111-2.

234. Ataç, B., Wagner, I., Horland, R., Lauster, R., Marx, U., Tonevitsky, G., Azar, R.P., and Lindner, G. (2013). Skin and hair on-a-chip : in vitro skin models versus ex vivo tissue maintenance with dynamic perfusion. Lab Chip *3*, 3555–3561. https://doi.org/10.1039/c3lc50227a.

235. Chung, H.H., Mireles, M., Kwarta, B.J., and Gaborski, T.R. (2018). Use of porous membranes in tissue barrier and co-culture models. Lab Chip *18*, 1671–1689. https://doi.org/10.1039/C7LC01248A.

236. Fernandez-Carro, E., Salomon-Cambero, R., Armero, L., Castro-Abril, H.A., Ayensa-Jiménez, J., Martínez, M.A., Ochoa, I., Alcaine, C., García, I., and Ciriza, J. (2023). Nanoparticles Stokes radius assessment through permeability coefficient determination within a new stratified epithelium on-chip model. Artif. Cells, Nanomed. Biotechnol. *51*, 466–475. https://doi.org/10.1080/21691401.2023.2253534.

237. Wong, K.H.K., Truslow, J.G., Khankhel, A.H., Chan, K.L.S., and Tien, J. (2013). Artificial lymphatic drainage systems for vascularized microfluidic scaffolds. J. Biomed. Mater. Res. *101*, 2181–2190. https://doi.org/10.1002/jbm.a.34524.

238. He, J., Zhu, L., Liu, Y., Li, D., and Jin, Z. (2014). Sequential assembly of 3D perfusable microfluidic hydrogels. J. Mater. Sci. Mater. Med. *25*, 2491–2500. https://doi.org/10.1007/s10856-014-5270-9.

239. Hu, Y., Azadi, G., and Ardekani, A.M. (2015). Microfluidic fabrication of shape-tunable alginate microgels: Effect of size and impact velocity. Carbohydr. Polym. *120*, 38–45. https://doi.org/10.1016/j.carbpol.2014.11.053.

240. Wang, C., Tanataweethum, N., Karnik, S., and Bhushan, A. (2018). Novel Microfluidic Colon with an Extracellular Matrix Membrane. ACS Biomater. Sci. Eng. *4*, 1377–1385. https://doi.org/10.1021/acsbiomaterials.7b00883.

241. Shim, K.-Y., Lee, D., Han, J., Nguyen, N.-T., Park, S., and Sung, J.H. (2017). Microfluidic gut-on-a-chip with three-dimensional villi structure. Biomed. Microdevices *19*, 37. https://doi.org/10.1007/s10544-017-0179-y.

242. Qiu, Y., Ahn, B., Sakurai, Y., Hansen, C.E., Tran, R., Mimche, P.N., Mannino, R.G., Ciciliano, J.C., Lamb, T.J., Joiner, C.H., et al. (2018). Microvasculature-on-a-chip for the long-term study of endothelial barrier dysfunction and microvascular obstruction in disease. Nat. Biomed. Eng. *2*, 453–463. https://doi.org/10.1038/s41551-018-0224-z.

243. Maxson, E.L., Young, M.D., Noble, C., Go, J.L., Heidari, B., Khorramirouz, R., Morse, D.W., and Lerman, A. (2019). In vivo remodeling of a 3D-Bioprinted tissue engineered heart valve scaffold. Bioprinting *16*, e00059. https://doi.org/10.1016/j.bprint.2019.e00059.

244. Matsusaki, M., Ikeguchi, H., Kubo, C., Sato, H., Kuramochi, Y., and Takagi, D. (2019). Fabrication of Perfusable Pseudo Blood Vessels by Controlling Sol–Gel Transition of Gellan Gum Templates. ACS Biomater. Sci. Eng. *5*, 5637–5643. https://doi.org/10.1021/acsbiomaterials.8b01272.

245. Cecen, B., Bal-Ozturk, A., Yasayan, G., Alarcin, E., Kocak, P., Tutar, R., Kozaci, L.D., Shin, S.R., and Miri, A.K. (2022). Selection of natural biomaterials for micro-tissue and organ-on-chip models. J. Biomed. Mater. Res. *110*, 1147–1165. https://doi.org/10.1002/jbm.a.37353.

246. Arık, Y.B., De Sa Vivas, A., Laarveld, D., Van Laar, N., Gemser, J., Visscher, T., Van Den Berg, A., Passier, R., and Van Der Meer, A.D. (2021). Collagen I Based Enzymatically Degradable Membranes for Organ-on-a-Chip Barrier Models. ACS Biomater. Sci. Eng. *7*, 2998–3005. https://doi.org/10.1021/acsbiomaterials.0c00297.

247. Wong, L., Pegan, J.D., Gabela-Zuniga, B., Khine, M., and McCloskey, K.E. (2017). Leaf-inspired microcontact printing vascular patterns. Biofabrication *9*, 021001. https://doi.org/10.1088/1758-5090/aa721d.

248. Mondrinos, M.J., Yi, Y.-S., Wu, N.-K., Ding, X., and Huh, D. (2017). Native extracellular matrix-derived semipermeable, optically transparent, and inexpensive membrane inserts for microfluidic cell culture. Lab Chip *17*, 3146–3158. https://doi.org/10.1039/C7LC00317J.

249. Passaniti, A., Kleinman, H.K., and Martin, G.R. (2022). Matrigel: history/background, uses, and future applications. J. Cell Commun. Signal. *16*, 621–626. https://doi.org/10.1007/s12079-021-00643-1.

250. Ahmed, T.A.E., Dare, E.V., and Hincke, M. (2008). Fibrin: A Versatile Scaffold for Tissue Engineering Applications. Tissue Eng. Part B Rev. *14*, 199–215. https://doi.org/10.1089/ten.teb.2007.0435.

251. Owczarzy, A., Kurasiński, R., Kulig, K., Rogóż, W., Szkudlarek, A., and Maciążek-Jurczyk, M. (2020). Collagen - structure, properties and application. Eng. Biomater. *156*, 17–23. https://doi.org/10.34821/ENG.BIOMAT.156.2020.17-23.

252. Palumbo, F.S., Federico, S., Pitarresi, G., Fiorica, C., and Giammona, G. (2020). Gellan gum-based delivery systems of therapeutic agents and cells. Carbohydr. Polym. *229*, 115430. https://doi.org/10.1016/j.carbpol.2019.115430.

253. Cheng, D., Jiang, C., Xu, J., Liu, Z., and Mao, X. (2020). Characteristics and applications of alginate lyases: A review. Int. J. Biol. Macromol. *164*, 1304–1320. https://doi.org/10.1016/j.ijbiomac.2020.07.199.

254. Yan, Y., Cao, Y., Cheng, R., Shen, Z., Zhao, Y., Zhang, Y., Zhou, G., and Sang, S. (2022). Preparation and In Vitro Characterization of Gelatin Methacrylate for Corneal Tissue Engineering. Tissue Eng. Regen. Med. *19*, 59–72. https://doi.org/10.1007/s13770-021-00393-6.

255. Sakr, M.A., Sakthivel, K., Hossain, T., Shin, S.R., Siddiqua, S., Kim, J., and Kim, K. (2022). Recent trends in gelatin methacryloyl nanocomposite hydrogels for tissue engineering. J. Biomed. Mater. Res. *110*, 708–724. https://doi.org/10.1002/jbm.a.37310.

256. Da Silva, K., Kumar, P., Van Vuuren, S.F., Pillay, V., and Choonara, Y.E. (2021). Three-Dimensional Printability of an ECM-Based Gelatin Methacryloyl (GelMA) Biomaterial for Potential Neuroregeneration. ACS Omega *6*, 21368–21383. https://doi.org/10.1021/acsomega.1c01903.

257. Yang, L., Shridhar, S.V., Gerwitz, M., and Soman, P. (2016). An *in vitro* vascular chip using 3D printing-enabled hydrogel casting. Biofabrication *8*, 035015. https://doi.org/10.1088/1758-5090/8/3/035015.

258. Qin, X., He, R., Chen, H., Fu, D., Peng, Y., Meng, S., Chen, C., and Yang, L. (2021). Methacrylated pullulan/polyethylene (glycol) diacrylate composite hydrogel for cartilage tissue engineering. J. Biomater. Sci. Polym. Ed. *32*, 1057–1071. https://doi.org/10.1080/09205063.2021.1899888.

259. Bandyopadhyay, A., Mandal, B.B., and Bhardwaj, N. (2022). 3D bioprinting of photo-crosslinkable silk methacrylate ( SilMA )-polyethylene glycol diacrylate ( PEGDA ) bioink for cartilage tissue engineering. J. Biomed. Mater. Res. *110*, 884–898. https://doi.org/10.1002/jbm.a.37336.

260. Okhovatian, S., Shakeri, A., Davenport Huyer, L., and Radisic, M. (2023). Elastomeric Polyesters in Cardiovascular Tissue Engineering and Organs-on-a-Chip. Biomacromolecules *24*, 4511–4531. https://doi.org/10.1021/acs.biomac.3c00387.

261. Yue, K., Trujillo-de Santiago, G., Alvarez, M.M., Tamayol, A., Annabi, N., and Khademhosseini, A. (2015). Synthesis, properties, and biomedical applications of gelatin methacryloyl (GelMA) hydrogels. Biomaterials *73*, 254–271. https://doi.org/10.1016/j.biomaterials.2015.08.045.

262. Joshi, P., Breaux, S., Naro, J., Wang, Y., Ahmed, M.S.U., Vig, K., and Auad, M.L. (2021). Synthesis and characterization of photopolymerizable hydrogels based on poly (ethylene glycol) for biomedical applications. J. Appl. Polym. Sci. *138*, 50489. https://doi.org/10.1002/app.50489.

263. Van Der Helm, M.W., Odijk, M., Frimat, J.-P., Van Der Meer, A.D., Eijkel, J.C.T., Van Den Berg, A., and Segerink, L.I. (2016). Direct quantification of transendothelial electrical resistance in organs-on-chips. Biosens. Bioelectron. *85*, 924–929. https://doi.org/10.1016/j.bios.2016.06.014.

264. Shrestha, J., Ghadiri, M., Shanmugavel, M., Razavi Bazaz, S., Vasilescu, S., Ding, L., and Ebrahimi Warkiani, M. (2019). A rapidly prototyped lung-on-a-chip model using 3D-printed molds. Organs-on-a-Chip *1*, 100001. https://doi.org/10.1016/j.ooc.2020.100001.

265. Polidoro, M.A., Ferrari, E., Marzorati, S., Lleo, A., and Rasponi, M. (2021). Experimental liver models: From cell culture techniques to microfluidic organs-on-chip. Liver Int. *41*, 1744–1761. https://doi.org/10.1111/liv.14942.

266. Kim, S., Lee, H., Chung, M., and Jeon, N.L. (2013). Engineering of functional, perfusable 3D microvascular networks on a chip. Lab Chip *13*, 1489–1500. https://doi.org/10.1039/c3lc41320a.

267. Kim, C., Kasuya, J., Jeon, J., Chung, S., and Kamm, R.D. (2015). A quantitative microfluidic angiogenesis screen for studying anti-angiogenic therapeutic drugs. Lab Chip *15*, 301–310. https://doi.org/10.1039/C4LC00866A.

268. Ayuso, J.M., Virumbrales-Muñoz, M., Lacueva, A., Lanuza, P.M., Checa-Chavarria, E., Botella, P., Fernández, E., Doblare, M., Allison, S.J., Phillips, R.M., et al. (2016). Development and characterization of a microfluidic model of the tumour microenvironment. Sci. Rep. *6*, 36086. https://doi.org/10.1038/srep36086.

269. Pasman, T., Grijpma, D., Stamatialis, D., and Poot, A. (2018). Flat and microstructured polymeric membranes in organs-on-chips. J. R. Soc. Interface *15*, 20180351. https://doi.org/10.1098/rsif.2018.0351.

270. Annabi, N., Selimović, Š., Acevedo Cox, J.P., Ribas, J., Afshar Bakooshli, M., Heintze, D., Weiss, A.S., Cropek, D., and Khademhosseini, A. (2013). Hydrogel-coated microfluidic channels for cardiomyocyte culture. Lab Chip *13*, 3569–3577. https://doi.org/10.1039/c3lc50252j.

271. Loessberg-Zahl, J., Beumer, J., Van Den Berg, A., Eijkel, J.C.T., and van der Meer, A.D. (2020). Patterning Biological Gels for 3D Cell Culture inside Microfluidic Devices by Local Surface Modification through Laminar Flow Patterning. Micromachines *11*, 1112. https://doi.org/10.3390/mi11121112.

272. Bunge, F., Driesche, S.v.d., and Vellekoop, M.J. (2017). Microfluidic Platform for the Long-Term On-Chip Cultivation of Mammalian Cells for Lab-On-A-Chip Applications. Sensors *17*, 1603. https://doi.org/10.3390/s17071603.

273. Hao, J., Zhao, W., Oh, J.M., and Shen, K. (2021). A Pillar-Free Diffusion Device for Studying Chemotaxis on Supported Lipid Bilayers. Micromachines *12*, 1254. https://doi.org/10.3390/mi12101254.

274. Soragni, C., Queiroz, K., Ng, C.P., Stok, A., Olivier, T., Tzagkaraki, D., Heijmans, J., Suijker, J., De Ruiter, S.P.M., Olczyk, A., et al. (2024). Phenotypic screening in Organ-on-a-Chip systems: a 1537 kinase inhibitor library screen on a 3D angiogenesis assay. Angiogenesis *27*, 37–49. https://doi.org/10.1007/s10456-023-09888-3.

275. Aung, A., Kumar, V., Theprungsirikul, J., Davey, S.K., and Varghese, S. (2020). An Engineered Tumor-on-a-Chip Device with Breast Cancer–Immune Cell Interactions for Assessing T-cell Recruitment. Cancer Res. *80*, 263–275. https://doi.org/10.1158/0008-5472.CAN-19-0342.

276. Brandenberg, N., and Lutolf, M.P. (2016). In Situ Patterning of Microfluidic Networks in 3D Cell-Laden Hydrogels. Adv. Mater. *28*, 7450–7456. https://doi.org/10.1002/adma.201601099.

277. Nikolaev, M., Mitrofanova, O., Broguiere, N., Geraldo, S., Dutta, D., Tabata, Y., Elci, B., Brandenberg, N., Kolotuev, I., Gjorevski, N., et al. (2020). Homeostatic mini-intestines through scaffold-guided organoid morphogenesis. Nature *585*, 574–578. https://doi.org/10.1038/s41586-020-2724-8.

278. Bayona, C., Olaizola-Rodrigo, C., Sharko, V., Ashrafi, M., Doblaré, M., Doblaré, M., Monge, R., Oliván, S., and Oliván, S. (2025). A Novel Multicompartment Barrier-Free Microfluidic Device Reveals the Impact of Extracellular Matrix Stiffening and Temozolomide on Immune-Tumor Interactions in Glioblastoma. Small *21*, e2409229. https://doi.org/10.1002/smll.202409229.

279. Weigl, B.H., and Yager, P. (1999). MICROFLUIDICS:Microfluidic Diffusion-Based Separation and Detection. Science *283*, 346–347.

280. Squires, T.M., and Quake, S.R. (2005). Microfluidics: Fluid physics at the nanoliter scale. Rev. Mod. Phys. *77*, 977–1026. https://doi.org/10.1103/RevModPhys.77.977.

281. Shchukin, D.G., Kommireddy, D.S., Zhao, Y., Cui, T., Sukhorukov, G.B., and Lvov, Y.M. (2004). Polyelectrolyte Micropatterning Using a Laminar-Flow Microfluidic Device. Adv. Mater. *16*, 389–393. https://doi.org/10.1002/adma.200305776.

282. Li, Z., Venkataraman, A., Rosenbaum, M.A., and Angenent, L.T. (2012). A Laminar-Flow Microfluidic Device for Quantitative Analysis of Microbial Electrochemical Activity. ChemSusChem *5*, 1119–1123. https://doi.org/10.1002/cssc.201100736.

283. Vulto, P., Podszun, S., Meyer, P., Hermann, C., Manz, A., and Urban, G.A. (2011). Phaseguides: a paradigm shift in microfluidic priming and emptying. Lab Chip *11*, 1596–1602. https://doi.org/10.1039/c0lc00643b.

284. Vulto, P., Huesgen, T., Albrecht, B., and Urban, G.A. (2009). A full-wafer fabrication process for glass microfluidic chips with integrated electroplated electrodes by direct bonding of dry film resist. J. Micromech. Microeng. *19*, 077001. https://doi.org/10.1088/0960-1317/19/7/077001.

285. Trietsch, S.J., Israëls, G.D., Joore, J., Hankemeier, T., and Vulto, P. (2013). Microfluidic titer plate for stratified 3D cell culture. Lab Chip *13*, 3548–3554. https://doi.org/10.1039/c3lc50210d.

286. Phurimsak, C., Yildirim, E., Tarn, M.D., Trietsch, S.J., Hankemeier, T., Pamme, N., and Vulto, P. (2014). Phaseguide assisted liquid lamination for magnetic particle-based assays. Lab Chip *14*, 2334–2343. https://doi.org/10.1039/c4lc00139g.

287. Yen, D.P., Ando, Y., and Shen, K. (2016). A cost-effective micromilling platform for rapid prototyping of microdevices. Technology *4*, 234–239. https://doi.org/10.1142/S2339547816200041.

288. Abidemi, J., and Thomas, H. (2021). OrganoPlate Micro-fluidic Microvessel Culture and Analysis. Bio-Protocol *11*, 3947. https://doi.org/10.21769/BioProtoc.4070.

289. Liu, V.A., and Bhatia, S.N. (2002). Three-Dimensional Photopatterning of Hydrogels Containing Living Cells. Biomed. Microdevices *4*, 257–266.

290. Albrecht, D.R., Tsang, V.L., Sah, R.L., and Bhatia, S.N. (2005). Photo- and electropatterning of hydrogel-encapsulated living cell arrays. Lab Chip *5*, 111–118. https://doi.org/10.1039/b406953f.

291. Liu Tsang, V., Chen, A.A., Cho, L.M., Jadin, K.D., Sah, R.L., DeLong, S., West, J.L., and Bhatia, S.N. (2007). Fabrication of 3D hepatic tissues by additive photopatterning of cellular hydrogels. FASEB J. *21*, 790–801. https://doi.org/10.1096/fj.06-7117com.

292. Khademhosseini, A., and Langer, R. (2007). Microengineered hydrogels for tissue engineering. Biomaterials *28*, 5087–5092. https://doi.org/10.1016/j.biomaterials.2007.07.021.

293. Ebrahimi, M., Ostrovidov, S., Salehi, S., Kim, S.B., Bae, H., and Khademhosseini, A. (2018). Enhanced skeletal muscle formation on microfluidic spun gelatin methacryloyl (GelMA) fibres using surface patterning and agrin treatment. J. Tissue Eng. Regen. Med. *12*, 2151–2163. https://doi.org/10.1002/term.2738.

294. Jiang, Z., Shaha, R., McBride, R., Jiang, K., Tang, M., Xu, B., Goroncy, A.K., Frick, C., and Oakey, J. (2020). Crosslinker length dictates step-growth hydrogel network formation dynamics and allows rapid on-chip photoencapsulation. Biofabrication *12*, 035006. https://doi.org/10.1088/1758-5090/ab7ef4.

295. Rajan, S.A.P., Skardal, A., and Hall, A.R. (2020). Multi-Domain Photopatterned 3D Tumor Constructs in a Micro-Physiological System for Analysis, Quantification, and Isolation of Infiltrating Cells. Adv. Biosyst. *4*, 1900273. https://doi.org/10.1002/adbi.201900273.

296. Ortiz-Cárdenas, J.E., Zatorski, J.M., Arneja, A., Montalbine, A.N., Munson, J.M., Luckey, C.J., and Pompano, R.R. (2022). Towards spatially-organized organs-on-chip: Photopatterning cell-laden thiol-ene and methacryloyl hydrogels in a microfluidic device. Organs. Chip. *4*, 100018. https://doi.org/10.1016/j.ooc.2022.100018.

297. Zhang, B., and Radisic, M. (2017). Organ-on-a-chip devices advance to market. Lab Chip *17*, 2395–2420. https://doi.org/10.1039/C6LC01554A.

298. Ying-Jin, S., Yuste, I., González-Burgos, E., and Serrano, D.R. (2025). Fabrication of organ-on-a-chip using microfluidics. Bioprinting *46*, e00394. https://doi.org/10.1016/j.bprint.2025.e00394.

299. TISSUSE (2025). Pioneering Human-on-a-Chip developments. https://www.tissuse.com/en/.

300. Mimetas (2025). Human Tissue Models for Better herapies. https://www.mimetas.com/en/home/.

301. Beonchip (2025). Organ-on-chip made easy. https://beonchip.com/.

302. AIM Biotech (2025). Explore AIM Biotech Solutions for Humanized Drug Discovery and Functional Precision Medicine. https://aimbiotech.com/.

303. CN-BIO Innovations (2025). Transform drug discovery with predictive human organ models. https://cn-bio.com/.

304. InSphero (2025). 3D In Vitro Models and Solutions for Drug Safety & Efficacy. https://insphero.com/.

305. Shakeri, A., Khan, S., Jarad, N.A., and Didar, T.F. (2022). The Fabrication and Bonding of Thermoplastic Microfluidics: A Review. Materials *15*, 6478. https://doi.org/10.3390/ma15186478.

306. Naikwadi, A.T., Sharma, B.K., Bhatt, K.D., and Mahanwar, P.A. (2022). Gamma Radiation Processed Polymeric Materials for High Performance Applications: A Review. Front. Chem. *10*, 837111. https://doi.org/10.3389/fchem.2022.837111.

307. Fifield, L.S., Pharr, M., Staack, D., Pillai, S.D., Nichols, L., McCoy, J., Faucette, T., Bisel, T.T., Huang, M., Hasan, M.K., et al. (2021). Direct comparison of gamma, electron beam and X-ray irradiation doses on characteristics of low-density polyethylene, polypropylene homopolymer, polyolefin elastomer and chlorobutyl rubber medical device polymers. Radiat. Phys. Chem. *186*, 109505. https://doi.org/10.1016/j.radphyschem.2021.109505.

308. Chen, Y., Neff, M., McEvoy, B., Cao, Z., Pezzoli, R., Murphy, A., Gately, N., Jnr, M.H., Rowan, N.J., and Devine, D.M. (2019). 3D printed polymers are less stable than injection moulded counterparts when exposed to terminal sterilization processes using novel vaporized hydrogen peroxide and electron beam processes. Polymer *183*, 121870. https://doi.org/10.1016/j.polymer.2019.121870.

309. Darwin Microfluidics (2025). HUMIMIC Chip3 & Chip3plus - 3-organ-chip. https://darwin-microfluidics.com/products/humimic-chip3-chip3plus-3-organ-chip/.

310. Labscoop (2025). HUMIMIC Organ-on-Chip2 - 96-well. https://labscoop.com/us/en/product/tss/humimic/c2-96-humimic-organ-on-chip2-96-well.

311. Fisher Scientific (2025). Emulate inc basic research chip kit- 24 pk. https://www.fishersci.com/shop/products/NC2892147/NC2892147.

312. Biocompare (2025). Chip-S1 Basic Research Kit (24-pack) from Emulate. https://www.biocompare.com/25138-Assay-Kit/21528639-Chip-S1-Basic-Research-Kit-24-pack/.

313. Core, G. (2023). Lab-on-a-chip—fostering a sustainable future. Front. Lab Chip Technol. *2*, 1239134. https://doi.org/10.3389/frlct.2023.1239134.

314. Özkayar, G., Lötters, J.C., Tichem, M., and Ghatkesar, M.K. (2022). Toward a modular, integrated, miniaturized, and portable microfluidic flow control architecture for organs-on-chips applications. Biomicrofluidics *16*, 021302. https://doi.org/10.1063/5.0074156.

315. Mastrangeli, M., Millet, S., the ORCHID partners, and van den Eijnden-van Raaij, J. (2019). Organ-on-Chip in Development: Towards a Roadmap for Organs-on-Chip. ALTEX *36*, 650–668. https://doi.org/10.14573/altex.1908271.

316. CEN, CENELEC and EUROoCS (2024). Focus Group Organ-on-Chip Standardization Roadmap. https://www.cencenelec.eu/news-events/news/2024/brief-news/2024-07-10-organ-on-chip/.

317. U.S. Food and Drug Administration (2025). FDA's ISTAND Pilot Program accepts a submission of first organ-on-a-chip technology designed to predict human drug-induced liver injury (DILI). https://www.fda.gov/drugs/drug-safety-and-availability/fdas-istand-pilot-program-accepts-submission-first-organ-chip-technology-designed-predict-human-drug.

318. European Medicines Agency (2025). New Approach Methodologies EU-IN Horizon Scanning Report. www.ema.europa.eu.

319. Low, L.A., Mummery, C., Berridge, B.R., Austin, C.P., and Tagle, D.A. (2021). Organs-on-chips: into the next decade. Nat. Rev. Drug Discov. *20*, 345–361. https://doi.org/10.1038/s41573-020-0079-3.

320. Mendes, M., Morais, A.S., Carlos, A., Sousa, J.J., Pais, A.C., Mihăilă, S.M., and Vitorino, C. (2025). Organ-on-a-chip: Quo vademus? Applications and regulatory status. Colloids Surf. B Biointerfaces *249*, 114507. https://doi.org/10.1016/j.colsurfb.2025.114507.